

Source Mechanism Inversion of Wastewater Injection Induced Earthquake in Pawnee, Oklahoma

Course Code: ESS492Y1

Author: Jia Yoong Chong

Student Number: 1001 204 252

Thesis supervisor: Dr. Qinya Liu

Date: April 8, 2019

Table of Content

Table of Contents

Abstract

1. Introduction

2. Data and Method

 2.1 Seismic Data

 2.2 Inversion Problem

 2.3 Observation and Waveform Data Processing

 2.4 Green's function

 2.5 Generalized “Cut-and-Paste” method

3. Result

4. Discussion

5. Conclusion

Acknowledgement

References

Appendix

Abstract

Pawnee M5.8 earthquake is the largest instrumentally recorded event in Oklahoma. It ruptured on a previously unmapped fault and triggered aftershocks along a complex conjugate fault system. Two M ≥ 3.5 earthquakes were detected along a mapped fault that is conjugate to the mainshock fault around 100 days before the mainshock. Another two earthquakes clusters have been detected in the region 40 days before. Regional earthquake trends have indicated high spatial and temporal correlation between earthquakes and high-volume disposal wells. This study summarizes an updated analysis of earthquakes source mechanisms in region nearby Pawnee that occurred from June 2016 to September 2016 by using general “Cut-and-Paste” (gCAP) method. Source mechanism inversion results shows Pawnee M5.8 mainshock may have been caused by destabilization of fault 3-4 km below the depth range where injection took place. In addition to geological evidence and injection parameters, our results shows Pawnee sequence was likely a result of left-lateral slip across the previously unmapped Sooner Lake Fault induced by wastewater injection. This mechanism has been suggested for characterizing the previously unmapped Sooner Lake Fault (Fielding et al., 2017).

1 Introduction

In recent decade, swarms of earthquake activities have flooded Oklahoma in United States followed by an increase of wastewater disposal activities due to hydraulic fracturing operations in the region. The widespread adoption of hydraulic fracturing for hydrocarbon resources in the Mississippi Lime has produced significant amount of wastewater that needs to be disposed. The Mississippian-age Caney Shale Formation beneath Oklahoma consist of lower, fissile shale intervals and an upper shale-siltstone interval in the Arkoma Basin. The main geological interest for oil & gas companies is the stratigraphically uniform Caney Shale Formation, containing substantial shale gas and coalbed methane resources (Andrews R.D., 2007). Hydraulic fracturing, commonly known as fracking, is an industrial practice of extracting oil and natural gas by means of injecting fluid into rock formations at high pressure. Fracture network, created by high pressure fluid, allows shale oil within the rocks to flow back with injected fluid for extraction. Additional saltwater is also injected deep underground to enhance oil and gas recovery (Rubinstein et. al., 2015). The recovered hydraulic fracturing fluid is then disposed in well 1-2 km below ground surface. The Arbuckle Group, beneath most of Oklahoma, is a favorable formation for wastewater disposal due to its highly porous and low pressure sediment layer overlying a crystalline basement (Chen et al., 2017). An average of 2.3 billion barrels of wastewater have been injected into the basement since 2011 (Hincks T et al., 2018).

These induced earthquakes often occurred in the form of swarm-like clustering without clear mainshock and exhibited spatio-temporal migrations that are regarded as manifestation of fluid propagation (Shapiro et al., 2002; McGarr, A. et al, 2017). However, regional earthquake trends indicate high spatial and temporal correlation between earthquakes and high-volume disposal wells (Walter et al., 2017). Previously recorded seismicities found within Precambrian crystalline basement suggests faults could have been reactivated by wastewater injection into Arbuckle Group (Keranen et al., 2013, 2014). Pawnee M5.8 earthquake is the largest instrumentally recorded event in Oklahoma, United States. Interestingly, the Pawnee M5.8 event is noted to have been preceded only by 3.9 Mw and 3.6 Mw earthquakes 100 days and 40 days before (Figure 1). Although the foreshocks and aftershocks of Pawnee sequence were sparse with magnitudes smaller than M4, this main shock appears to have been induced by high-volume wastewater disposal within 10km from the mainshock epicenter (McGarr et al., 2017). Wastewater injection may have locally increased the pore fluid pressure and reduced the effective stress along faults, resulting in induced seismicity (Hincks et al., 2018). Foreshock activities within the conjugate fault system too have been identified with instantaneous response to fluctuation in injection rate at 95% confidence interval (Chen et al., 2015).

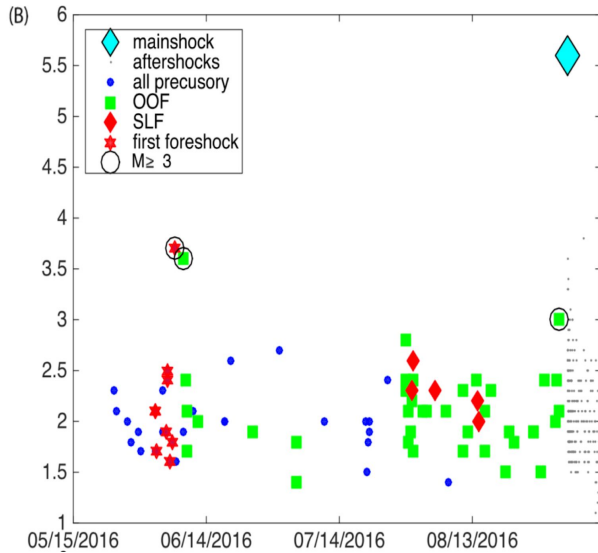


Figure 1. Timeline of Pawnee Earthquake Sequence 120 days period before the mainshock (Chen et al., 2017). Magnitude of located seismicity (refer to legend) and detected earthquake catalogues. OOF and SLF refers to the fault where earthquakes are located. Mainshock occurred on Sept. 2, 2016.

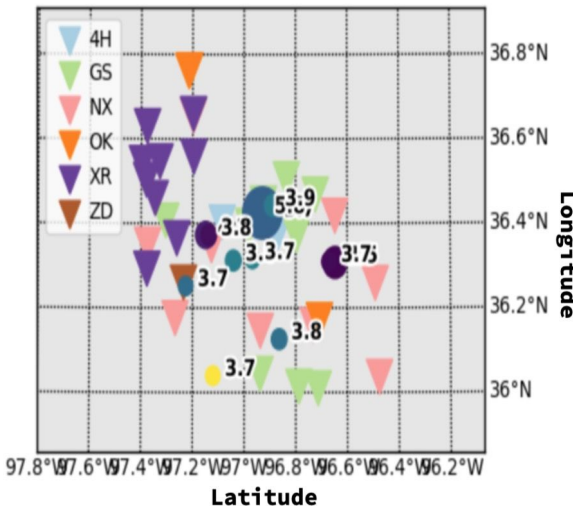
An important task in seismology is to compute the moment tensor of seismic event using seismic observations. Moment tensor solution can provide fundamental information on focal mechanisms and event magnitude of earthquakes. This study aims to conduct an updated analysis of moment tensor inversions for earthquakes source mechanisms in region nearby Pawnee that occurred from June 2016 to September 2016 by using general “Cut-and-Paste” (gCAP) method. Analyzing moment tensors for an ensemble of events would provide updated information about the inducing mechanisms, size, focal depth and orientation of fractures. Combining the moment tensor solution catalogue with wastewater injection parameters, we seek to better understand the nature of earthquake sequence occurred in Pawnee, Oklahoma. This constitutes an essential step in the industrial practice of seismic monitoring.

2 Data and Method

2.1 Seismic Data

Waveform data are requested from Incorporated Research Institution for Seismology (IRIS) web service via Obspy, a Python framework for processing seismological data. Seismic waveforms used in this study consists three-component recordings from stations of selected telemetered networks. The distribution of seismic stations ranging 30 km-300 km from epicenters shows a good azimuthal coverage around events of interest (Figure 2a). The requested seismic waveforms consist of three-component recording from AG, GM, GS, N4, NX, OK, PN, TA, TX, US, Y9 telemetered networks (Figure 2b).

a.)



b.)

1. AG: Arkansas Seismic Network
2. GS/GM: US Geological Survey Networks
3. N4: Central and Eastern US Networks
4. NX: Nanometric Research Networks
5. OK: Oklahoma Seismic Network
6. PN: PEPP-Indiana
7. TA: USArray Transportable Array
8. TX: Texas Seismological Network
9. US: United States National Seismic Network
10. XR: Seismicity near the Nemaha fault in northern Oklahoma
11. YW: IRIS Community Wavefield Experiment in Oklahoma
12. Y9: Rapid response for fairview aftershock in Oklahoma

Figure 2: a.) Distribution of seismograph stations (inverted colored triangles) of various networks, and epicenter of earthquakes (circles, with magnitudes). b.) Abbreviations of telemetered networks used in collecting waveform data.

Table 1: Catalogue of 4 events chosen for inversion.

Magnitude Catalogue (Mw)	Event Time (Date/Time)	Hypocenter depth (m)	Epicenter location [latitude, longitude]
3.6	2016-09-03 12:58:37.800000Z	6.162	+36.423, -96.909
5.8	2016-09-03 12:02:44.400000Z	5.557	+36.425, -96.929
3.6	2016-07-21 21:33:30.900000Z	10.354	+36.355, -97.091
3.9	2016-06-08 16:50:41.700000Z	6.632	+36.443, -96.888

Events selected for inversion are based on proximity to disposal wells and Pawnee main shock epicenter. In addition, the timeline in Figure 1 is also used as guide for selecting events' date. Careful screening process has been made to get rid of stations with poor recordings, usually due to instrument limitations. Example of poor recordings includes clipping, glitches and noises. Clipped waveforms, with high signal-to-noise ratios and missing high-amplitude data, have to be removed from the estimation of magnitudes and other earthquake properties. Screening ensures exclusion of poor stations in inversion process to yield better inversion results.

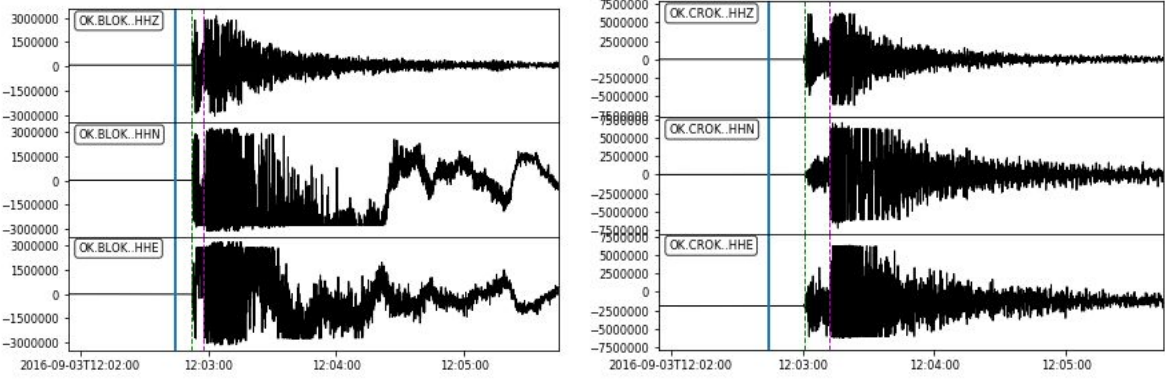


Figure 3: Examples of observational waveform on stations that exhibits glitches (left) and clipping (right).

2.2 Inversion Problem

Waveforms recorded at seismic stations consist of three components and can be written as:

$$W(t) = S(t) * G(t) * I(t).$$

where $S(t)$ represents source function, $G(t)$ represents Green's functions, and $I(t)$ represents instrument response. To retrieve source parameters for an earthquake event, it is necessary to deconvolve instrument response, $I(t)$ and Green's functions $G(t)$ from the actual observation, $W(t)$. After the waveform data are obtained, it is necessary for the instrument responses to be removed. Therefore, the waveform data is in displacement or in velocity, $u(t) = S(t) * G(t)$. The corresponding synthetic displacement $s(t)$ for a double-couple source is just a convolution product of source function, $S(t)$ and Green's function, $G(t)$. The synthetic displacement function can be written as:

$$s(t) = M \circ \sum A_i(\phi - \theta, \delta, \delta) G_i(t)$$

Where $G_i(t)$ are Green's functions, A_i are radiation coefficients (ϕ is station azimuth, θ , δ and δ represents strike, dip and rake respectively). $M \circ$ is scalar moment. Grid search is performed in all possible solutions of strike, dip, and rake to obtain the best fit by finding the minimal residual between the data and synthetics. Hence it is necessary to prepare process observational waveform data, compute Green's functions and derive focal mechanism solutions.

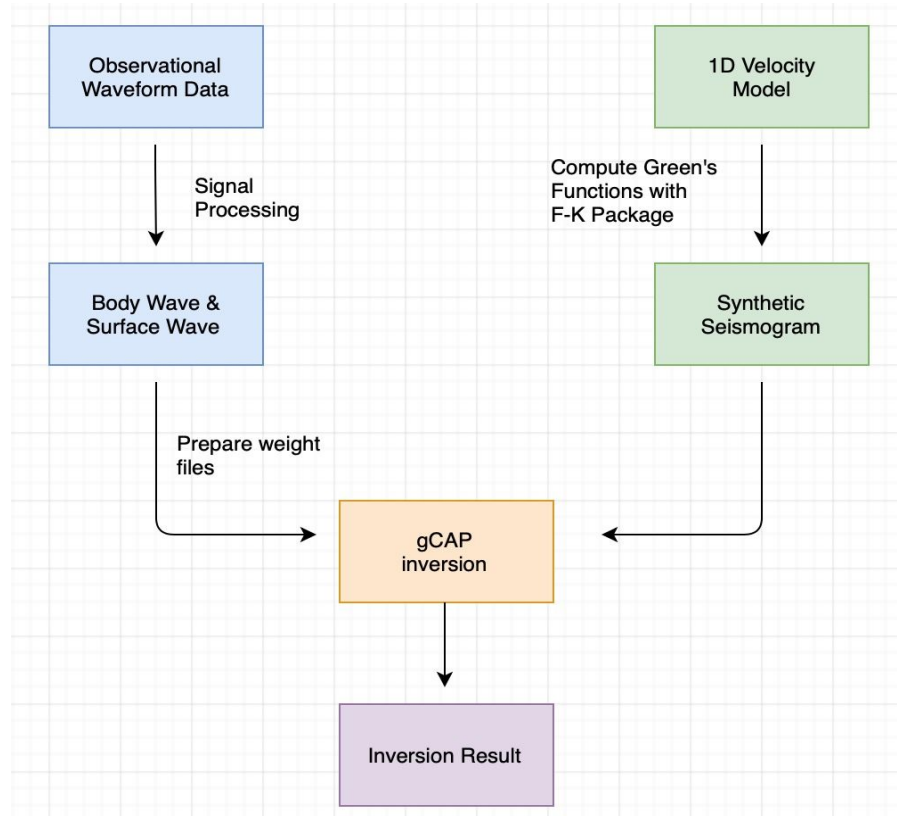


Figure 4: Flowchart shows the source mechanism inversion workflow structure.

2.3 Preparing Seismogram

Waveform data requested from IRIS web service requires signal processing. With built-in functions of Obspy, the instrument response of each seismic trace are removed. Instrument response often include full-response information by stage such as ground motion, sensor, digitizer, and any digital filtering. Removal of mean and linear trends in waveforms is also performed. Each seismic trace is processed into Seismic Analysis Code (SAC) format with correct header information including event latitude and longitude, station latitude and longitude. Reference time for each seismic trace are set at origin time of the event. The epicentral distance and azimuth headers are also set into the correct format. The unit of three-component seismograms velocity is converted from m/s into cm/s to produce meaningful magnitudes. Waveform at each station are cut into the equal length, and named as r, t, z for convention. The three component seismograms are rotated to the great circle.

2.4 Green's functions

In seismology, Green's functions is the theoretical response of a basic moment tensor component based on a velocity model. Each theoretical response of a basic moment tensor corresponds to a fundamental Green's function. Given a velocity model, synthetic seismograms can be constructed by summing up the weighted Green's functions for each basis moment tensor. Green's functions can be computed with Haskell propagator matrix FK

method, developed by Zhu and Rivera, 2002, with an assumed Earth structure . Green's functions, computed with FK package, are named ###.grn.[0-8] where ### represents distance. All Green's functions computed from one source depth are placed in a single directory named "chelsea_#", where chelsea represents name of 1-D velocity model and # represents the source depth in meters. The computed Green's functions are in SAC format with two time marks set: t1 for first P arrival and t2 for first S arrival. Green's functions for each stations are set with initial time headers to match with the event time of observational waveform.

In this study, an appropriate 1-D velocity model in Chelsea, Oklahoma has been chosen to compute Green's functions with FK package. The construction of Chelsea velocity model was based on seismic refraction (Mitchell and Landisman, 1970). The attenuation models (Qs and Qp) have been modified according to documentations specified in FK package. The final simplified 1-D velocity model represents a crustal structure with 4 velocity layers and with low velocity zone preserved in the study area.

T	Vp	Vp/Vs	rho	Qs	Qp
3.1	3.048	1.732	2.46	730	1460
23	3.677	1.732	2.81	1700	3400
20.2	4.168	1.732	3.08	1700	3400
0.0	4.723	1.732	3.39	1700	3400

Figure 5. The 1-D velocity model of Chelsea, Oklahoma in the format of thickness(km), P-wave velocity/S-wave velocity, Density(g/cm3), attenuation of Qs and Qp.

2.5 Generalized “Cut-and-Paste” method

The generalized “Cut-and-Paste” (gCAP) method was developed by Dr. Lupei Zhu and Dr. Helmberger to compute focal mechanism solutions. The seismic waveforms are first cut into Pnl window (two P-wave windows on the vertical and radial components) and surface wave window (all three surface wave components). The observational and synthetic waveforms generated from same set of parameters are fitted and cross-correlated. To optimize fitting for inversions, the Pnl and surface wave window are each filtered with different frequencies. In this study, the Pnl window has been filtered between 0.08 and 0.4 Hz with a 35-s-long window length, while the surface wave window is filtered between 0.05 and 0.10 Hz with a 70-s-long window length. Due to the potential inaccuracies inherent in assumed velocity model and epicenter location, gCAP allows synthetic waveforms to time-shift within an assigned range. This time shift allowance can improve cross-correlation coefficients and reduce effect of data inaccuracies. In this study, Pnl waves are allowed to shift within 2 seconds and surface waves are allowed to shift within 5 seconds. Amplitude of

synthetics waveforms (e.g Pnl/surface wave) can also be adjusted to increase the stability and resolution of focal mechanism solution.

The gCAP method requires a weight.dat file consists of station information and weights for each different time windows during inversion. The structure of weight.dat file can be formatted as: station_name distance w1 w2 w3 w4 w5 tp ts. To note, the distance (in format of dist.grn.?) shows the names of Green's functions to be used and w1 to w5 represents the weight for 5 segments of waveforms: PnlZ, PnlR, Z, R, T. In addition, tp represents first P arrival time and ts stands for initial time shift for surface waves (positive means data is delayed). It is also possible to turn off certain components by setting the corresponding weighting parameters (w1 to w5) to be 0. This could ensure reduction of potential data errors during inversion.

With the previously processed waveform data, FK computed Green's functions and weight.dat file, gCAP would perform a grid search of source mechanism parameters in specific search range and step size a shown in Table 2. This allows the assessment of the whole parameter space volume. Synthetic waveform and observation are then into five different 5 segment windows: PnlZ, PnlR, Z, R, T. The synthetic and observed waveform segment pairs will be fitted against one another. This process is continued for every station included in the inversion until a minimum misfit is found. The cross-correlation coefficient is calculated for the fitting of all segment pairs. To obtain best focal depth, the entire grid search process is repeated over 2km, 3km, 4km, 5km, 6km and 7km. The inversion results for different depths is compared and plotted on a misfit graph. The inversion result with minimum misfit represents the best-fit source mechanism solution.

Table 2 : Ranges and step sizes of each of the parameters used in inversion process.

Parameter	Range	Step size
Mw	[1,10]	0.1
Strike	[0,360]	1
Dip	[0,90]	1
Rake	[-180,180]	1
Depth	[2km,7km]	1km

3 Result

3.1 Inversion Result

Inversion result from September 3, 2016 Pawnee earthquake shows above-average waveform fitting between observational waveform and synthetic waveforms. The focal mechanism and moment magnitude of inversion are resulted from best-fitting solutions of each station's vertical Pnl waves (Pz), radial Pnl waves (Pr), vertical surface waves(Sz), radial surface waves (Sr) and transverse surface waves (Sh). This moment tensor solution can be displayed visually with a beach-ball diagram located on the upper left corner of sample output. Notice that Figure 5 only shows a portion of the inversion result. For complete inversion catalog, please refer to Appendix A.

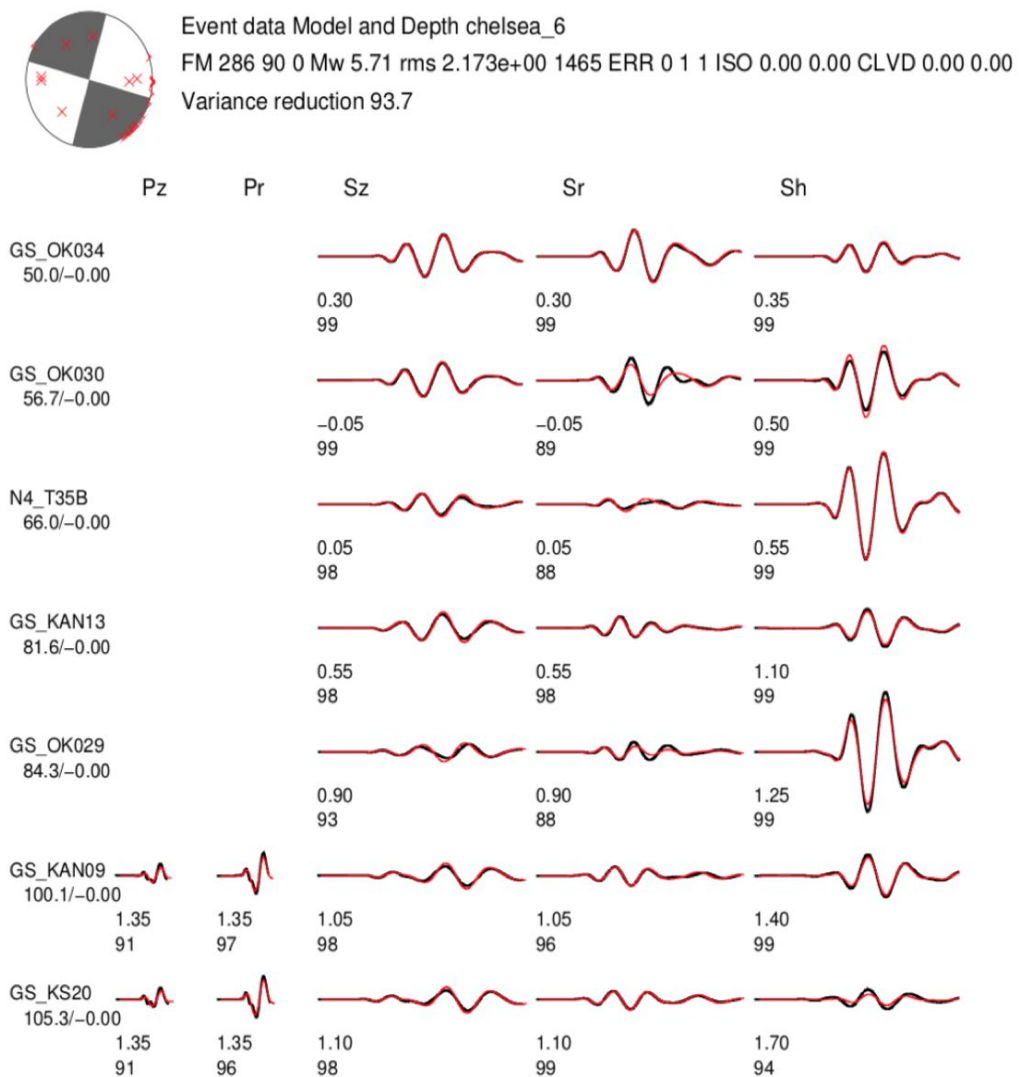


Figure 6: gCAP inversion result and waveform fits of the mainshock at source depth of 6km.

Stations are arranged by its epicentral distance, which is shown in km below the station name. Black traces are observed waveforms and red traces are predicted waveforms. The numbers below each waveform segment refers to the time shift in seconds (top), and waveform cross-correlation coefficient in percentage (bottom). Stations used in the inversion process are labelled as red dots on the beach ball on upper left corner. First line of inversion output in the format: Event data Model and Depth chelsea_6 FM 286 90 0 Mw 5.71 rms 2.173e+00 1465 ERR 0 1 1 ISO 0.00 0.00 CLVS 0.00 0.00. This means that the best-fit fault plane solution is strike 286, dip 90, and rake 0 degrees, with the axial lengths of the 1- σ error ellipsoid of 0, 1, and 1 degrees. The gCAP method also estimates the moment magnitude of mainshock event as Mw 5.71. The inversion results for other 3 events related to the Pawnee mainshock are shown in Figure 6.

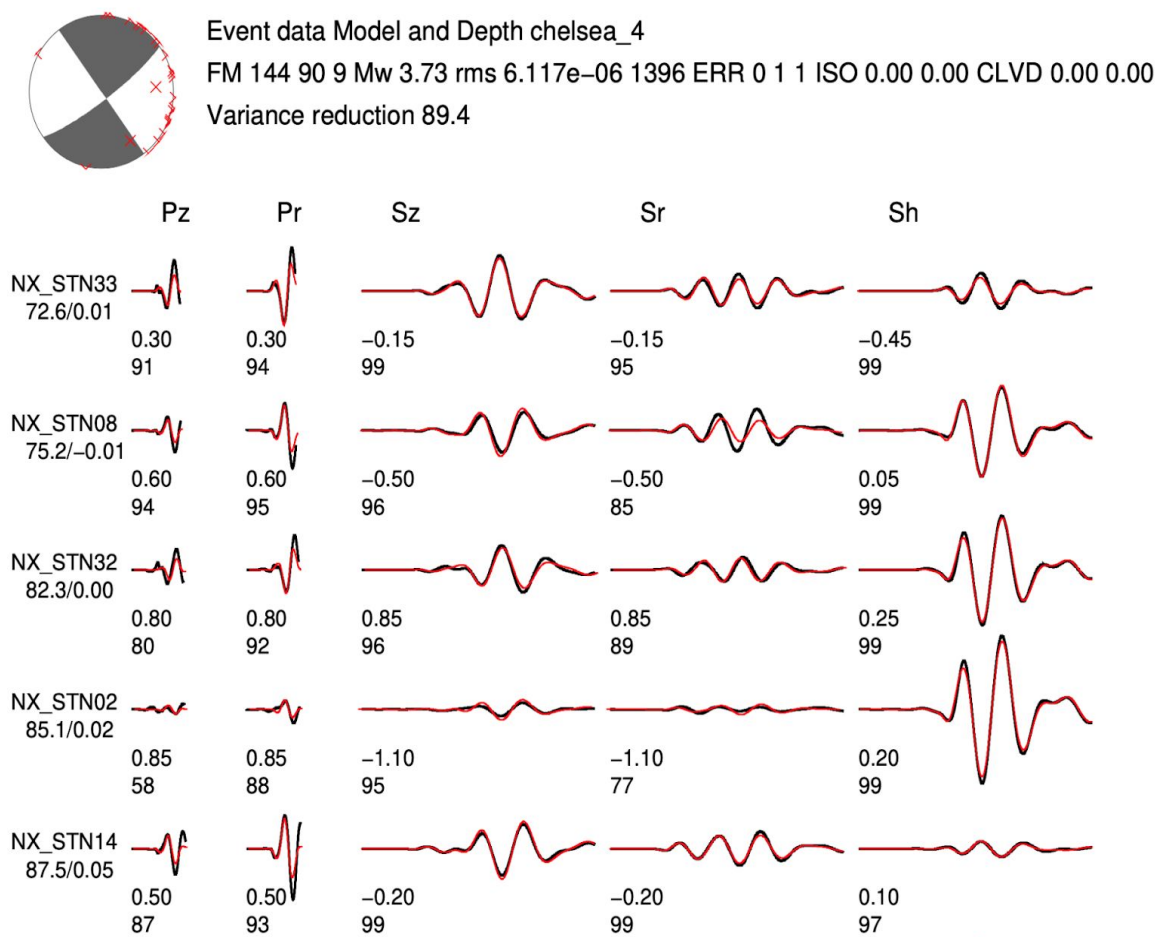


Figure 7. Sample inversion output for the event 2016-07-21T21:33:30.900000Z at depth 4 km.

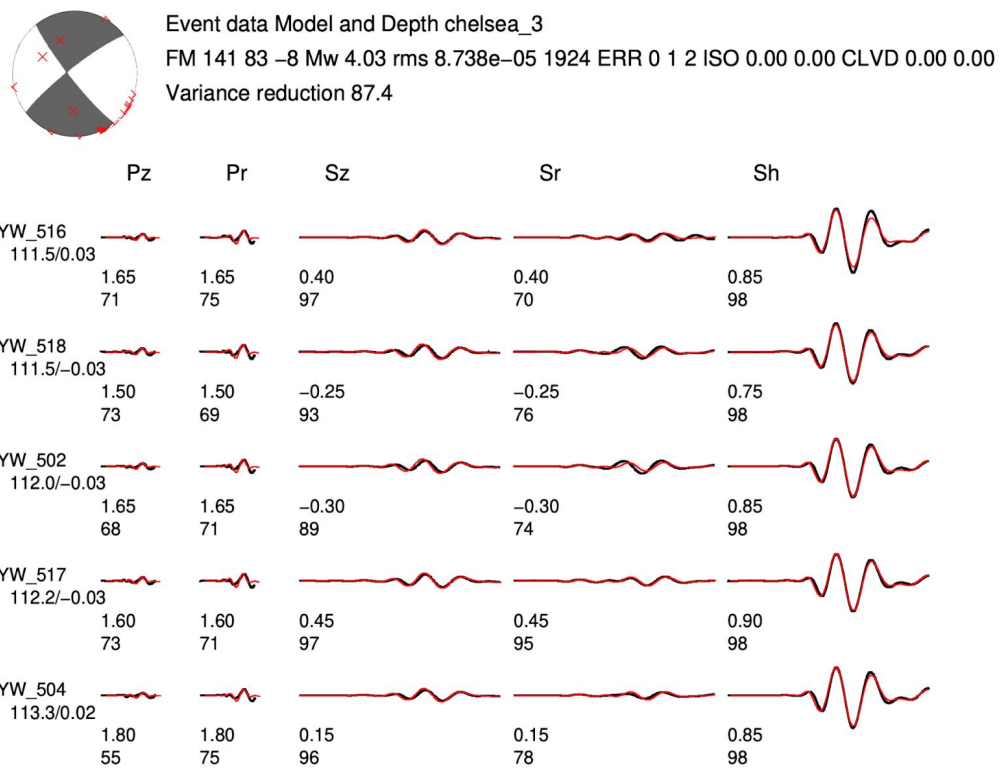


Figure 8. Sample inversion output for the event b.) 2016-06-08T16:50:41.700000Z at depth 3km.

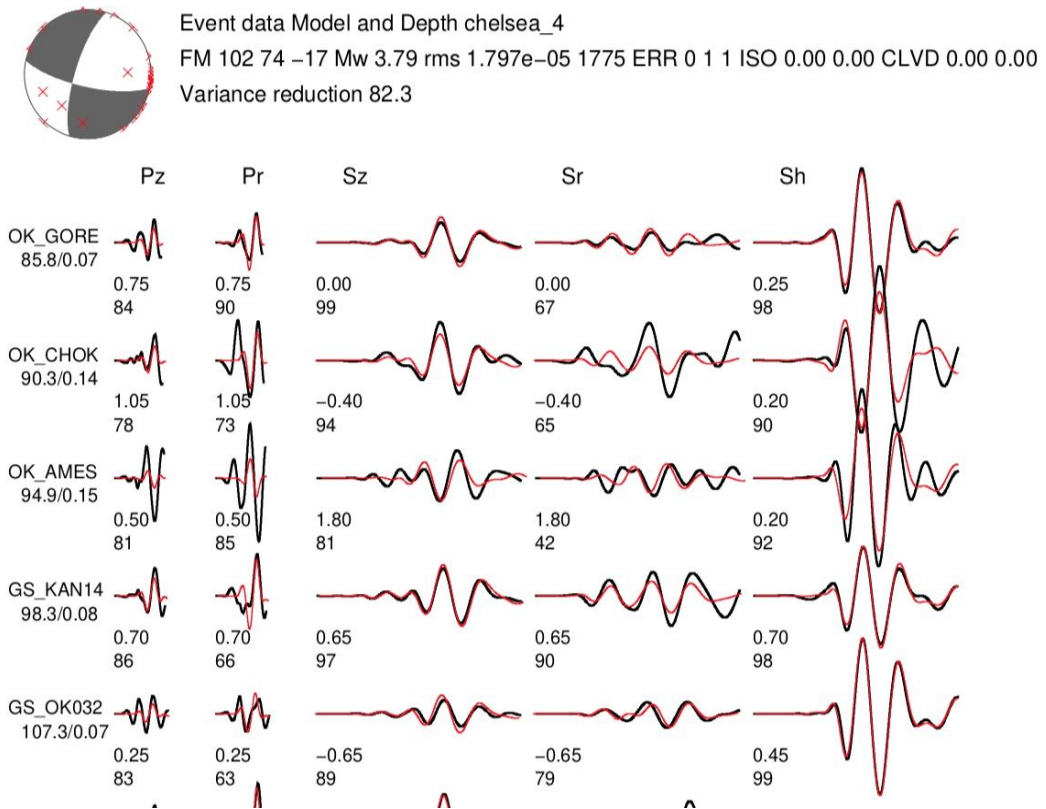


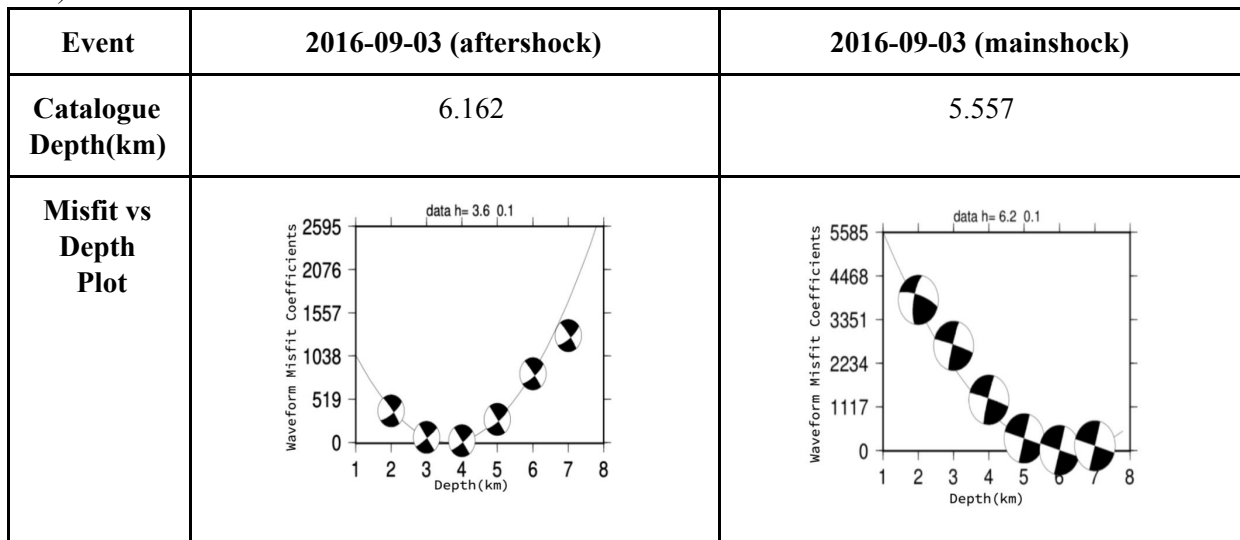
Figure 9 : Sample inversion output for the event 2016-09-03T12:58:37.800000Z 3.6 6.162 at depth 4 km.

3.2 Best Fit Focal Depth

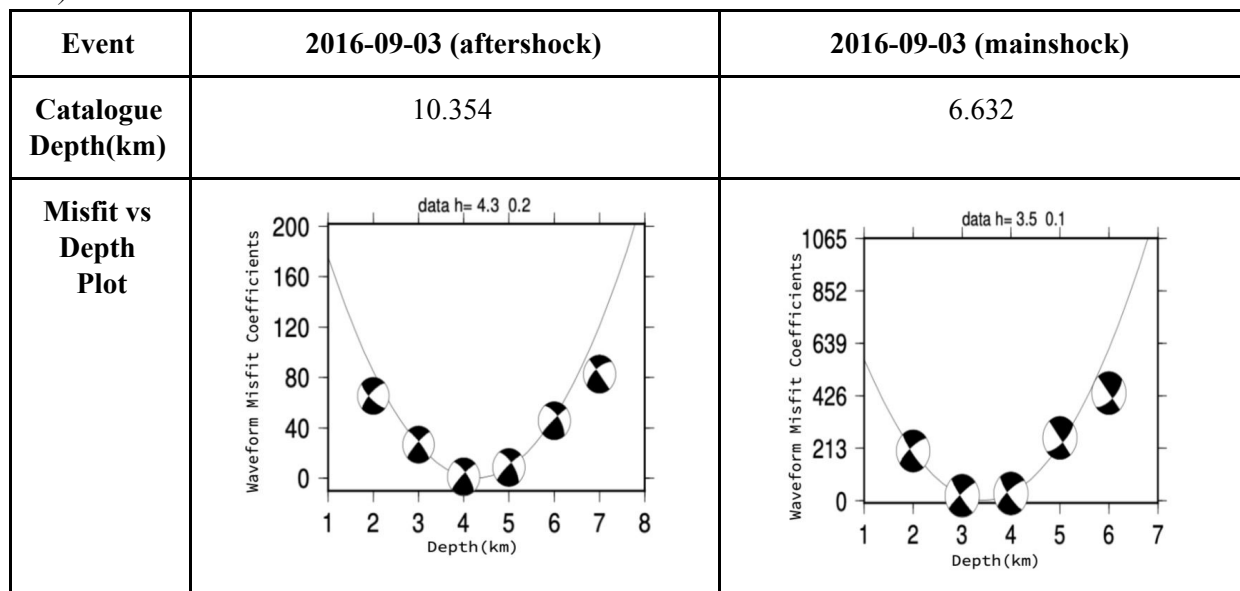
The inversion process is iterated over a number of different focal depths in order to obtain the best-fitting focal depth. The process is iterated from 2 km to 7km with a step size of 1 km. The six inversion results produces six focal mechanisms at different focal depths. Each inversion output is assigned which a variance reduction, which indicates the reliability of inversion result. The higher score of variance reduction indicates better inversion. To determine best-fitting focal depth, the inversion results at different focal depths are plotted on a misfit graphs. X-axis represents focal depths (in km), and Y-axis represents waveform misfit. The best-fit focal depths yielded from gCAP is compared against to the catalogue depth in Table 3.

Table 3 a & b: Summary of catalogue depths and best estimated focal depths with plots of waveform misfit coefficients (Y-axis) versus the centroid depth in km (X-axis) for 4 events.

a.)



b.)

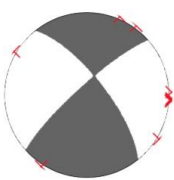
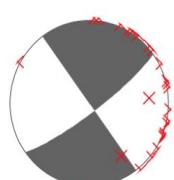


3.3 Moment Tensor Solution

Moment tensor solution mathematically describes the rupture source that produces the seismic waves in terms of fault plane orientation and its slipping direction. It usually takes at least 10 records and good azimuthal coverage of seismograph stations to produce a reasonable focal mechanism diagram. The faulting geometry is graphically represented by the beach-ball plot, a lower-hemisphere stereographic projection surrounding the earthquake source. Each beach ball would produce two candidate nodal planes. The fault plane responsible for the earthquake will be parallel to one of the nodal planes. The other nodal plane, known as auxiliary plane, is orthogonal to the fault plane. The two candidate nodal planes can generate the same waveforms as observed; however only one of the two planes is responsible for generating the earthquake. The two nodal planes separating opposite quadrants are filled with black (compressional quadrants) and white (dilatational quadrants).

Analysis of several focal mechanism solutions suggest thrust mechanism with the primary fault plane are either NW-SE or NE-SW. To differentiate the fault plane from auxiliary plane, it is necessary to look into other geological or geophysical evidences. The beach balls, at best-fitting focal depth, for each event are summarized in Table 4.

Table 4 : Detailed summary of inversion results for 4 events analyzed in this study.

Focal Mechanisms Solution				
Event (Day/Time)	2016-09-03 12:58:37	2016-09-03 12:02:44	2016-07-21 21:33:30	2016-06-08 16:50:41
Plane solution (strike/dip/rake)	321/72/10	286/90/0	144/90/09	141/83/-8
Catalogue magnitude (Mw)	3.6	5.8	3.6	3.9
Estimated magnitude (Mw)	3.79	5.71	3.73	4.03
Variance reduction	82.3	93.7	89.4	87.4

4 Discussion

The gCAP method can reduce uncertainties from velocity structures by separating the entire seismograms into Pnl and surface wave segments and allowing for relative time shift between them. Close stations with epicentral distances less than 100 km are excluded so that the point-source approximation used in the inversion is valid. Estimated centroid depth of the mainshock is noted similar to the catalogue depth; however, for smaller-magnitude events, the centroid depths are likely to be underestimated. This maybe due to inaccuracies inherent in velocity model. The moments magnitude estimated with gCAP method is consistent to that of catalogue, differs at most only by 0.2Mw. In this study, reliable inversion results are obtained with high correlation coefficients between observational and synthetics. It is also noted that events analyzed in this study have similar focal mechanism to each other, indicating likelihood of originating from same fault plane.

Moment tensor solutions of all events analyzed in this study suggests a strike-slip mechanism with almost-vertical nodal planes. To distinguish the fault plane from auxiliary plane, understanding of local geological features is required. The Pawnee earthquake sequence occurred within a conjugate fault system (Figure 8) that consists Sooner Lake Fault (SLF), segment of Labette Fault (OOF) and Watchorn Fault. The intersection of multiple fault trends is known as Pawnee Triple Junction, where the mainshock ruptured (Chen et al., 2017). One of the fault planes is noted to have similar geometry to our west-northwest oriented nodal plane. This fault, known as Sooner Lake fault, is a left-lateral almost-vertical fault striking west-northwestward. In addition, the catalogue shows the 4 events analyzed in the study are located along this fault. Several disposal wells are also noted nearby the area (Figure 8).

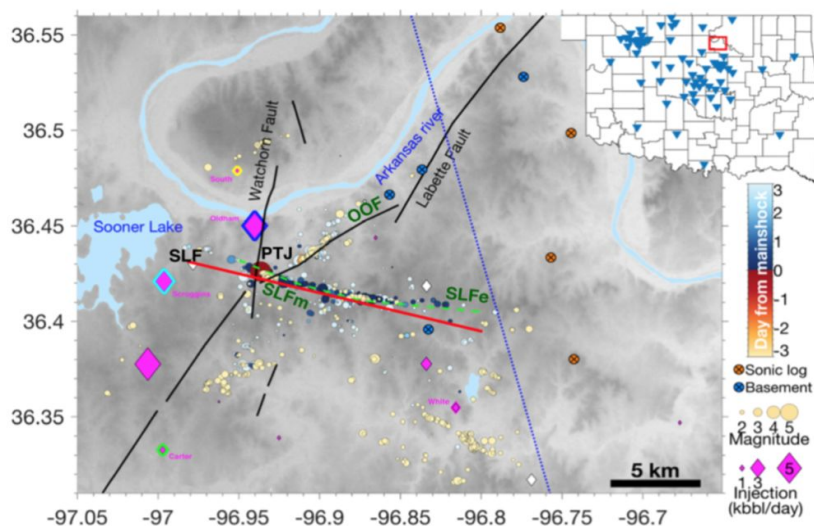


Figure 10: Map view of Pawnee earthquake region. Pink diamonds refer to disposal wells scaled by averaged injection volume since 2015. White diamonds refer to inactive disposal wells. Green dashed line shows segments of Sooner Lake Fault. Black lines refers to previously mapped faults by Oklahoma Geological Survey. PTJ is abbreviated as Pawnee Triple Junction, an intersection of multiple fault trends. Red line shows segments segments of Sooner Lake Fault.

Injection often took place at depth of 1–2 km within the Arbuckle sediment layer, while most of the earthquakes occurred in the deeper crystalline basement (Figure 9b) . Active wastewater injection in close proximity to the conjugate fault system may have reduced effective stress and caused the reactivation of pre-existing faults in the crystalline basement. Small amplitude fluctuation in injection rate within 10km from mainshock epicenter has been reported since May 2016. Subsequently, two peaks in seismicity rate correspond to the two M3.5+ earthquakes 100 days before and two swarms 40 days before the Pawnee M5.8 event have been detected. Rapid response to small fluctuations in injection rates indicates that the conjugate fault system is sensitive to small stress perturbations prior to mainshock rupture (Chen et al., 2017). This suggests that the foreshocks, leading up to mainshock rupture, are likely related to injection.

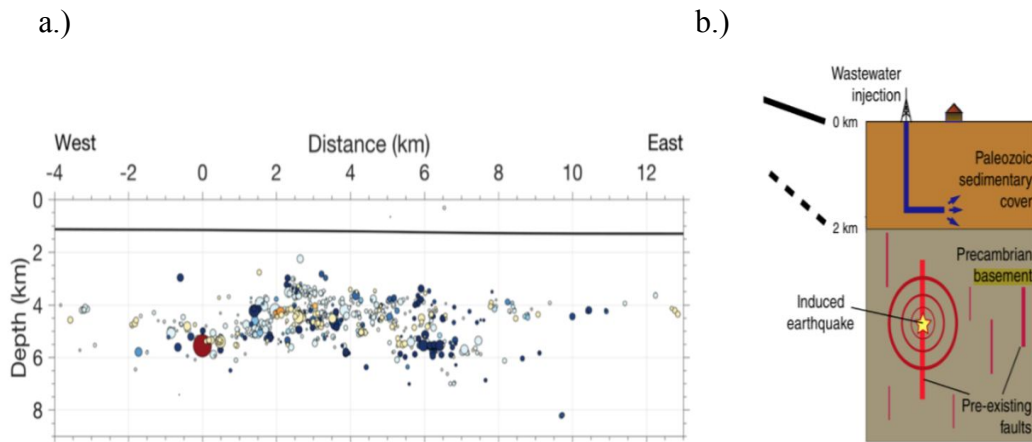


Figure 11: a.) Cross-section view of Sooner Lake Fault segment. Mainshock is denoted as red circle and located at distance 0. Rest of earthquake events are shown in other colored balls. The black line represents the boundary between Arbuckle Group and basement (Chen et al., 2017) . b.) Illustration of wastewater injection depth and possible existing faults buried in depth greater than 2km (Grandin et al., 2017).

Recent study shows that the M5.8 accounts for nearly all of the accumulated moment related to wastewater injection (McGarr et al., 2017). Hence, Pawnee M5.8 mainshock may be caused by destabilization of fault 3–4 km below the depth range where injection took place (Figure 9b). Triggering process of Pawnee earthquake may also be due to precursory seismic slips on the same fault plane within the conjugate fault system.(Chen et al., 2017). Combining fault plane solutions for analyzed events and injection parameters, it is very likely that the Pawnee sequence was a result of left-lateral slip across Sooner Lake Fault induced by wastewater injection. This mechanism has been suggested for characterizing the previously unmapped Sooner Lake Fault. (McGarr et al., 2017).

Conclusion

The main purpose of this study is to present updated source mechanism solutions for earthquakes source mechanisms in region nearby Pawnee that occurred from June 2016 to September 2016 by using general “Cut-and-Paste” (gCAP) method. With observational and synthetic waveforms, our inversion results indicates the Pawnee sequence is dominated by a left-lateral strike-slip mechanism. The moment tensor solutions and location of this earthquake sequence suggest activation of NW-SE striking and vertically dipping Sooner Lake Fault. Accurate estimation of source mechanisms are keys for providing insights about fracture behaviors, which is important for microseismic monitoring of hydraulic fracturing operations.

Acknowledgement

Earthquake waveforms are provided by GM, GS, N4, NX, OK, TA, US, Y9 stations and downloaded from IRIS web service through Obspy. Green's functions were computed with FK software package developed by Dr. Lupei Zhu and Rivera. Source mechanism inversion was obtained with gCAP software package developed by Dr. Lupei Zhu and Helmberger. Disposal well data are obtained from Oklahoma Corporation Commission (OCC) and Environmental Protection Agency (EPA). I thank supervisor Dr. Qinya Liu for her invaluable scientific guidance, Yiru Zhou and Chuangxin Lin for their technical help.

References

Andrews, R.D., 2007, Stratigraphy, production, and reservoir characteristics of the Caney Shale in southern Oklahoma: Shale Shaker 58, 9-25.

Chen, X., Nakata, N., Pennington. C, Haffener. J, Chang. J.C, He. X, Zhan. Z, Ni.S & Walter. J (2017) The Pawnee Earthquake as a result of interplay among injection, faults and foreshocks, Nature,Scientific Report 7, 4945

Darold. A.P, Holland A.A, Jennifer K.M., Gibson A.R. (2015). Oklahoma Earthquake Summary Report 2014. Oklahoma Geological Survey OF1 – 2015

Fielding. E.J, Sangha. S.S, Bakaert. D.P.S., Samsonov S.V., Chang. J.C. (2017) Surface Deformation of North-Central Oklahoma Related to the 2016 Mw 5.8 Pawnee Earthquake from SAR Interferometry Time Series. Seismological Research Letters, vol-8, no-4, doi: 10.1785/0220170010

Elebiju, O. O., Matson, S., Randy Keller, G. & Marfurt, K. J. (2011). Integrated geophysical studies of the basement structures, the Mississippi chert, and the Arbuckle Group of Osage County region, Oklahoma. *AAPG Bulletin* **95**, 371–393

Grandin, R., Vallee, M., Lacassin, R., (2017) Rupture Process of the Mw 5.8 Pawnee Oklahoma, Earthquake from Sentinel-1 InSAR and Seismological Data. *Seismological Research Letters* 88(4), 994 – 1004

Hincks, T., Aspinall, W., Cooke, R., Gernon, T. (2018) Oklahoma's induced seismicity strongly linked to wastewater injection depth. *Science* 362(6415).

Holland A. (August 2011) Examination of Possibly Induced Seismicity from Hydraulic Fracturing in the Eola Field, Garvin Country, Oklahoma. Oklahoma Geological Survey. Open-file report, OF1-2011.

Holland, A. A. Preliminary fault map of Oklahoma.(2015). *Oklahoma Geological Survey Open File Report OF3–2015*

Keranen, K.M., Weingarten, M., Abers, G., Bekins, B., and Ge. S., (2014). Sharp increase in central Oklahoma seismicity since 2008 induced by massive wastewater injection 345, 448–451.

Llenos, A. L. & Michael, A. (2013). Modeling Earthquake Rate Changes in Oklahoma and Arkansas: Possible Signatures of Induced Seismicity. *Bull. Seismol. Soc. Am.* 103, 2850–2861.

McGarr, A., B. Bekins, N. Burkardt, J. Dewey, P. Earle, W. Ellsworth, S. Ge, S. Hickman, A. Holland, E. Majer, J. Rubinstein, and A. Shee-han (2015). Coping with earthquakes induced by fluid injection, *Science* 347, 6224, 830–831, doi: 10.1126/science.aaa0494.

McGarr, A., Barbour, A.J. (2017). Wastewater Disposal and Earthquake Sequences During 2016 near Fairview, Pawnee, and Cushing Oklahoma. *Geophysical Research Letters*, 10.1002 /2017GLO75258, 9330-9336

Mitchell, B.J. and M. Landisman, 1970, Interpretation of a Crustal Section across Oklahoma, *Geol. Soc. Amer. Bul* 81(9), p. 2647-2656.

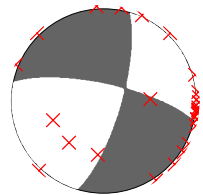
Raleigh, B. C., Healy, J. H. & Bredehoeft, J. D.(1976). An experiment in earthquake control at Rangely, Colorado. *Science* .

- Rubinstein, J.L. and Mahani, A.B. (August 2015). Myths and Facts on Waste Water Injection, Hydraulic Fracturing, Enhanced Oil Recovery, and Induced Seismicity. *Seismological Research Letters* 84(4), 1-8
- Segall, P. & Lu, S. Injection-induced seismicity: Poroelastic and earthquake nucleation effects. *Journal of Geophysical Research: Solid Earth* 120, 1–22 (2015).
- Shapiro, S. A., Rothert, E., Rath, V. & Rindschwentner J. (2002). Characterization of fluid transport properties of reservoirs using induced microseismicity. *Geophysics* 67, 212–220.
- Walsh, F. R. & Zoback, M. D. (2015). Oklahoma's recent earthquakes and saltwater disposal. *Science Advances* 1, 1–9
- Walters, R., M. Zoback, J. Baker, and G. Beroza (2015). Characterizing and responding to seismic risk associated with earthquakes potentially triggered by saltwater disposal and hydraulic fracturing, *Seis- mol. Res. Lett.* 86, no. 4, doi: 10.1785/0220150048.
- Walter, J. I., Chang, J. C., & Dotray, P (2017).. Foreshock seismicity suggests gradual differential stress increase in the months prior to the 3 September 2016 Mw 5.8 Pawnee earthquake. *Seismol. Res. Lett.*, *in press* doi:[10.1785/0220170007](https://doi.org/10.1785/0220170007)
- Zhu, L., & Helmberger, D. V. (1996). Advancement in source estimation techniques using broadband regional seismograms. *Bulletin of the Seismological Society of America* 86(5), 1634-1641.
- Zhu, L. & Rivera, L., 2002. A note on the dynamic and static displacements from a point source in multi-layered media, *Geophys. J. Int.* 148, 619–627.

Appendix

A. Full Inversion Results For Event on 2016-06-08

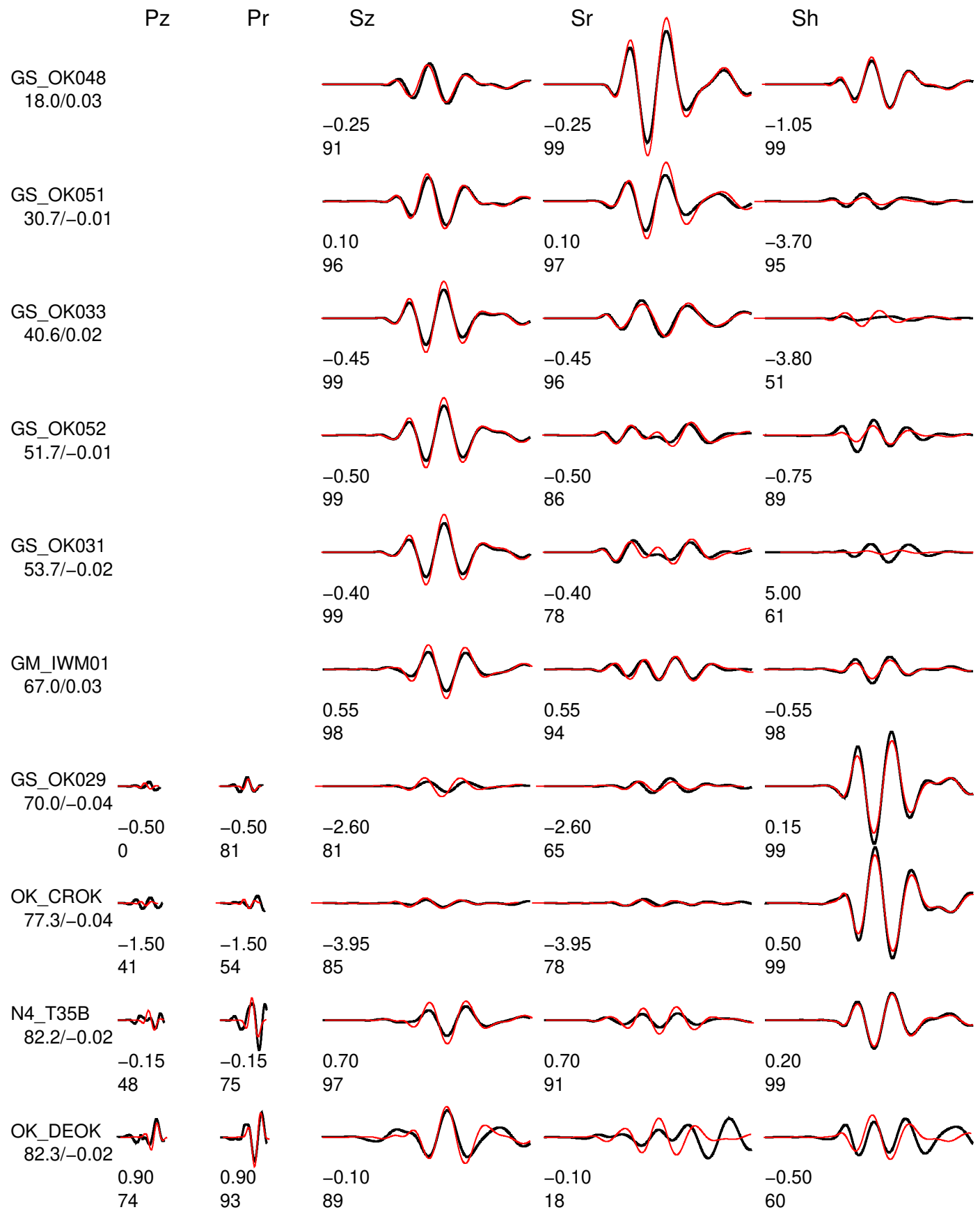
A.1 Inversion Result at depth of 2km

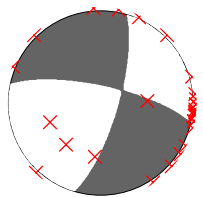


Event data Model and Depth chelsea_2

FM 282 75 -16 Mw 3.75 rms 1.902e-05 1776 ERR 0 1 2 ISO 0.00 0.00 CLVD 0.00 0.00

Variance reduction 81.3

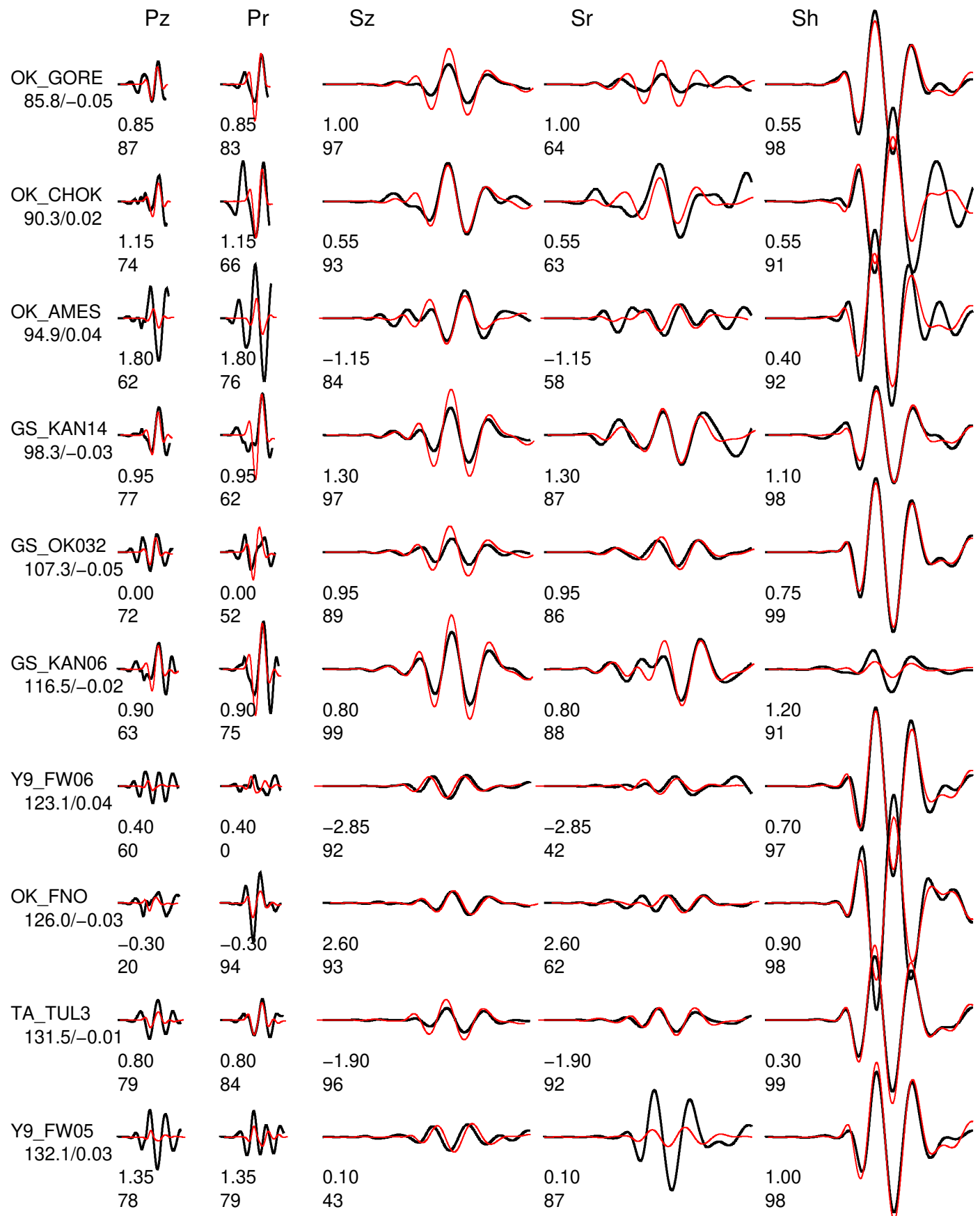


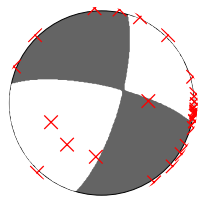


Event data Model and Depth chelsea_2

FM 282 75 -16 Mw 3.75 rms 1.902e-05 1776 ERR 0 1 2 ISO 0.00 0.00 CLVD 0.00 0.00

Variance reduction 81.3

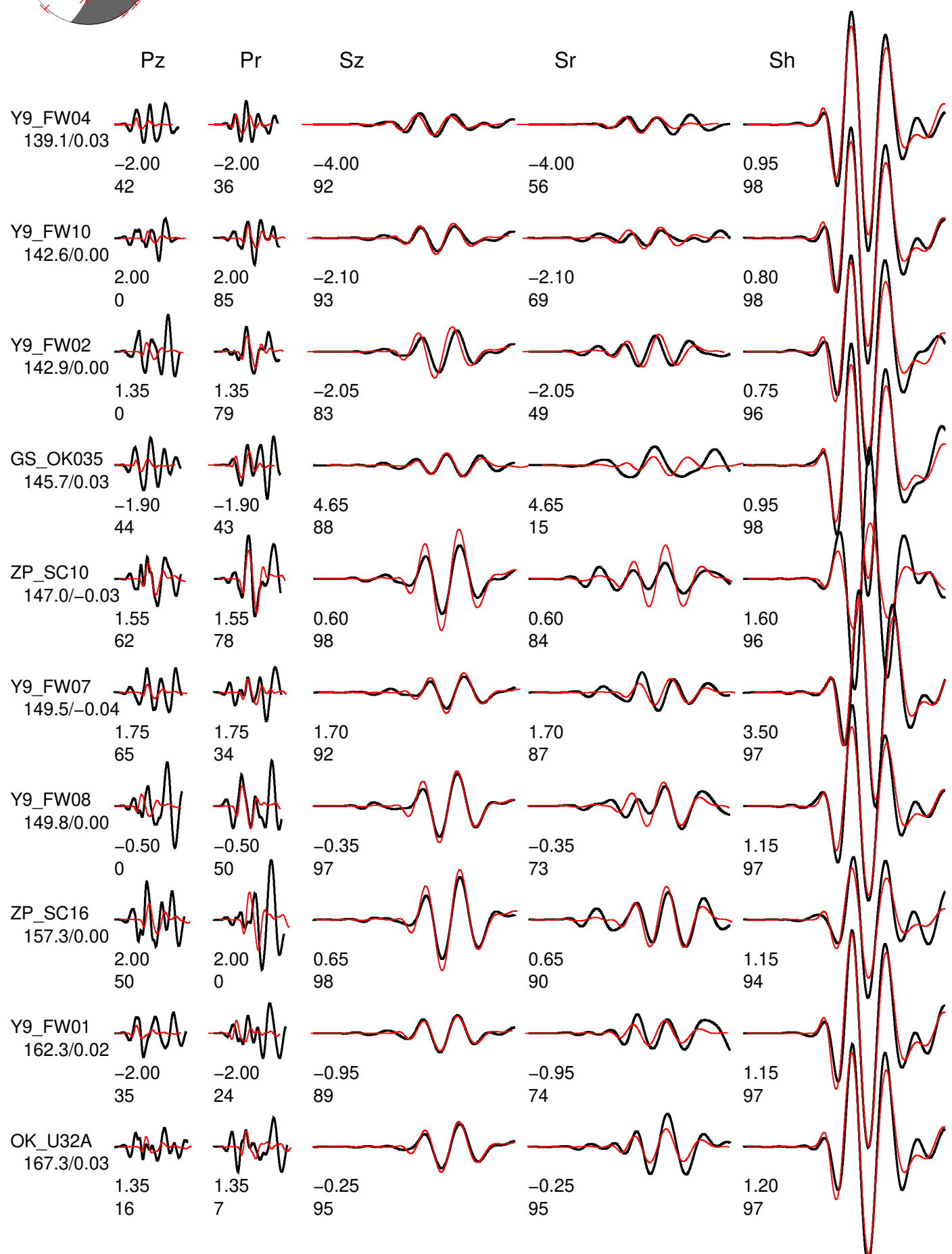


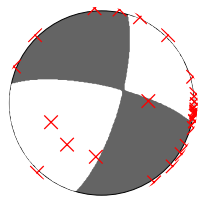


Event data Model and Depth chelsea_2

FM 282 75 –16 Mw 3.75 rms 1.902e-05 1776 ERR 0 1 2 ISO 0.00 0.00 CLVD 0.00 0.00

Variance reduction 81.3

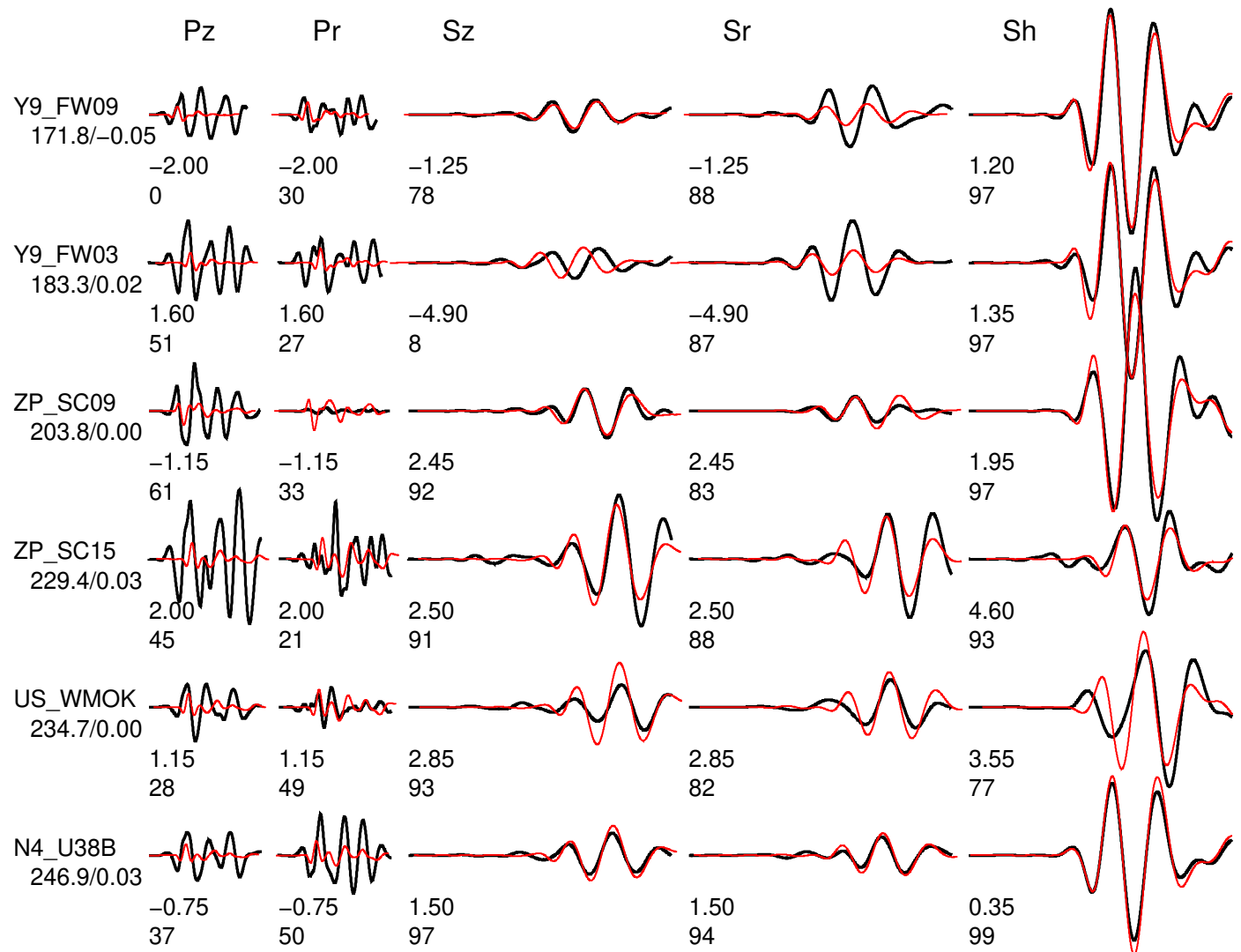




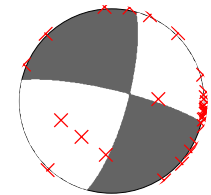
Event data Model and Depth chelsea_2

FM 282 75 –16 Mw 3.75 rms 1.902e-05 1776 ERR 0 1 2 ISO 0.00 0.00 CLVD 0.00 0.00

Variance reduction 81.3



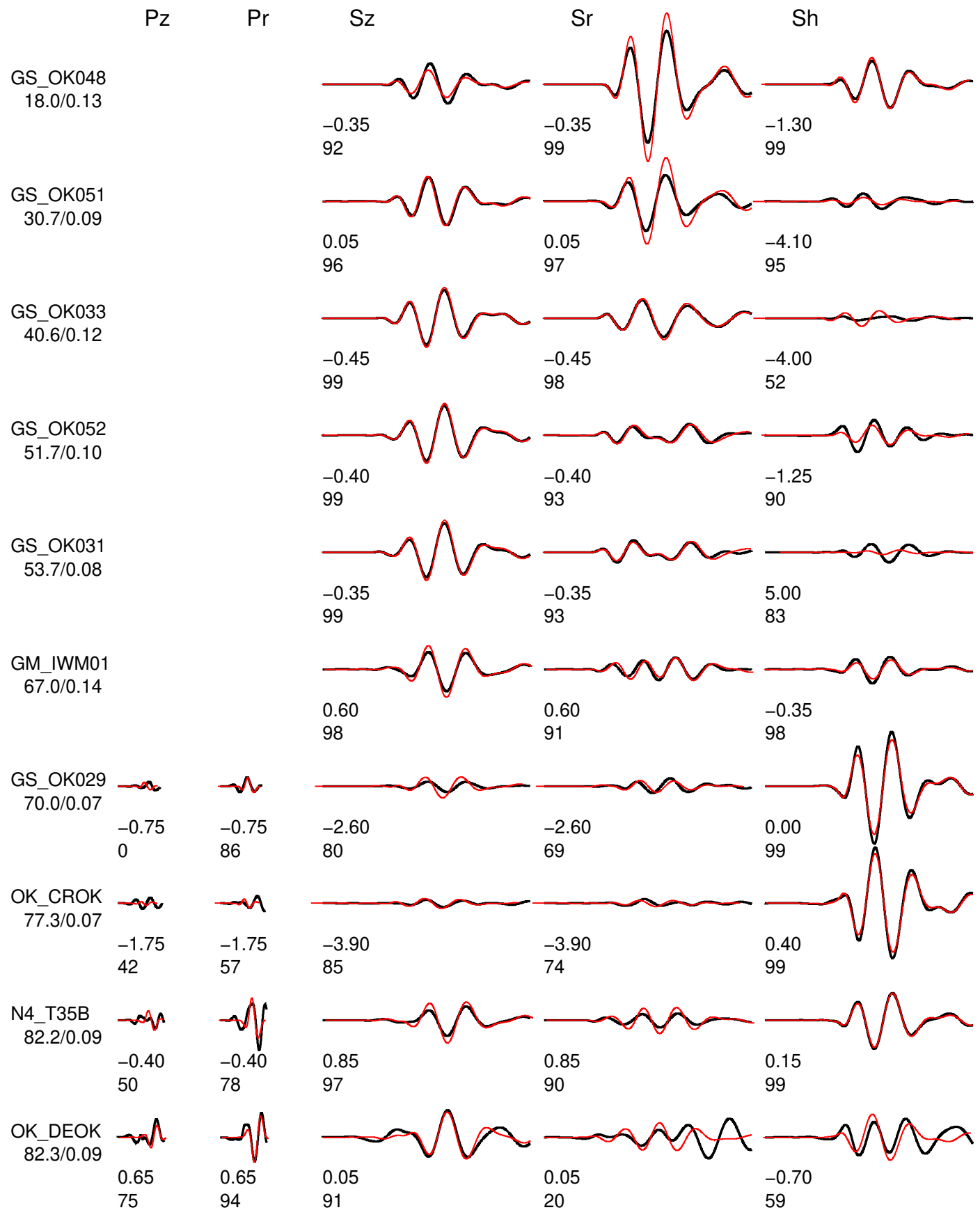
A.2 Inversion Result at depth of 3km

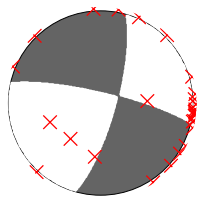


Event data Model and Depth chelsea_3

FM 283 80 -14 Mw 3.76 rms 1.826e-05 1775 ERR 0 1 2 ISO 0.00 0.00 CLVD 0.00 0.00

Variance reduction 82.0

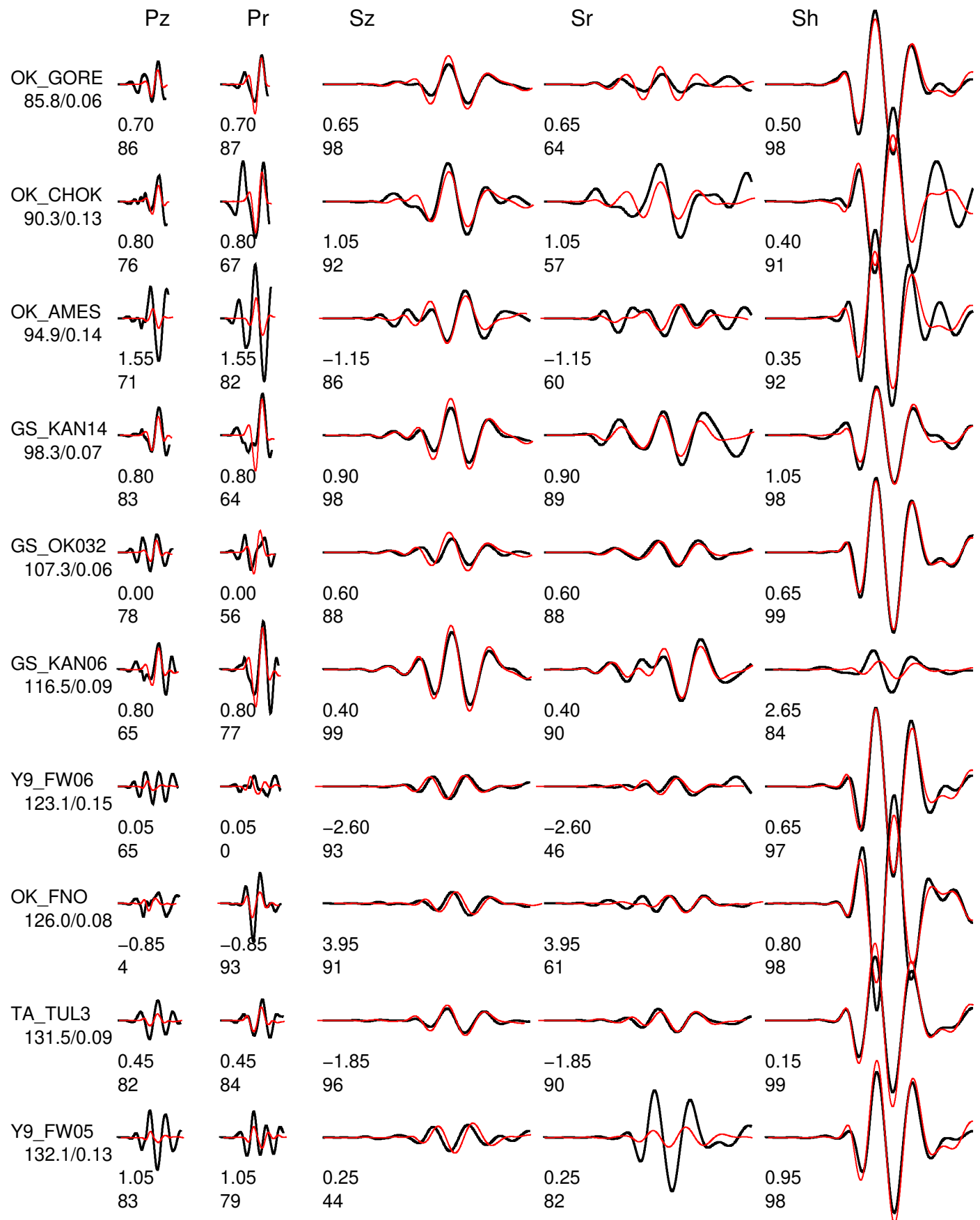


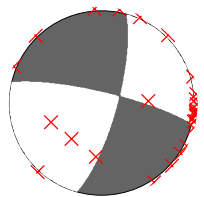


Event data Model and Depth chelsea_3

FM 283 80 -14 Mw 3.76 rms 1.826e-05 1775 ERR 0 1 2 ISO 0.00 0.00 CLVD 0.00 0.00

Variance reduction 82.0

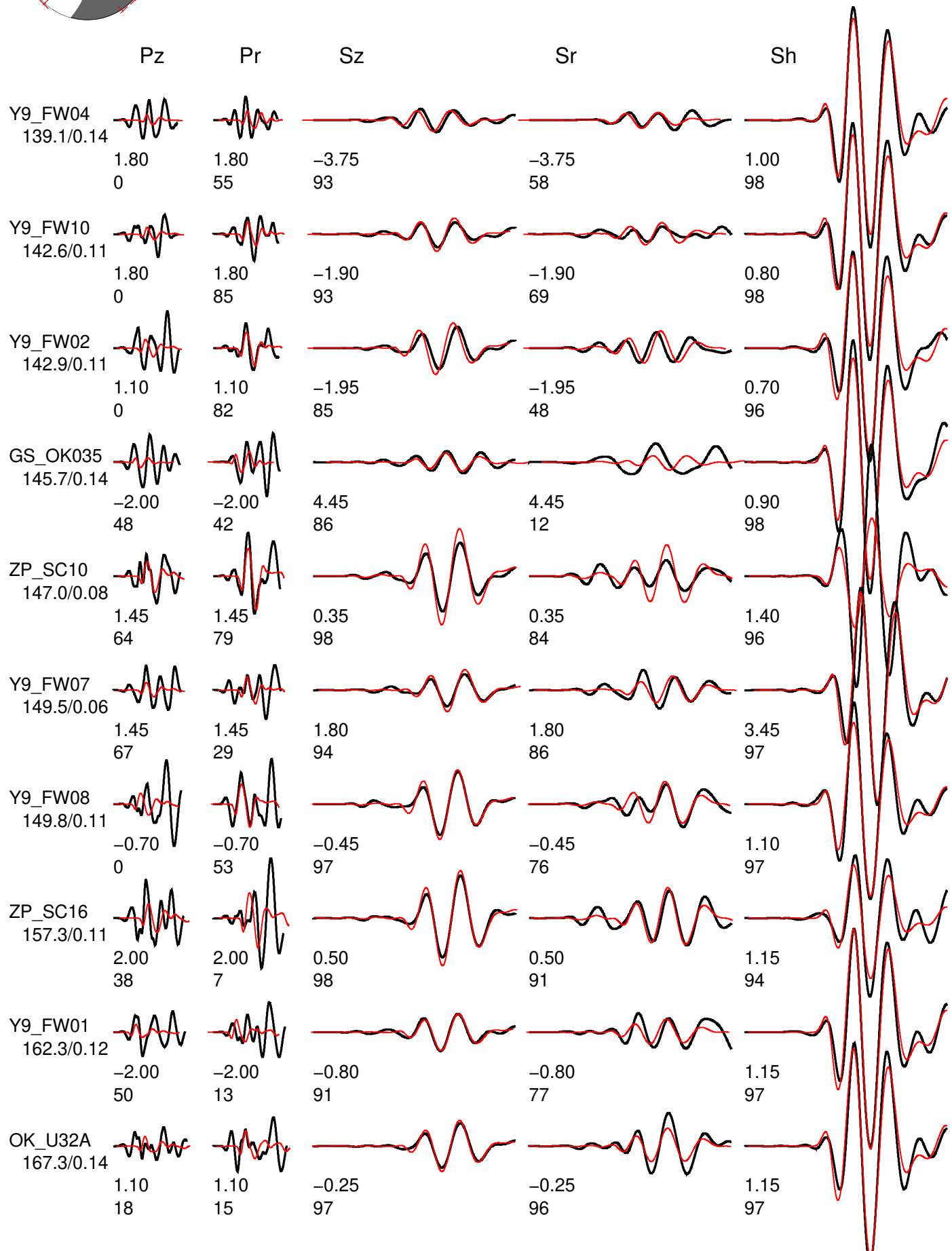


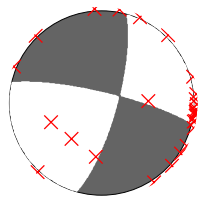


Event data Model and Depth chelsea_3

FM 283 80 -14 Mw 3.76 rms 1.826e-05 1775 ERR 0 1 2 ISO 0.00 0.00 CLVD 0.00 0.00

Variance reduction 82.0

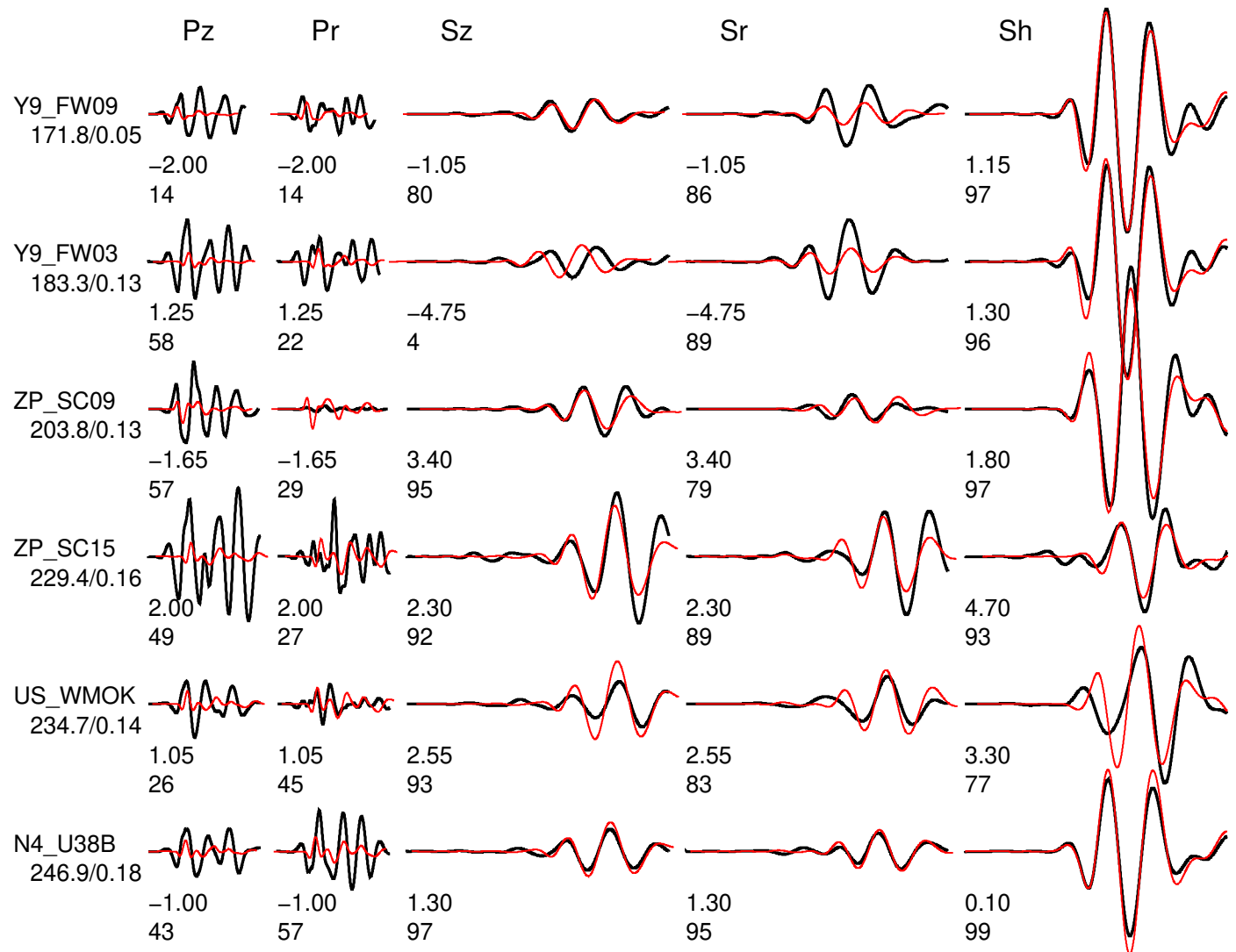




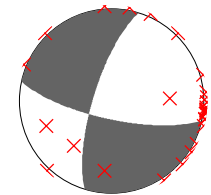
Event data Model and Depth chelsea_3

FM 283 80 -14 Mw 3.76 rms 1.826e-05 1775 ERR 0 1 2 ISO 0.00 0.00 CLVD 0.00 0.00

Variance reduction 82.0



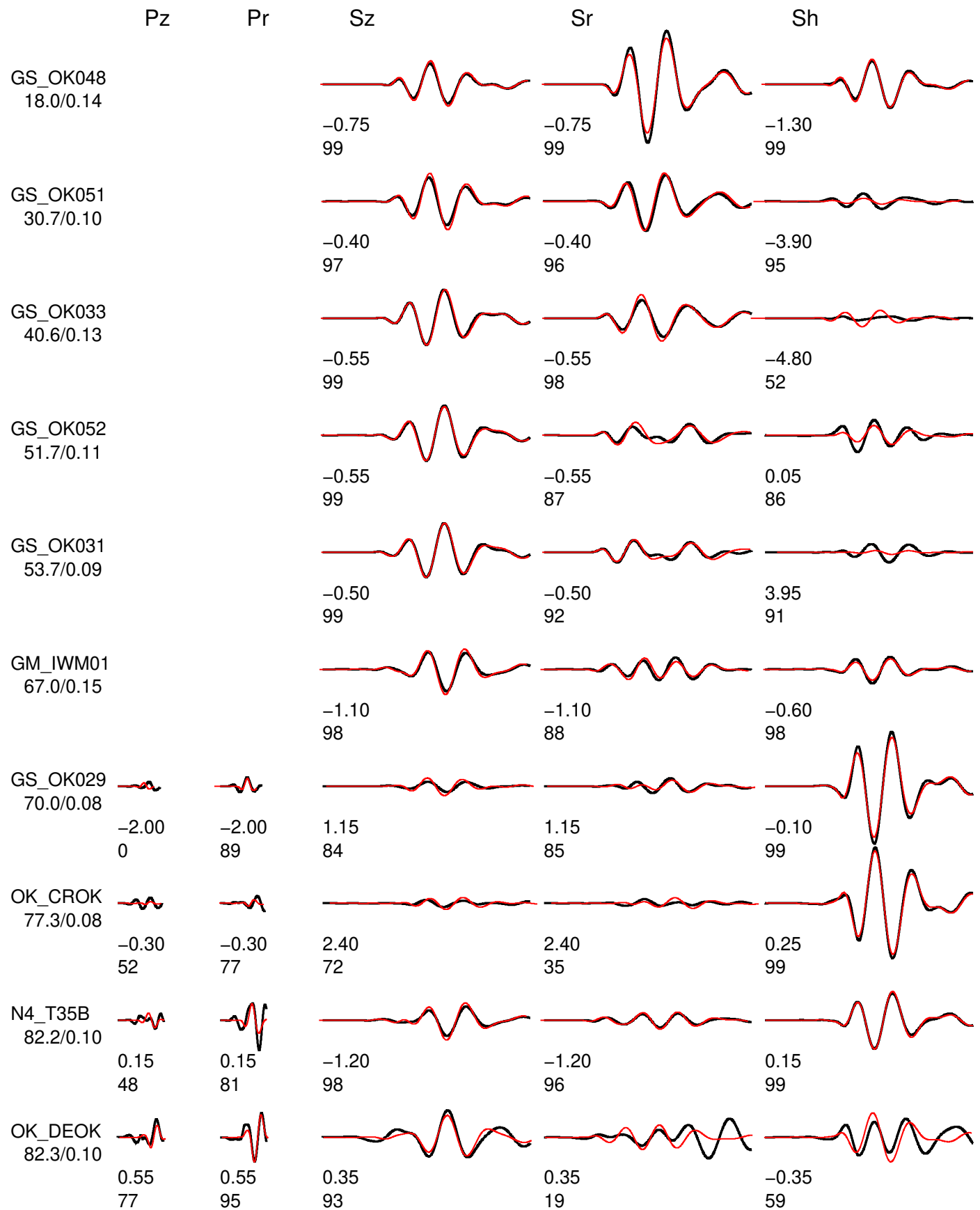
A.3 Inversion Result at depth of 4km

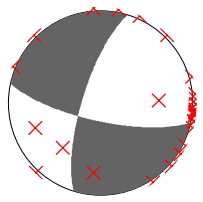


Event data Model and Depth chelsea_4

FM 102 74 -17 Mw 3.79 rms 1.797e-05 1775 ERR 0 1 1 ISO 0.00 0.00 CLVD 0.00 0.00

Variance reduction 82.3

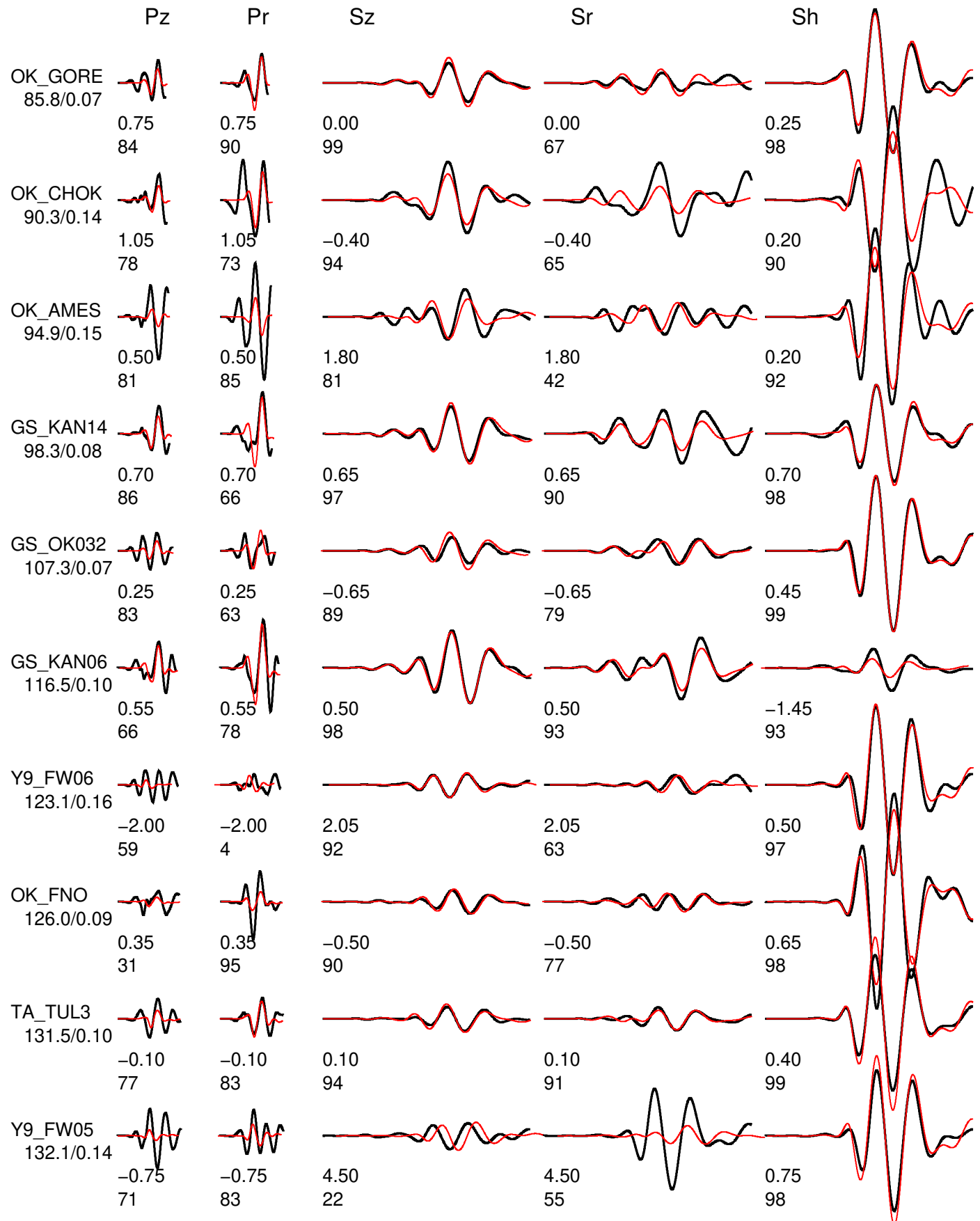


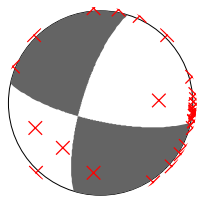


Event data Model and Depth chelsea_4

FM 102 74 -17 Mw 3.79 rms 1.797e-05 1775 ERR 0 1 1 ISO 0.00 0.00 CLVD 0.00 0.00

Variance reduction 82.3

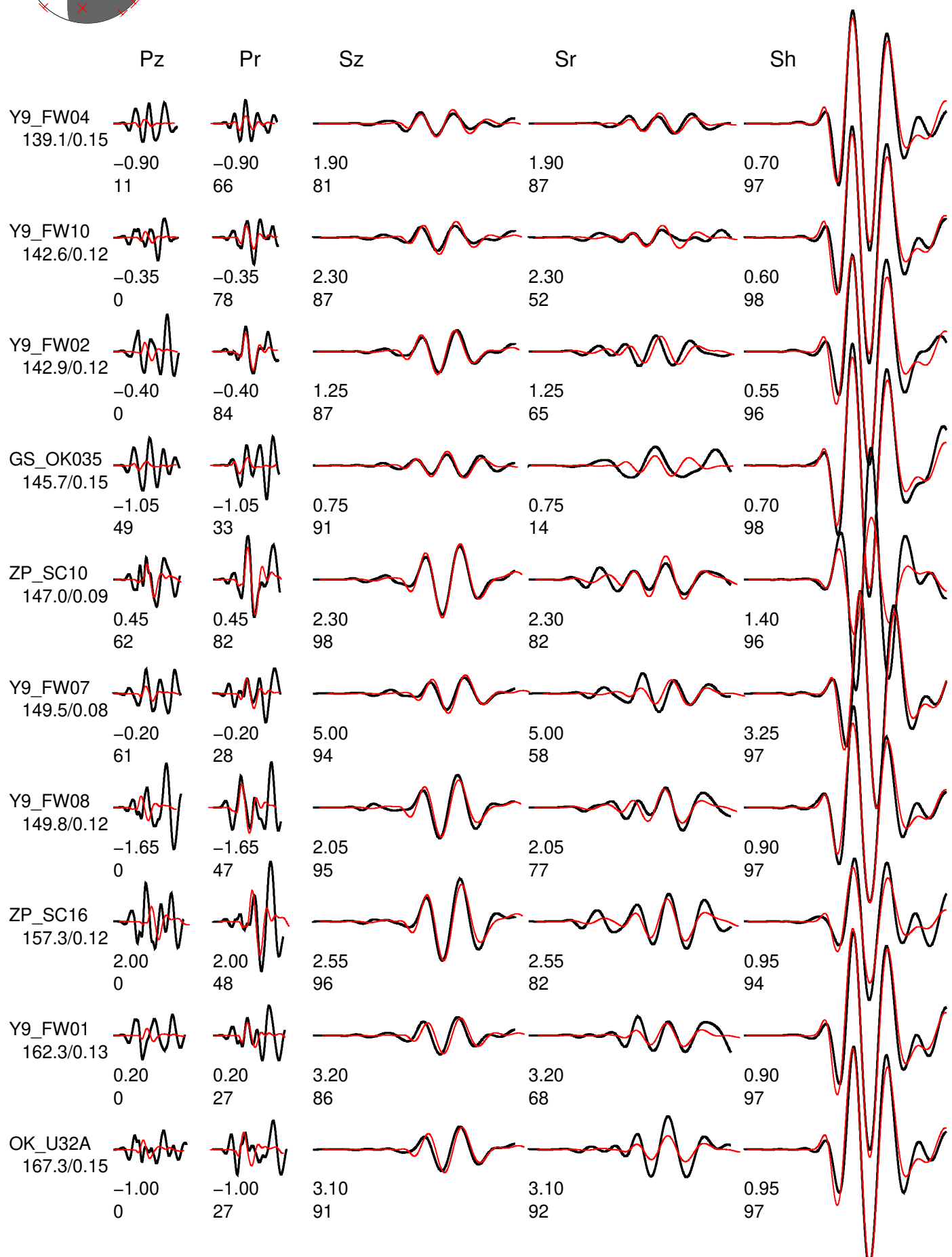


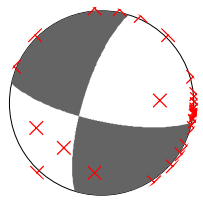


Event data Model and Depth chelsea_4

FM 102 74 -17 Mw 3.79 rms 1.797e-05 1775 ERR 0 1 1 ISO 0.00 0.00 CLVD 0.00 0.00

Variance reduction 82.3

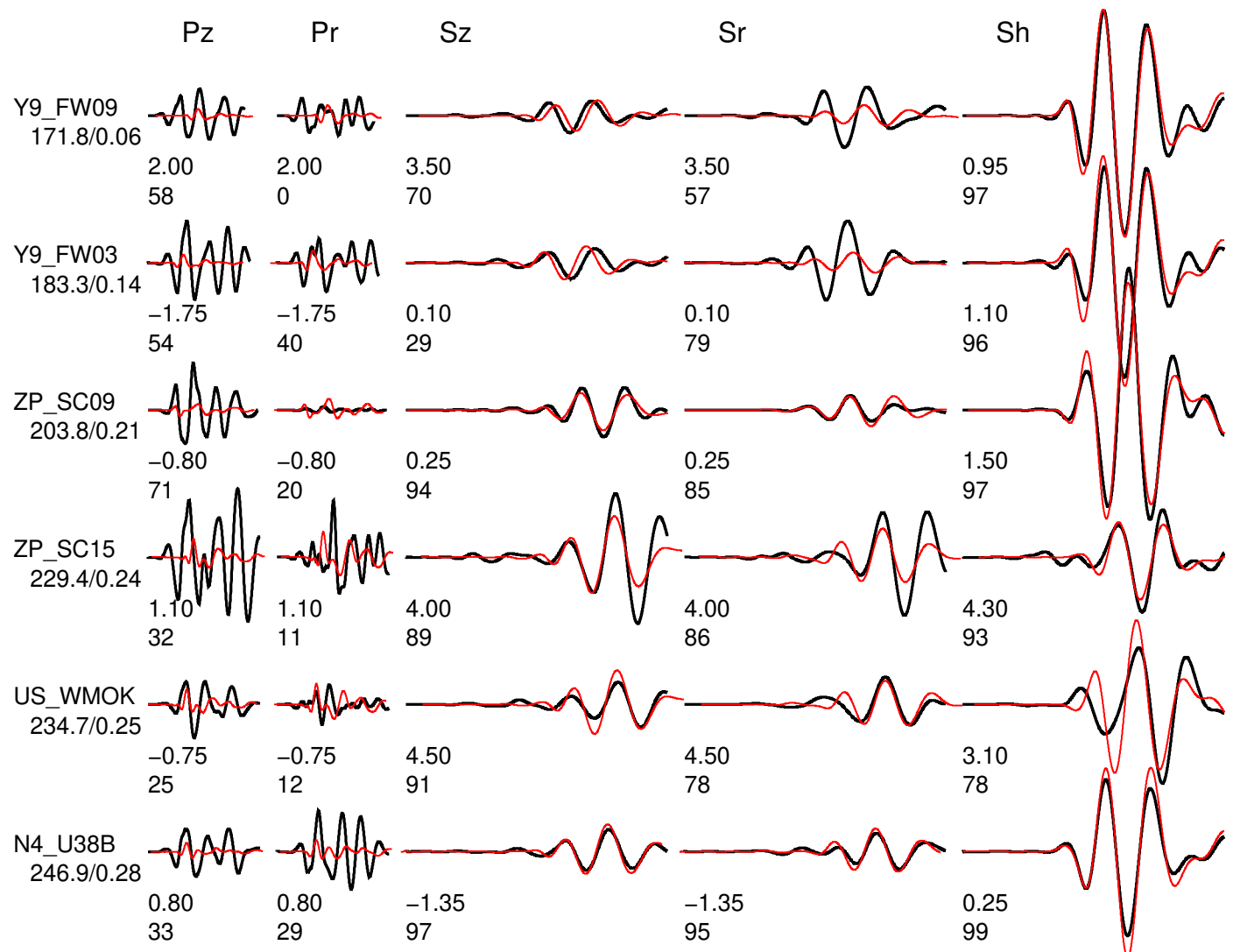




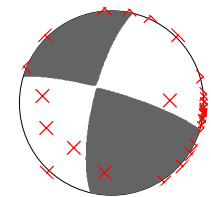
Event data Model and Depth chelsea_4

FM 102 74 -17 Mw 3.79 rms 1.797e-05 1775 ERR 0 1 1 ISO 0.00 0.00 CLVD 0.00 0.00

Variance reduction 82.3



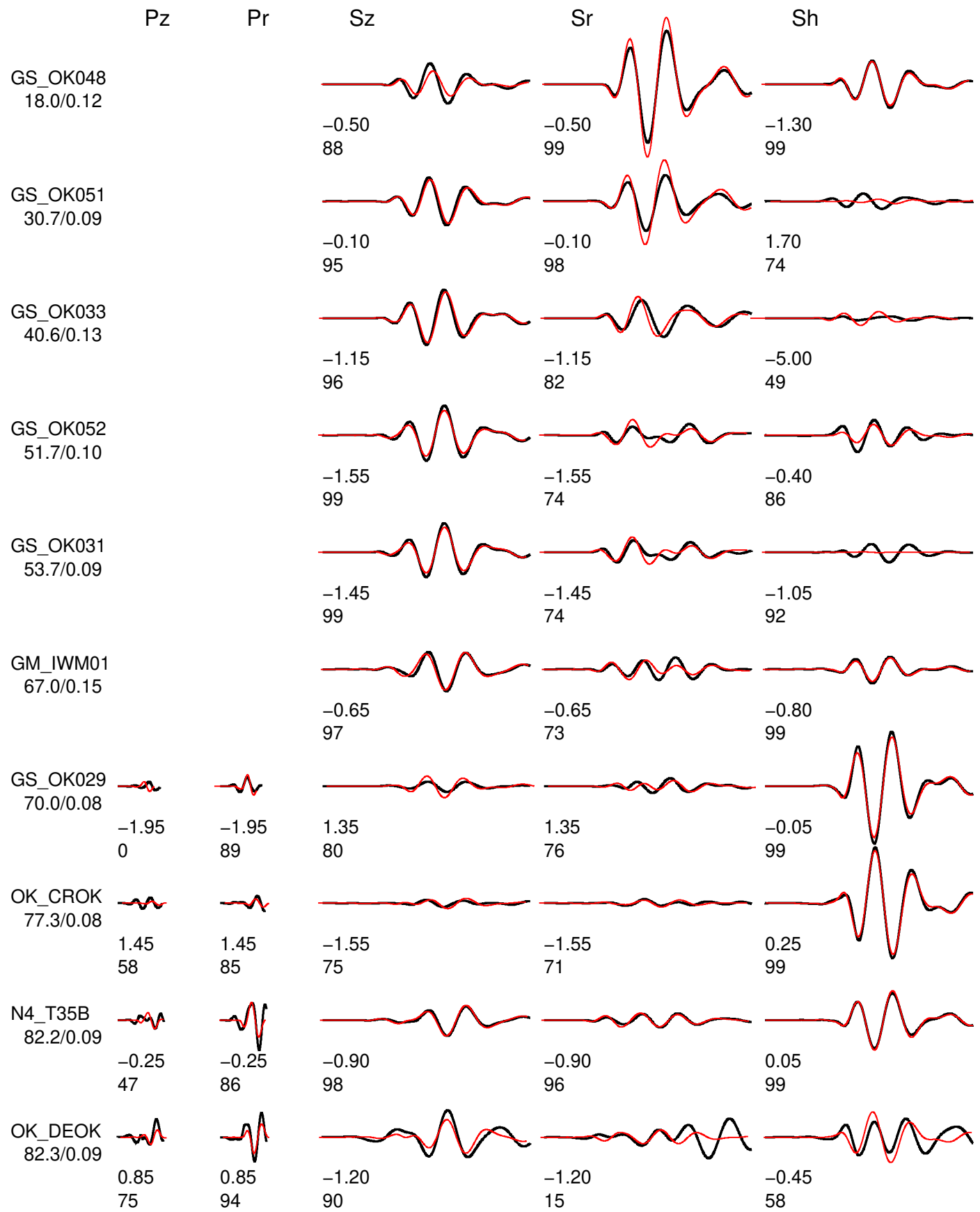
A.4 Inversion Result at depth of 5km

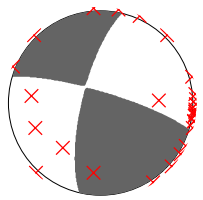


Event data Model and Depth chelsea_5

FM 287 80 17 Mw 3.79 rms 1.872e-05 1775 ERR 0 1 2 ISO 0.00 0.00 CLVD 0.00 0.00

Variance reduction 81.6

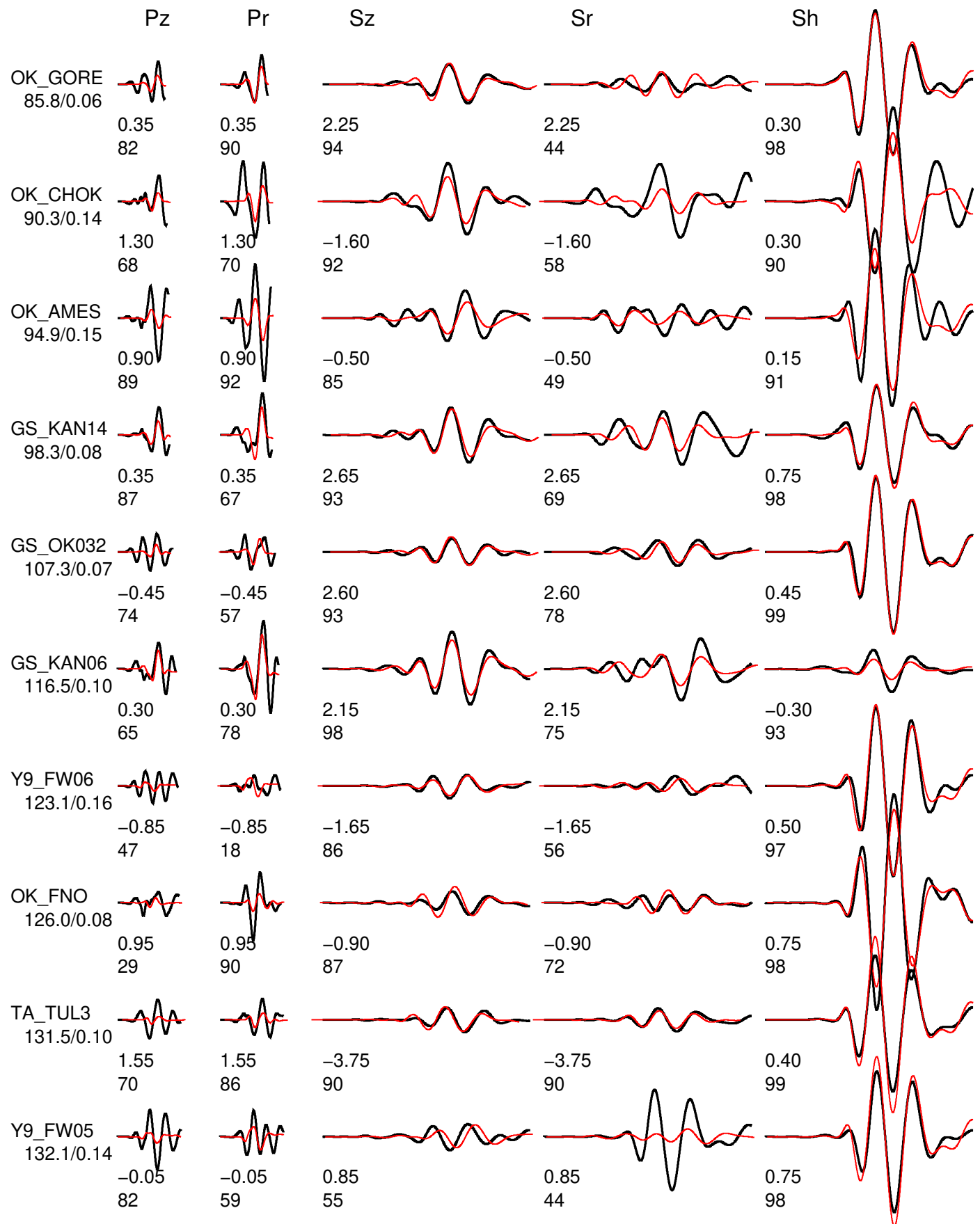


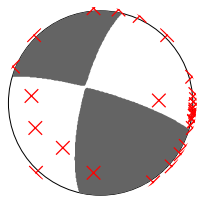


Event data Model and Depth chelsea_5

FM 287 80 17 Mw 3.79 rms 1.872e-05 1775 ERR 0 1 2 ISO 0.00 0.00 CLVD 0.00 0.00

Variance reduction 81.6

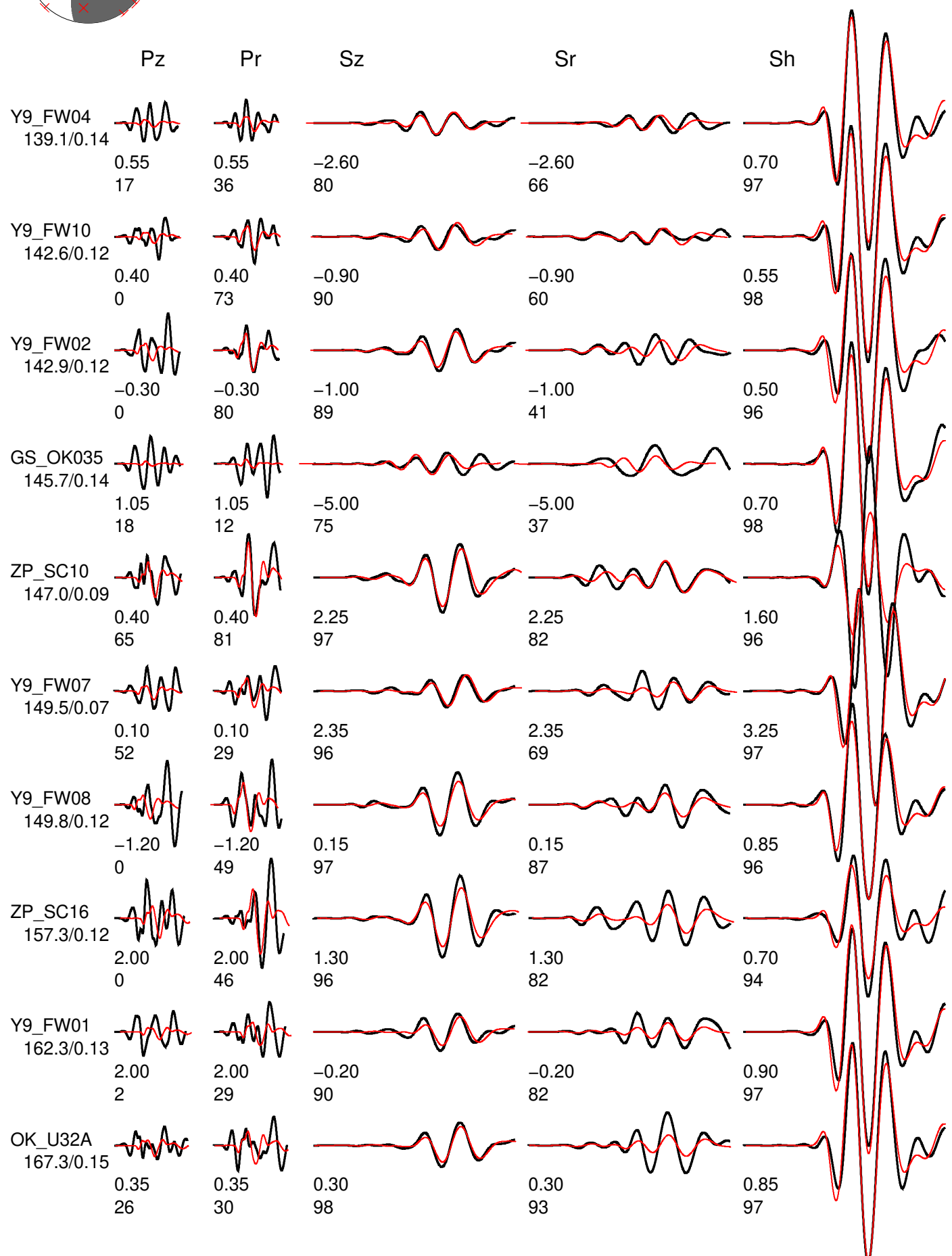


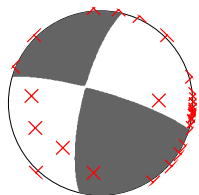


Event data Model and Depth chelsea_5

FM 287 80 17 Mw 3.79 rms 1.872e-05 1775 ERR 0 1 2 ISO 0.00 0.00 CLVD 0.00 0.00

Variance reduction 81.6

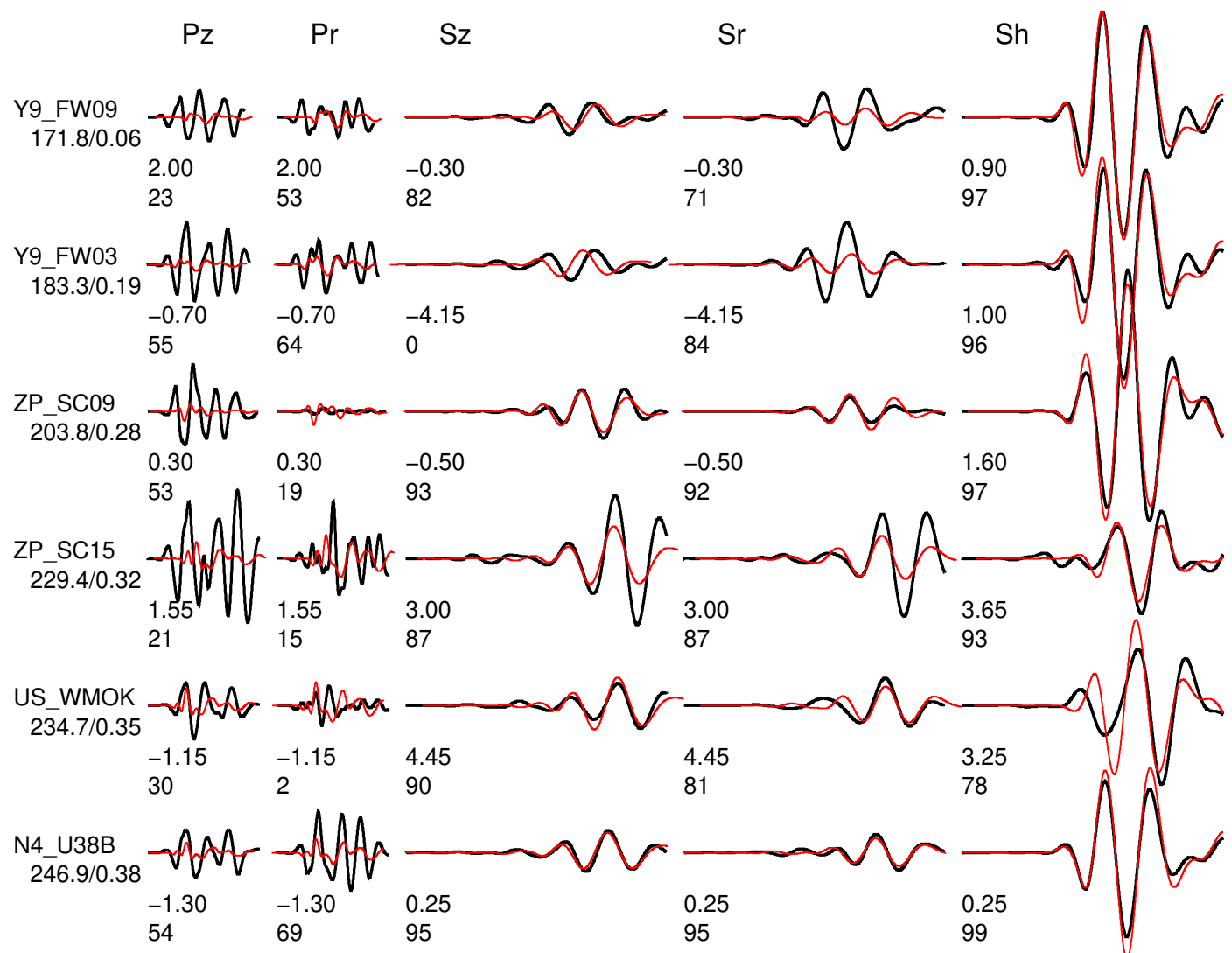




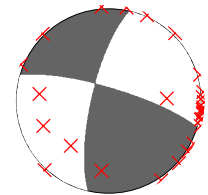
Event data Model and Depth chelsea_5

FM 287 80 17 Mw 3.79 rms 1.872e-05 1775 ERR 0 1 2 ISO 0.00 0.00 CLVD 0.00 0.00

Variance reduction 81.6



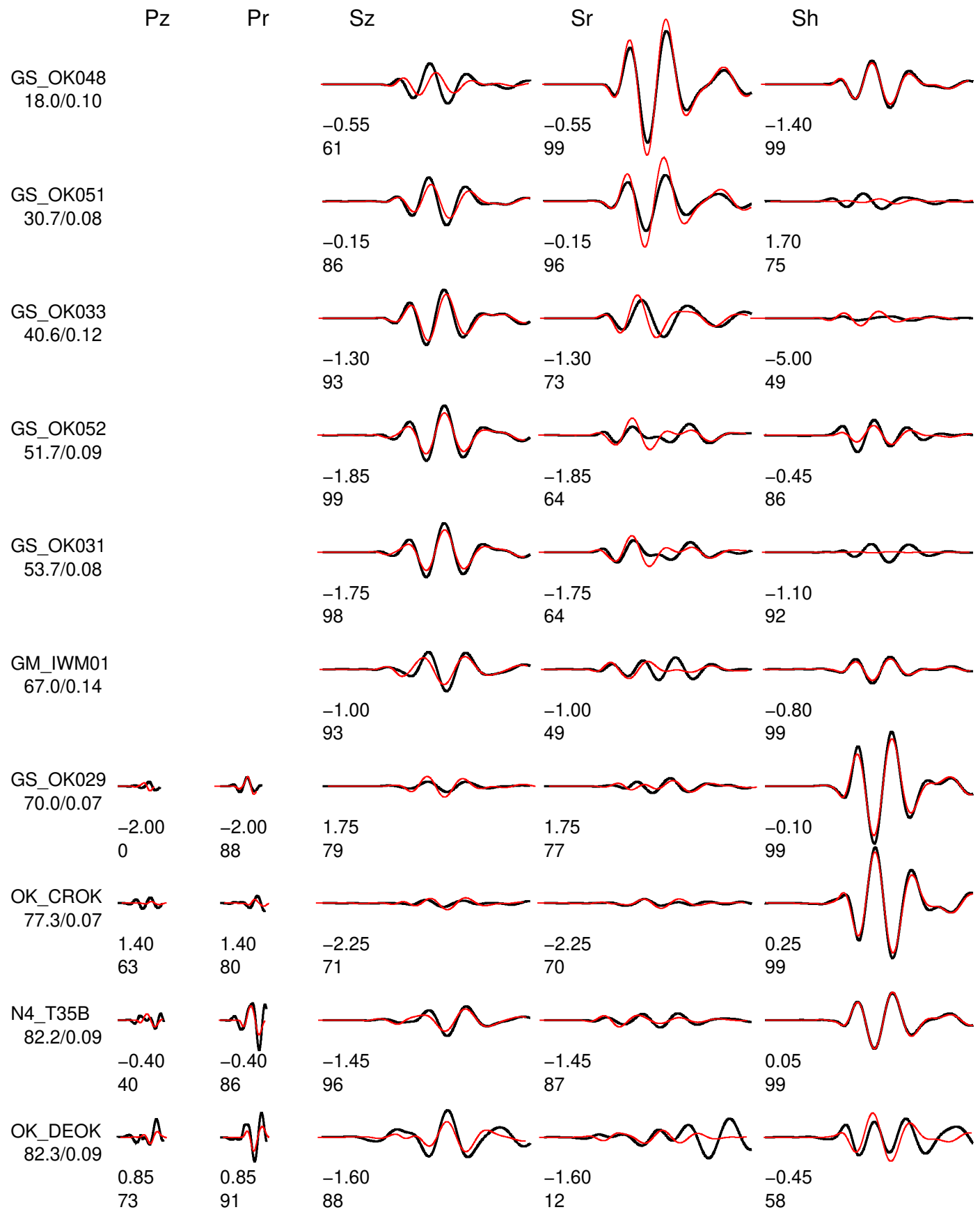
A.5 Inversion Result at depth of 6km

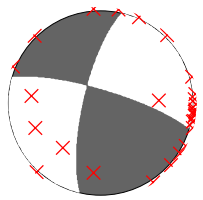


Event data Model and Depth chelsea_6

FM 286 78 16 Mw 3.79 rms 2.056e-05 1775 ERR 0 1 2 ISO 0.00 0.00 CLVD 0.00 0.00

Variance reduction 79.8

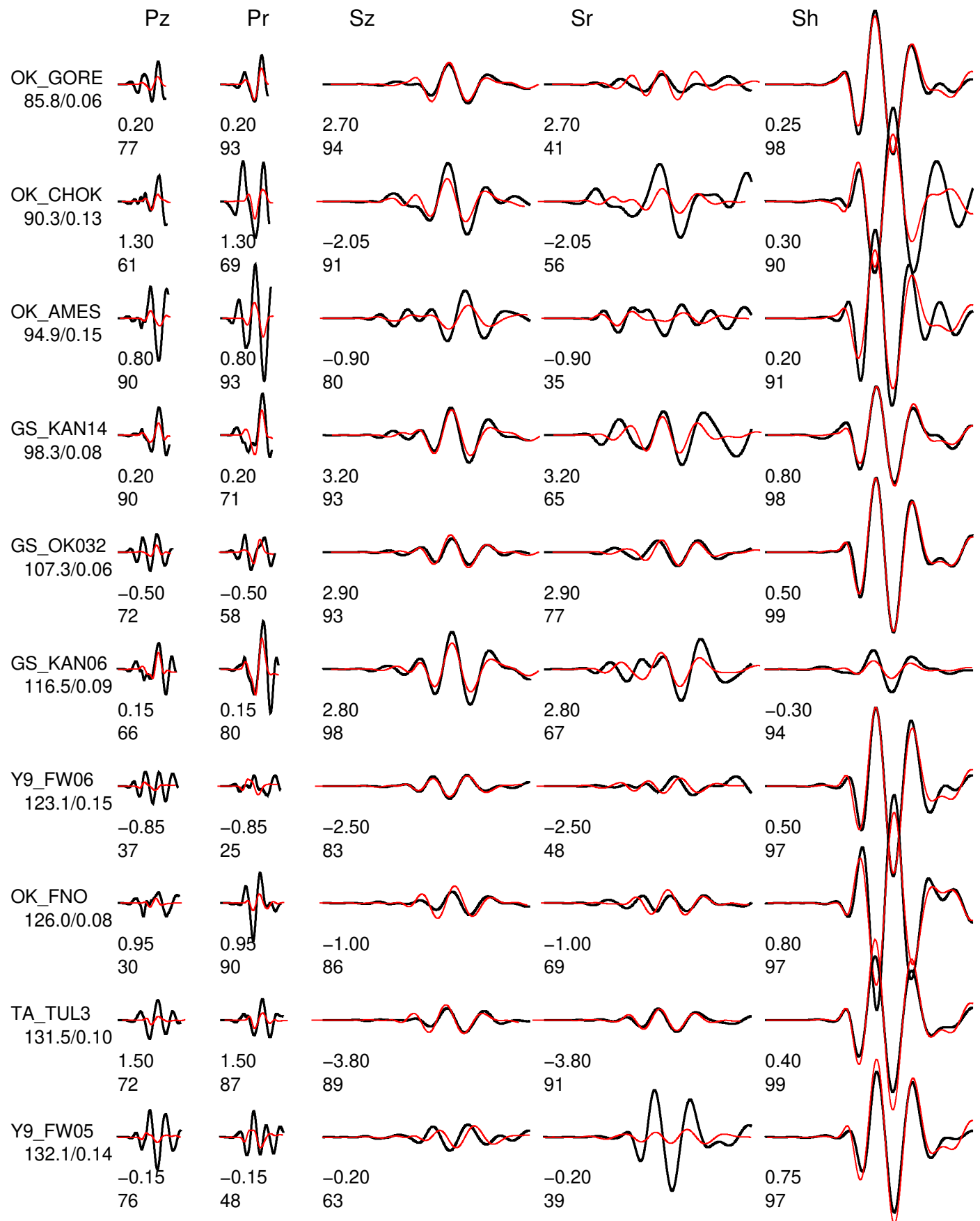


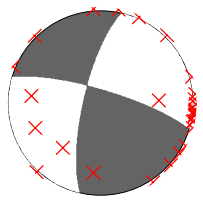


Event data Model and Depth chelsea_6

FM 286 78 16 Mw 3.79 rms 2.056e-05 1775 ERR 0 1 2 ISO 0.00 0.00 CLVD 0.00 0.00

Variance reduction 79.8

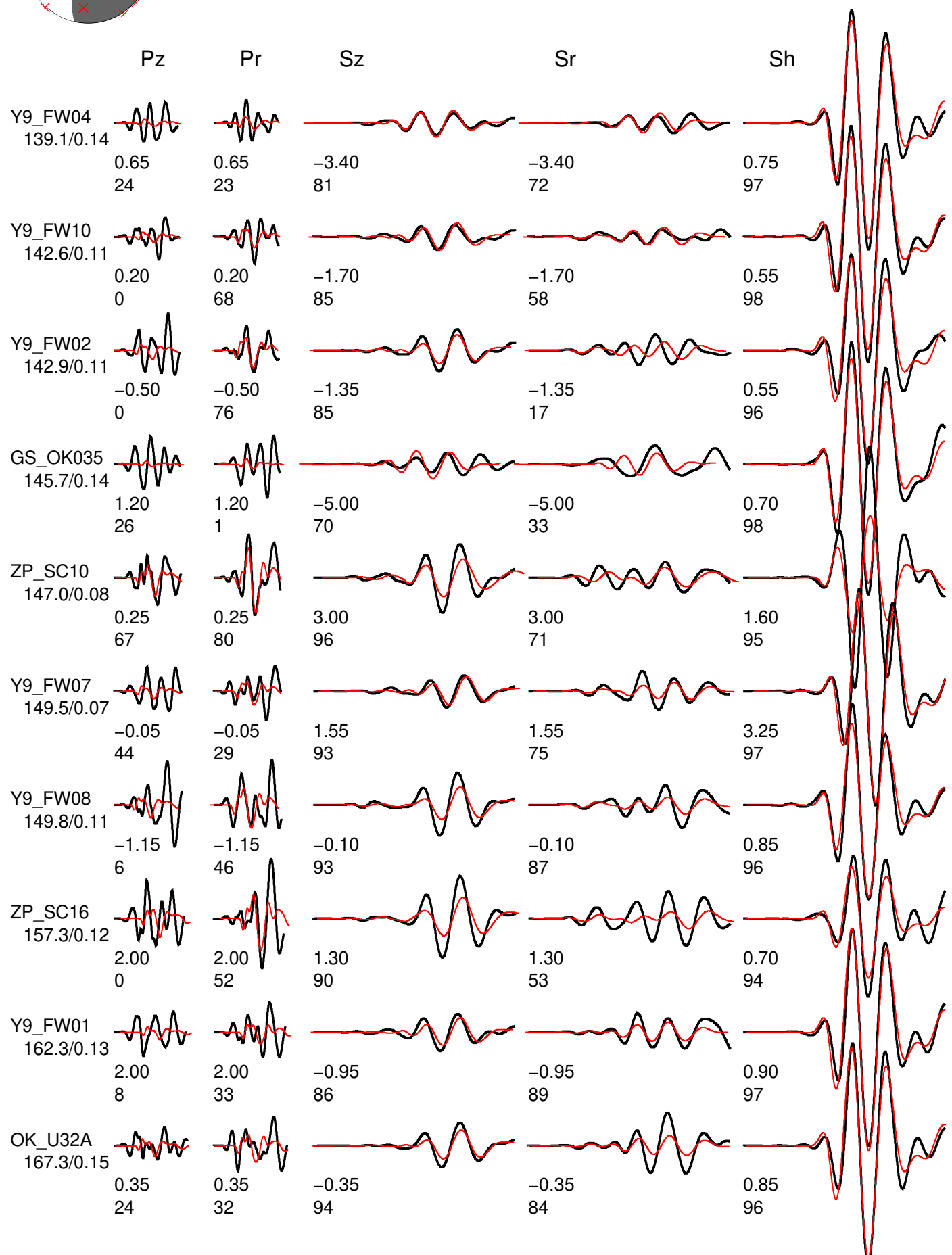


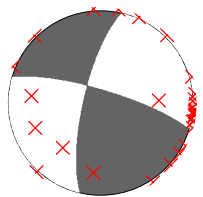


Event data Model and Depth chelsea_6

FM 286 78 16 Mw 3.79 rms 2.056e-05 1775 ERR 0 1 2 ISO 0.00 0.00 CLVD 0.00 0.00

Variance reduction 79.8

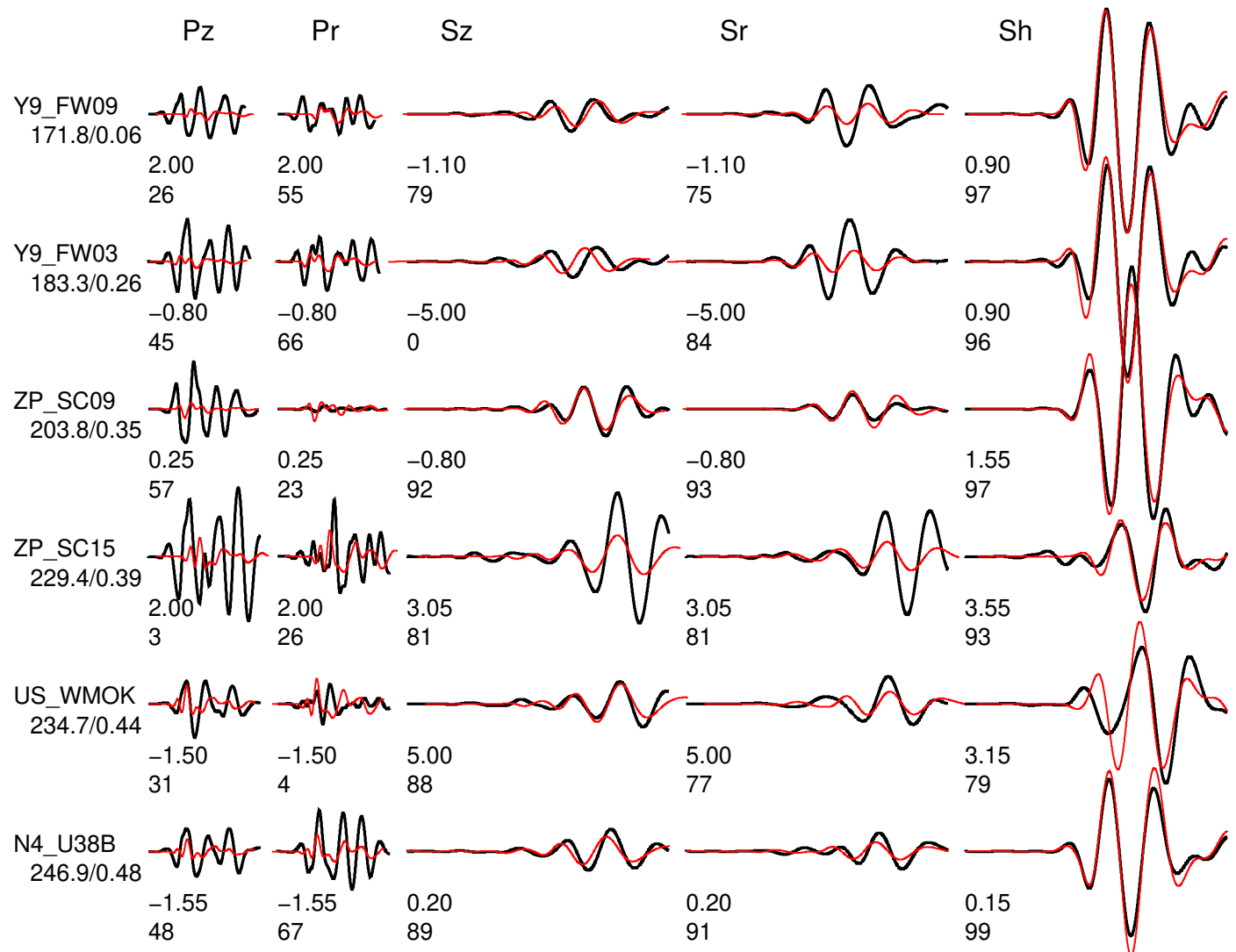




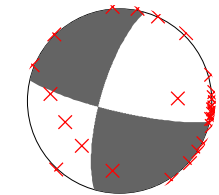
Event data Model and Depth chelsea_6

FM 286 78 16 Mw 3.79 rms 2.056e-05 1775 ERR 0 1 2 ISO 0.00 0.00 CLVD 0.00 0.00

Variance reduction 79.8



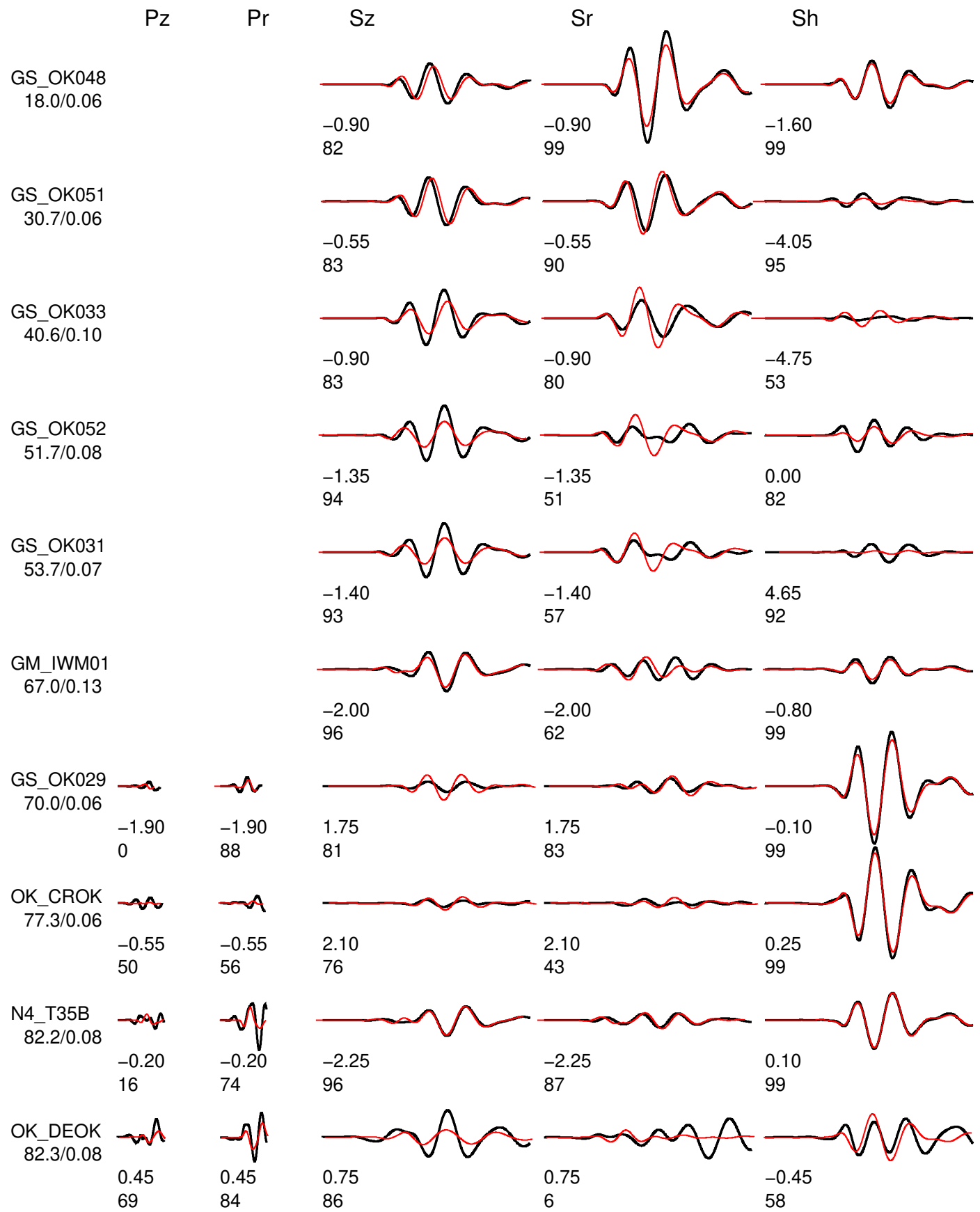
A.6 Inversion Result at depth of 7km

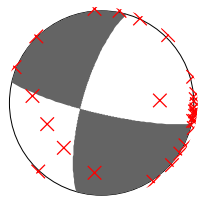


Event data Model and Depth chelsea_7

FM 103 80 -17 Mw 3.79 rms 2.305e-05 1775 ERR 1 1 1 ISO 0.00 0.00 CLVD 0.00 0.00

Variance reduction 77.3

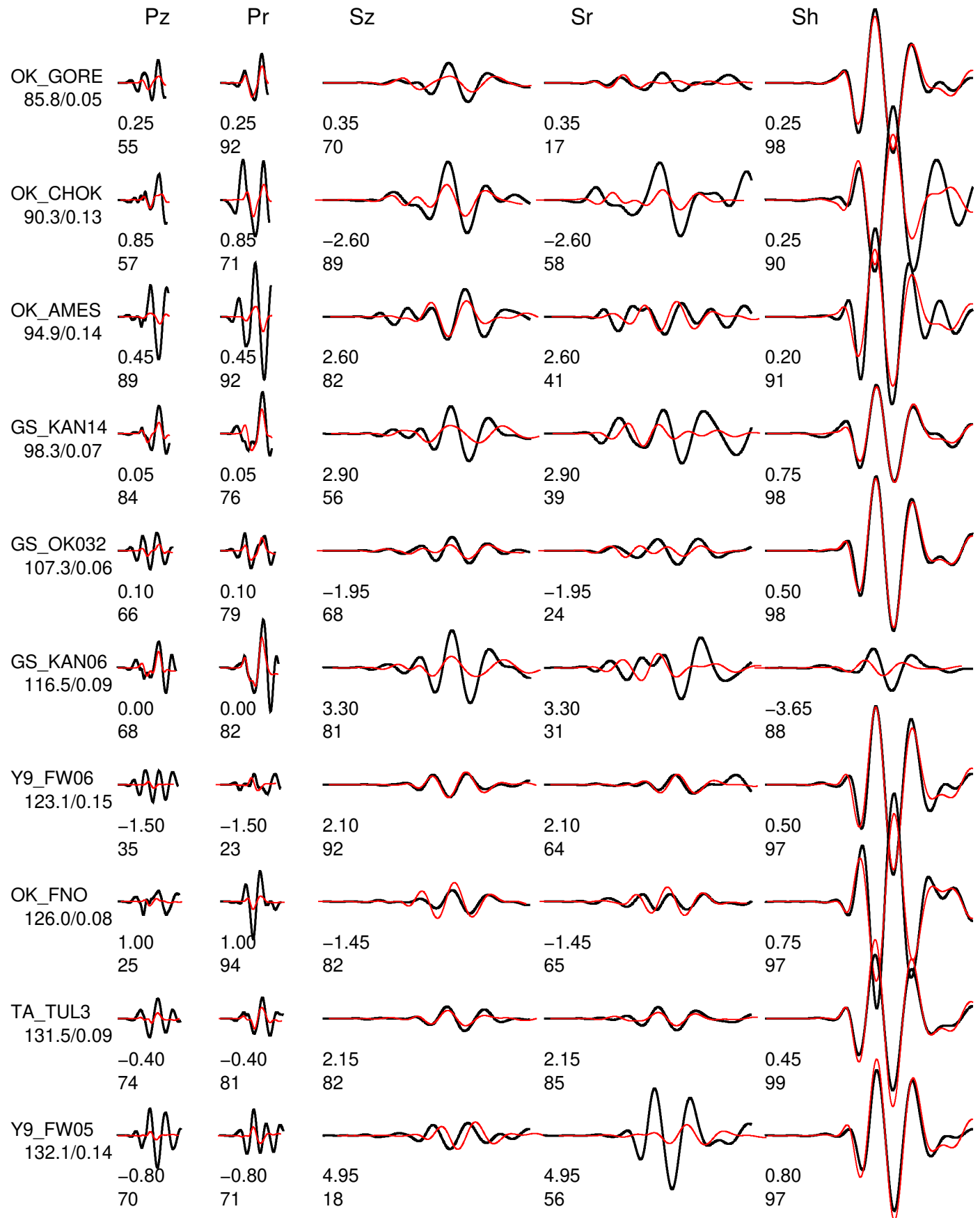


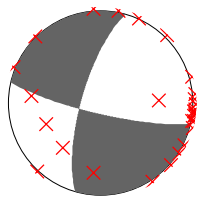


Event data Model and Depth chelsea_7

FM 103 80 -17 Mw 3.79 rms 2.305e-05 1775 ERR 1 1 1 ISO 0.00 0.00 CLVD 0.00 0.00

Variance reduction 77.3

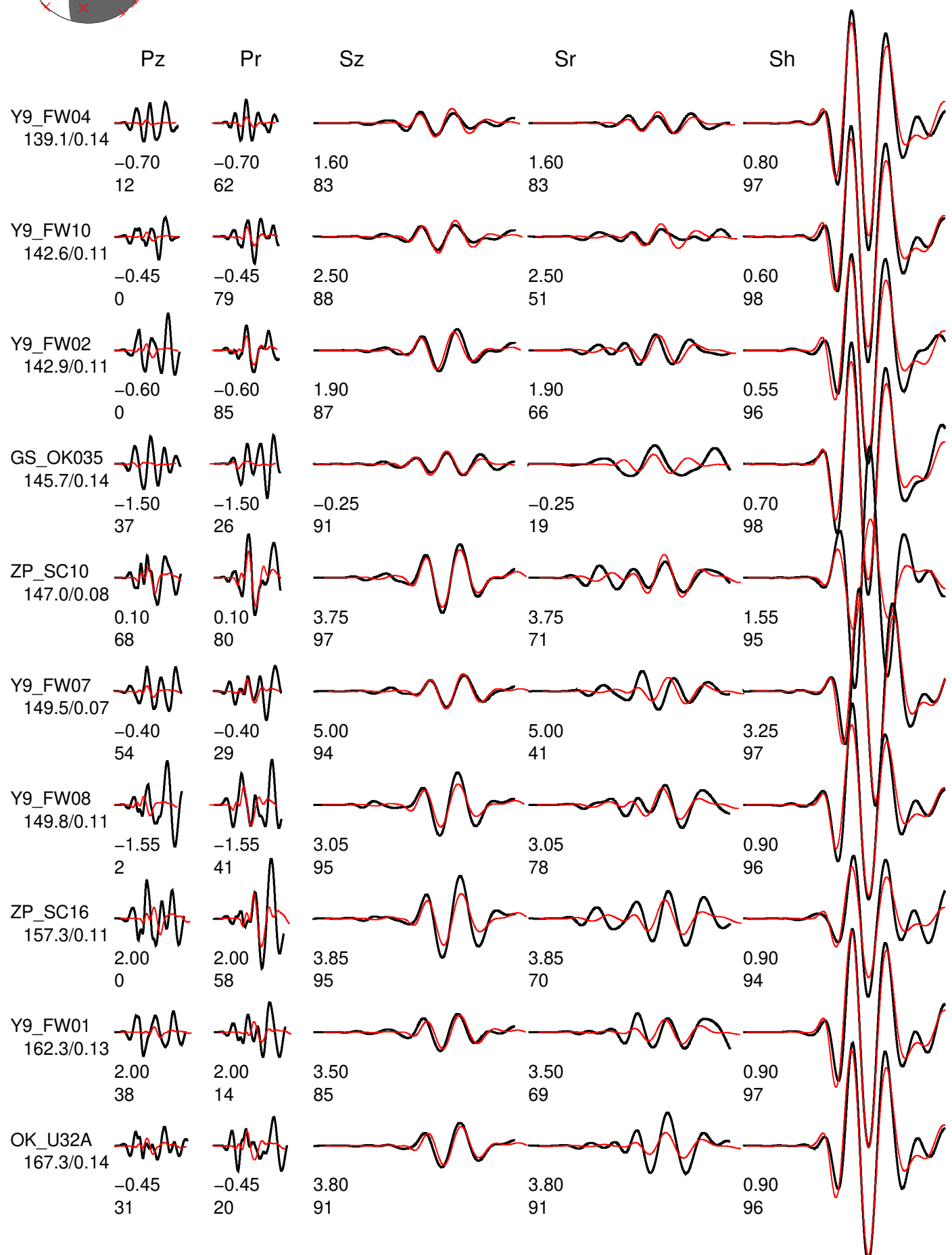


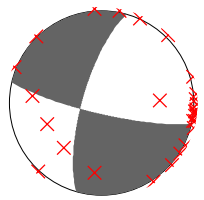


Event data Model and Depth chelsea_7

FM 103 80 -17 Mw 3.79 rms 2.305e-05 1775 ERR 1 1 1 ISO 0.00 0.00 CLVD 0.00 0.00

Variance reduction 77.3

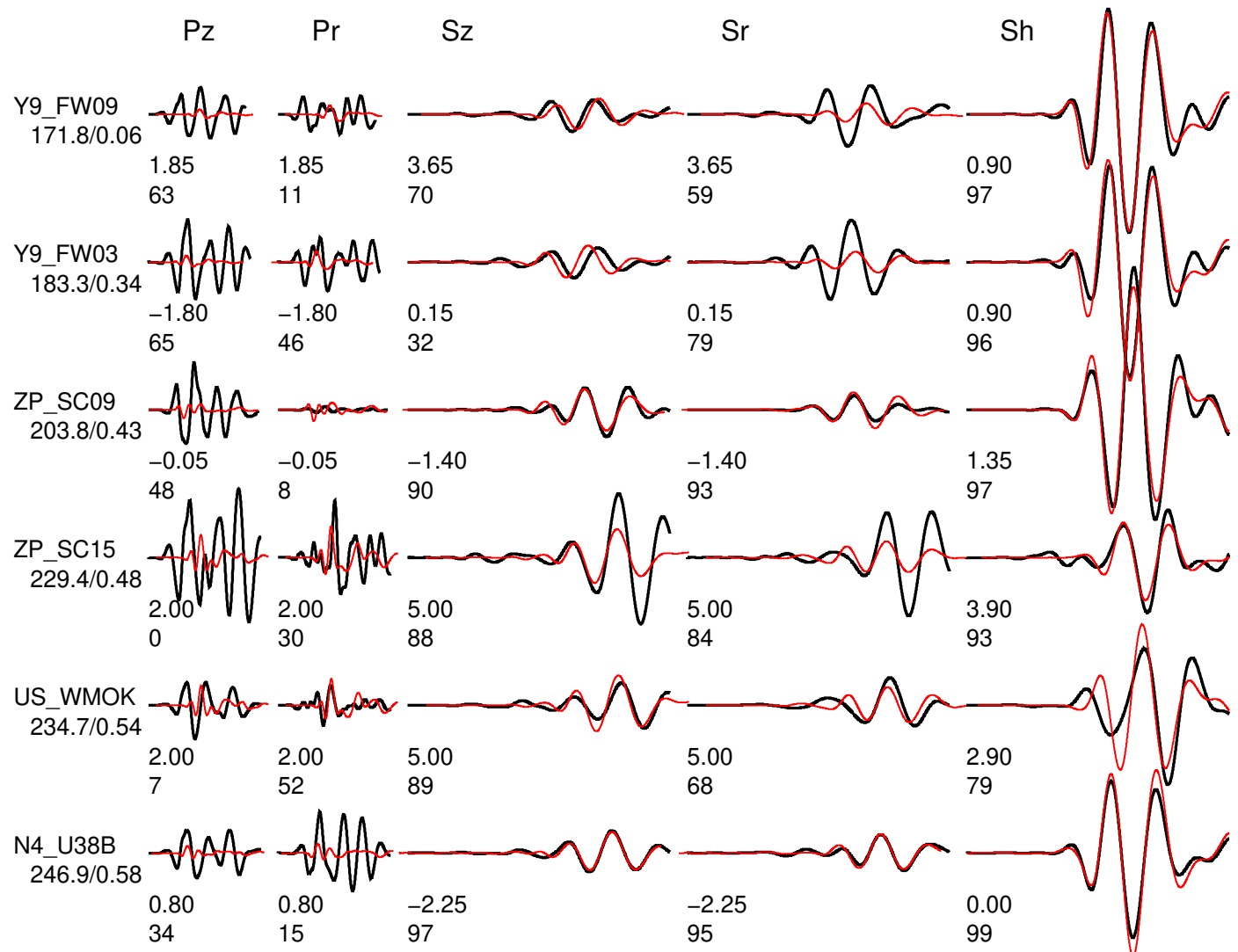




Event data Model and Depth chelsea_7

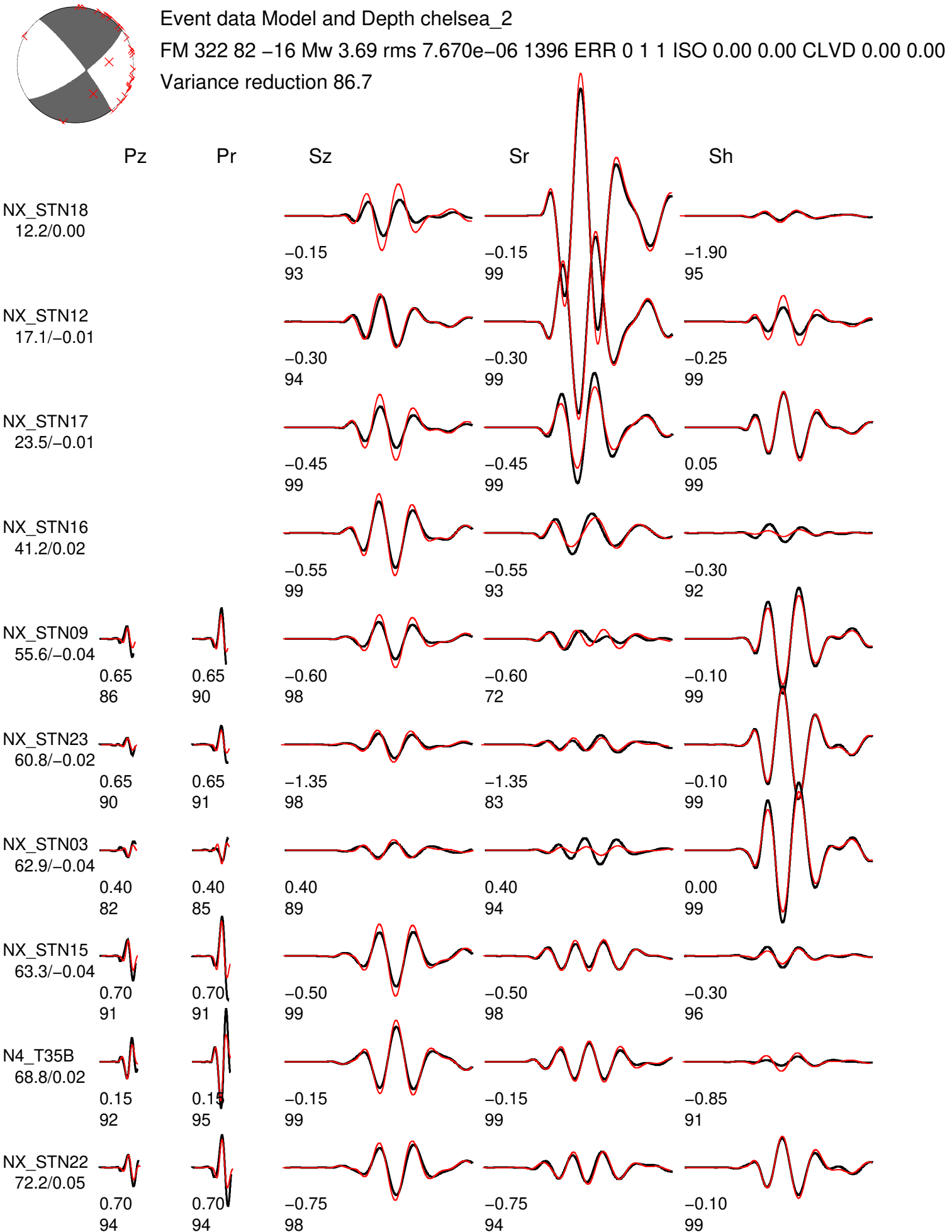
FM 103 80 -17 Mw 3.79 rms 2.305e-05 1775 ERR 1 1 1 ISO 0.00 0.00 CLVD 0.00 0.00

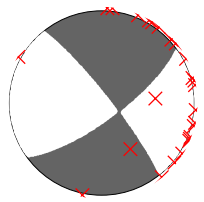
Variance reduction 77.3



B. Full Inversion Results For Event on 2016-07-21

B.1 Inversion Result at depth of 2km

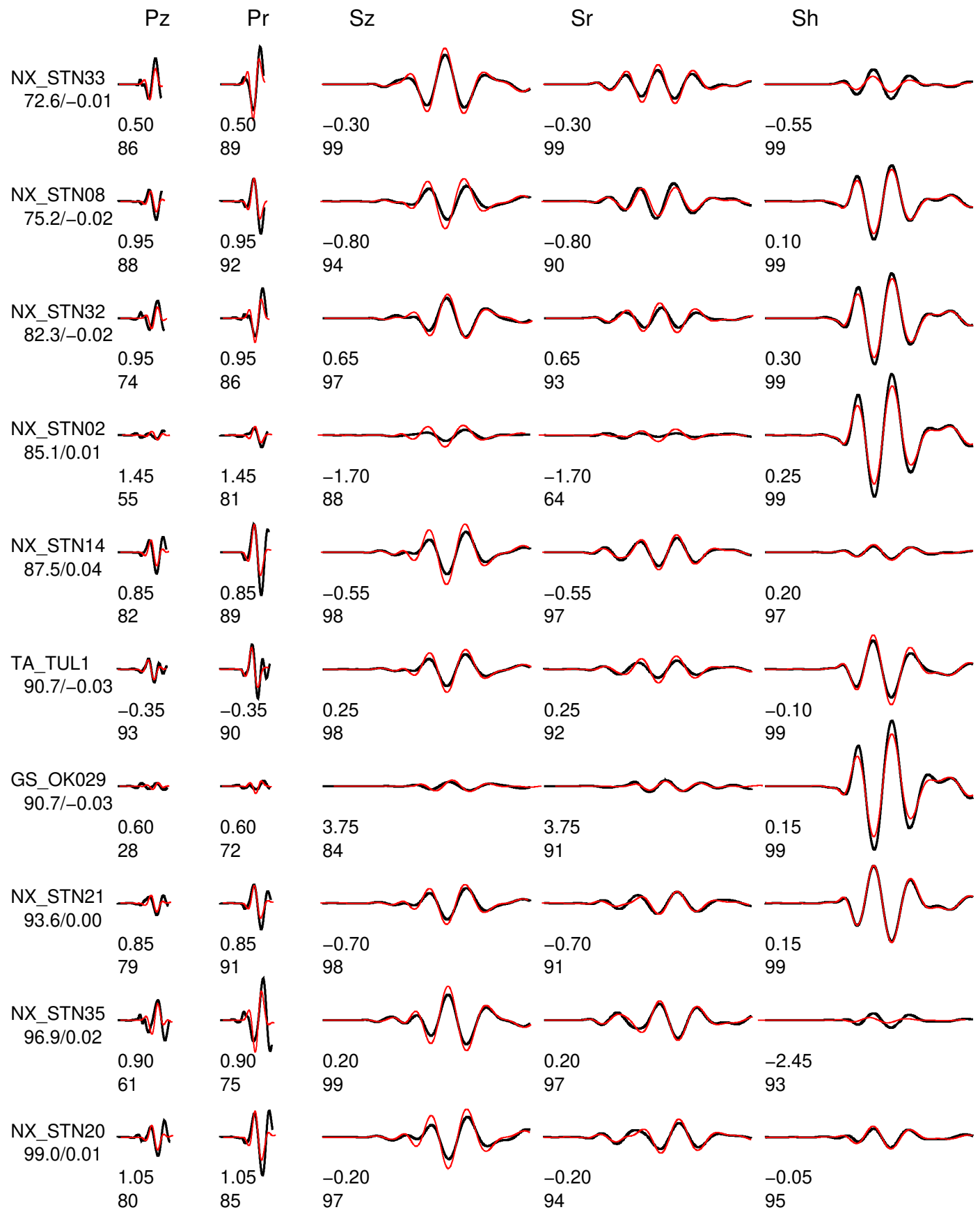


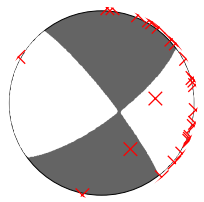


Event data Model and Depth chelsea_2

FM 322 82 -16 Mw 3.69 rms 7.670e-06 1396 ERR 0 1 1 ISO 0.00 0.00 CLVD 0.00 0.00

Variance reduction 86.7

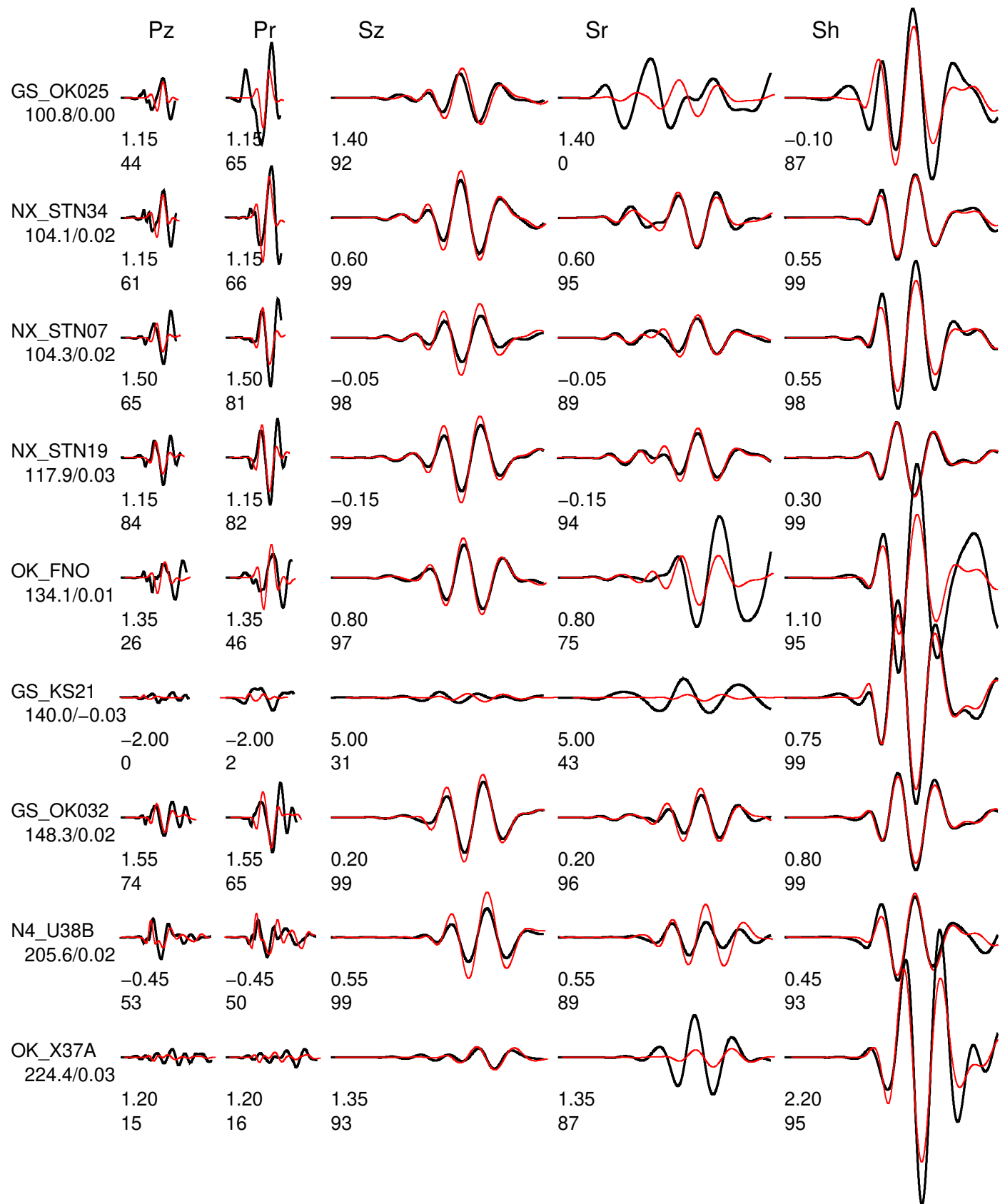




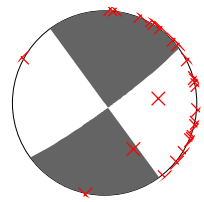
Event data Model and Depth chelsea_2

FM 322 82 -16 Mw 3.69 rms 7.670e-06 1396 ERR 0 1 1 ISO 0.00 0.00 CLVD 0.00 0.00

Variance reduction 86.7



B.2 Inversion Result at depth of 3km



Event data Model and Depth chelsea_3

FM 144 90 5 Mw 3.70 rms 6.300e-06 1396 ERR 0 2 2 ISO 0.00 0.00 CLVD 0.00 0.00

Variance reduction 89.1

Pz

Pr

Sz

Sr

Sh

NX_STN18
12.2/-0.02

-0.15
99

-0.15
99

-1.55
96

NX_STN12
17.1/-0.01

-0.40
99

-0.40
99

-0.25
99

NX_STN17
23.5/-0.01

-0.30
99

-0.30
99

-0.05
99

NX_STN16
41.2/0.02

-0.30
99

-0.30
98

-5.00
94

NX_STN09
55.6/-0.03
0.30
88

0.30
93

-0.20
99

-0.20
75

-0.15
99

NX_STN23
60.8/-0.02
0.20
95

0.20
95

-0.55
99

-0.55
85

-0.15
99

NX_STN03
62.9/-0.03
0.50
94

0.50
90

-1.05
93

-1.05
83

-0.10
99

NX_STN15
63.3/-0.03
0.45
92

0.45
93

-0.10
99

-0.10
98

-0.10
95

N4_T35B
68.8/0.03
0.00
92

0.00
96

0.00
99

0.00
96

-0.60
92

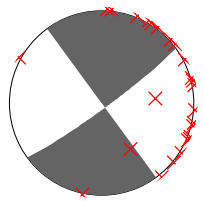
NX_STN22
72.2/-0.04
0.55
96

0.55
95

-0.15
99

-0.15
95

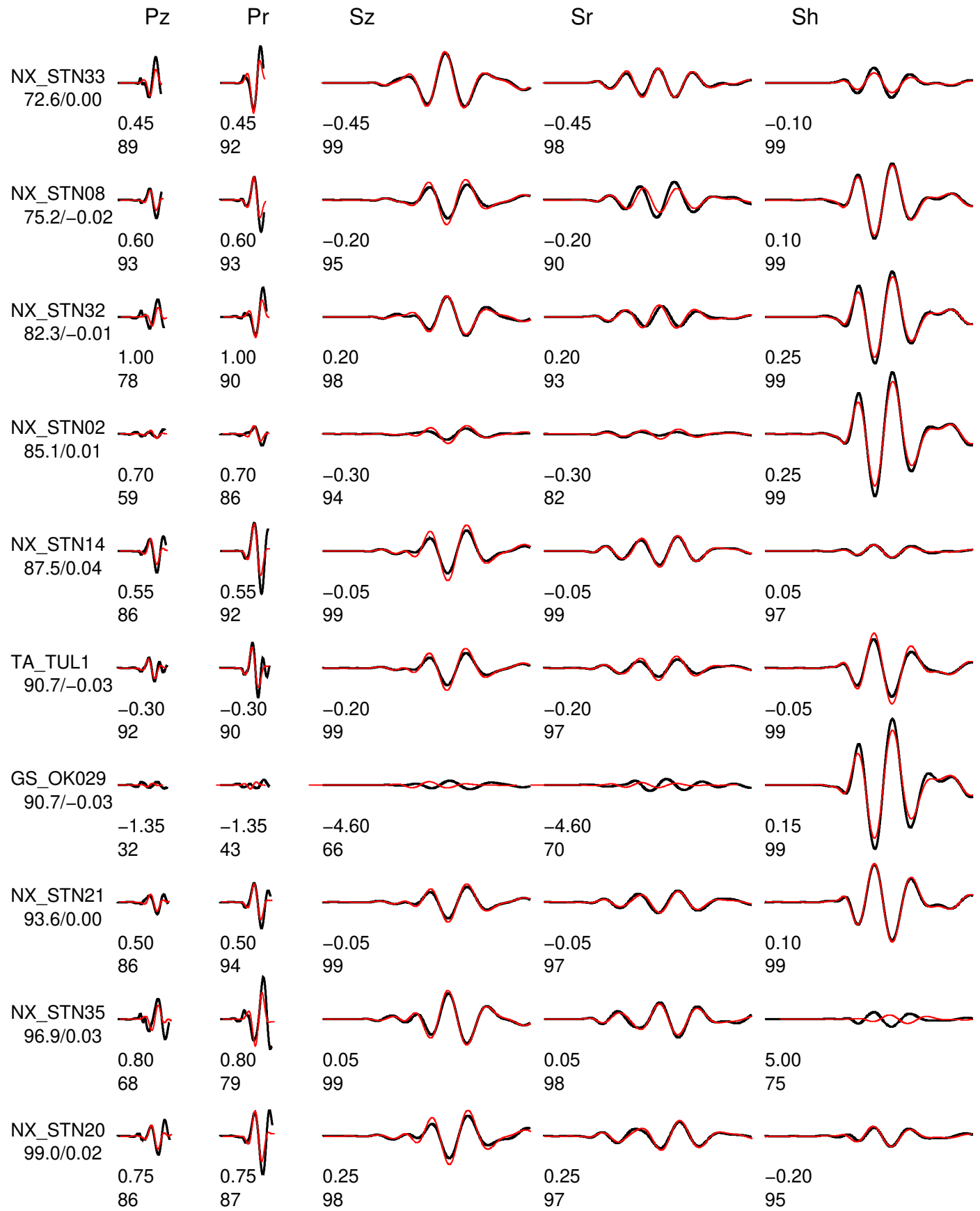
-0.10
99

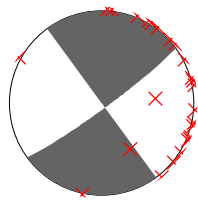


Event data Model and Depth chelsea_3

FM 144 90 5 Mw 3.70 rms 6.300e-06 1396 ERR 0 2 2 ISO 0.00 0.00 CLVD 0.00 0.00

Variance reduction 89.1

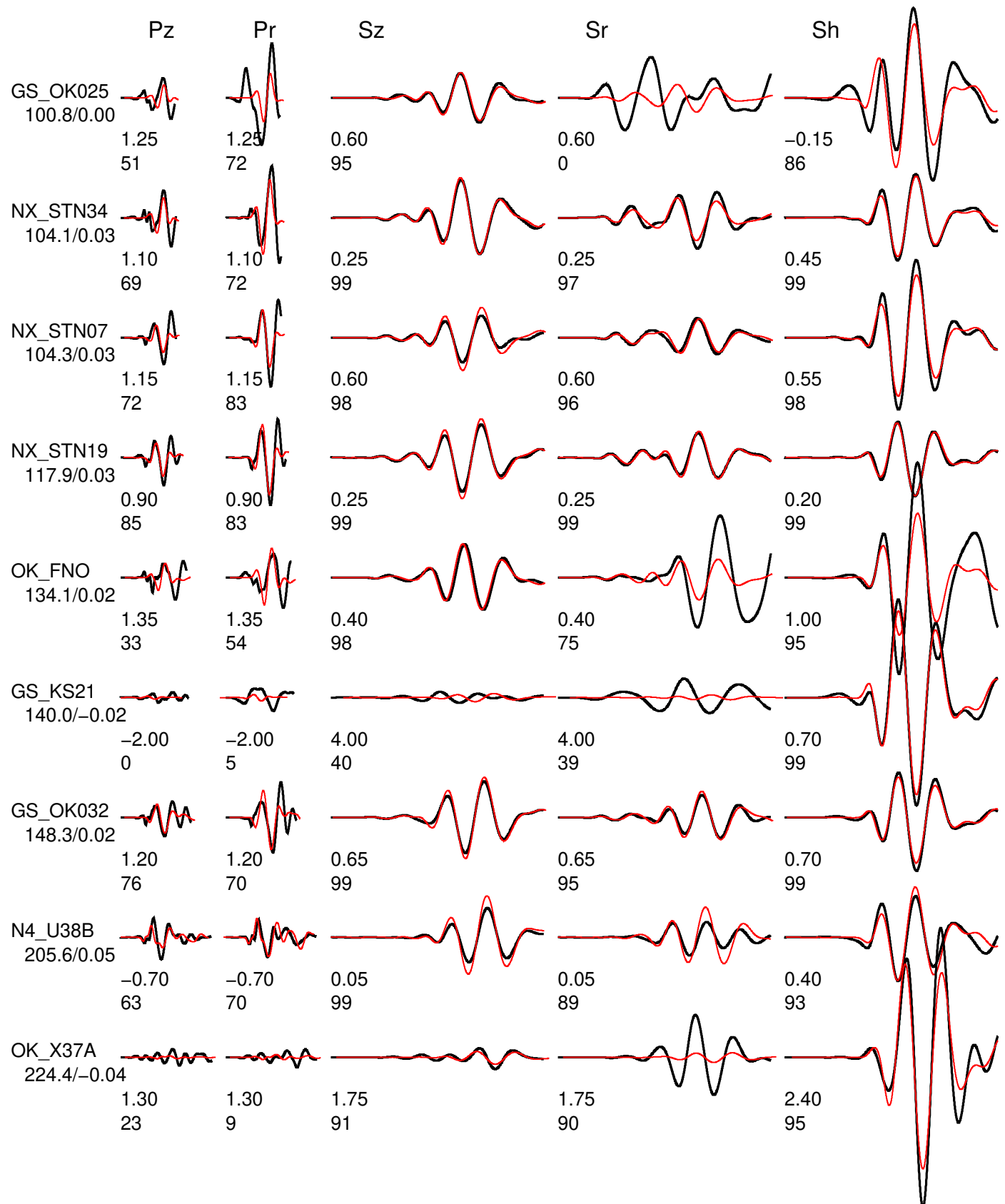




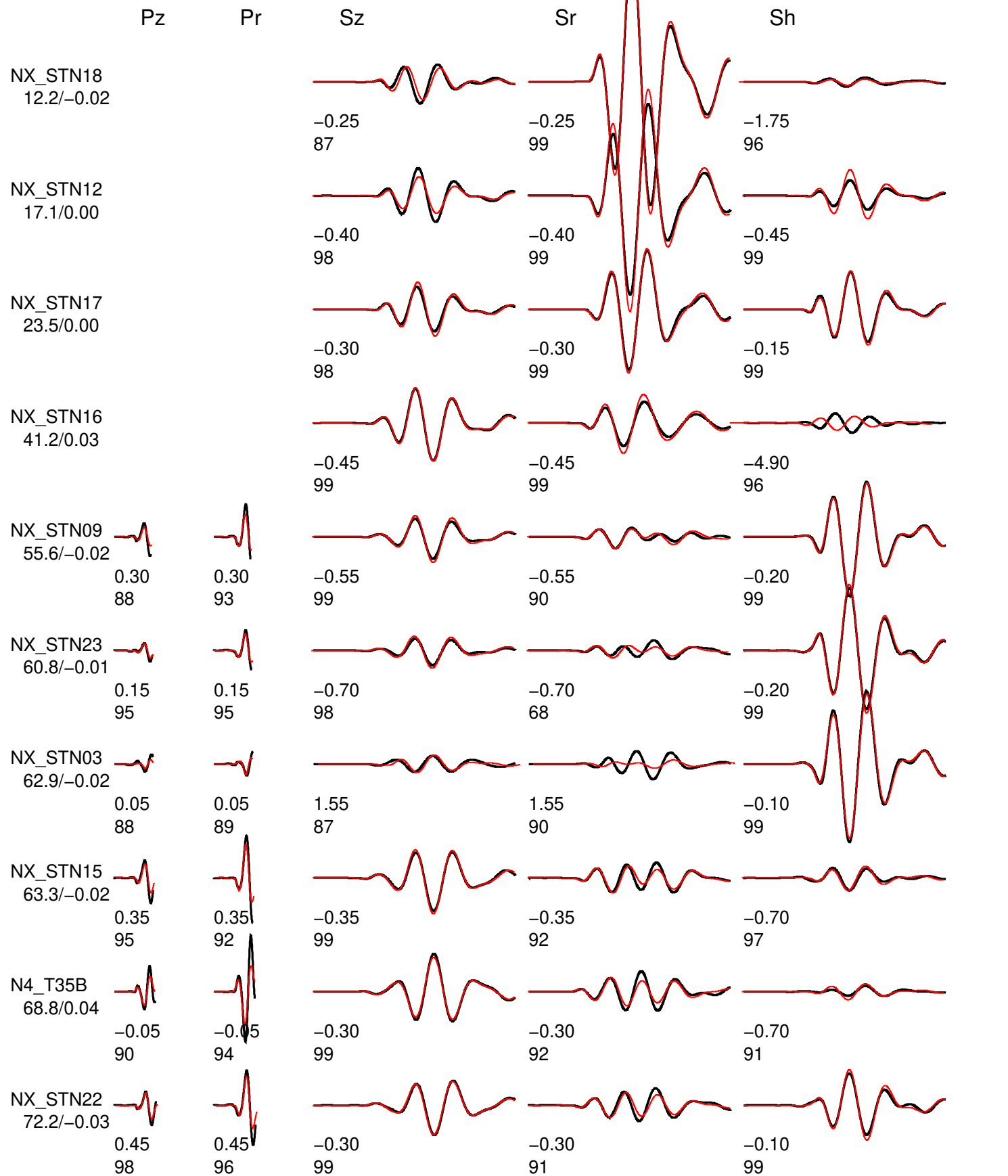
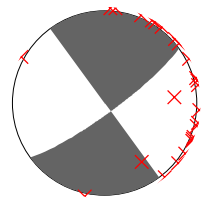
Event data Model and Depth chelsea_3

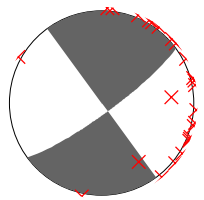
FM 144 90 5 Mw 3.70 rms 6.300e-06 1396 ERR 0 2 2 ISO 0.00 0.00 CLVD 0.00 0.00

Variance reduction 89.1



B.3 Inversion Result at depth of 4km

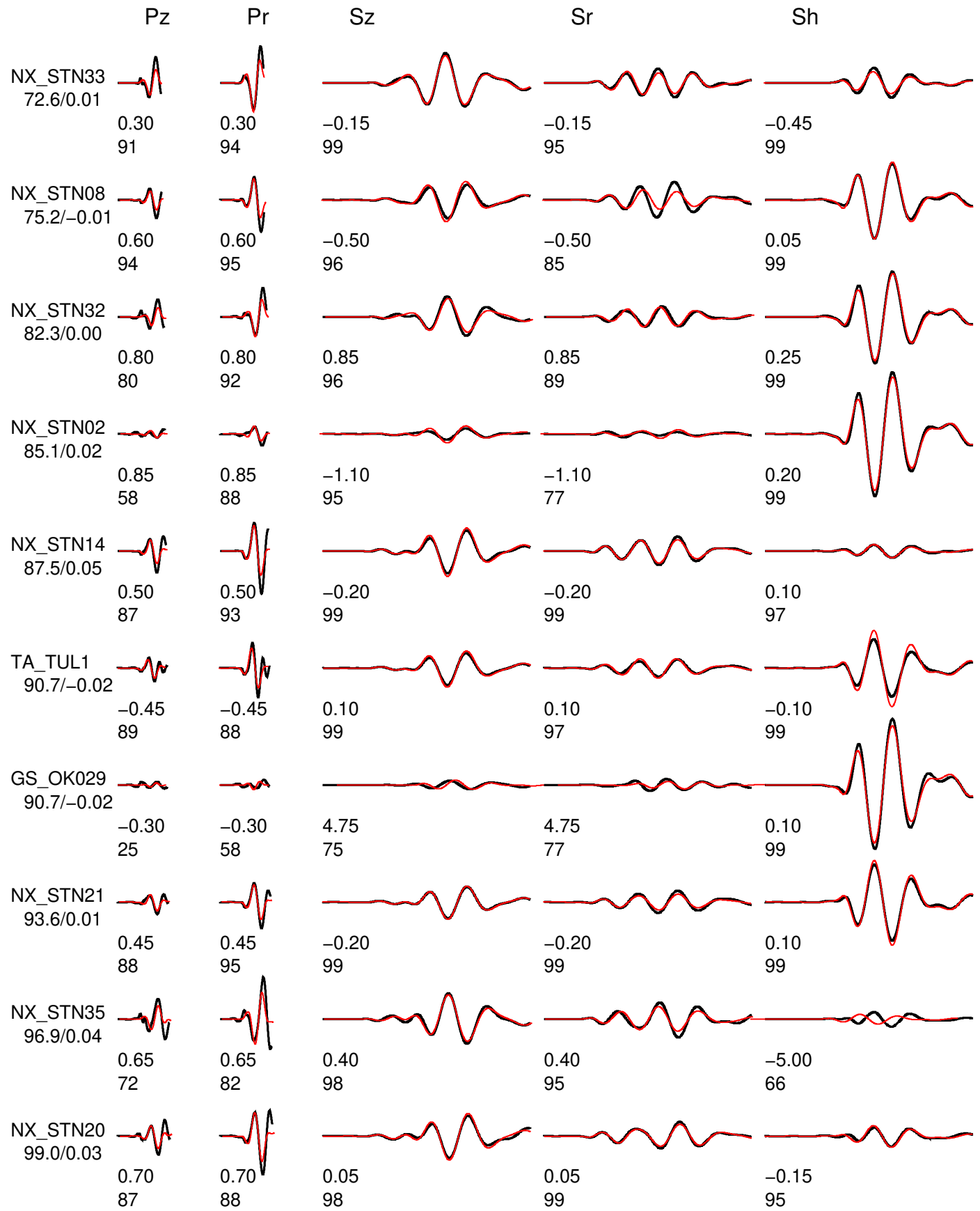


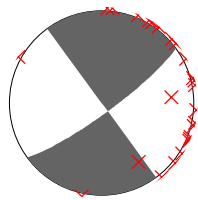


Event data Model and Depth chelsea_4

FM 144 90 9 Mw 3.73 rms 6.117e-06 1396 ERR 0 1 1 ISO 0.00 0.00 CLVD 0.00 0.00

Variance reduction 89.4

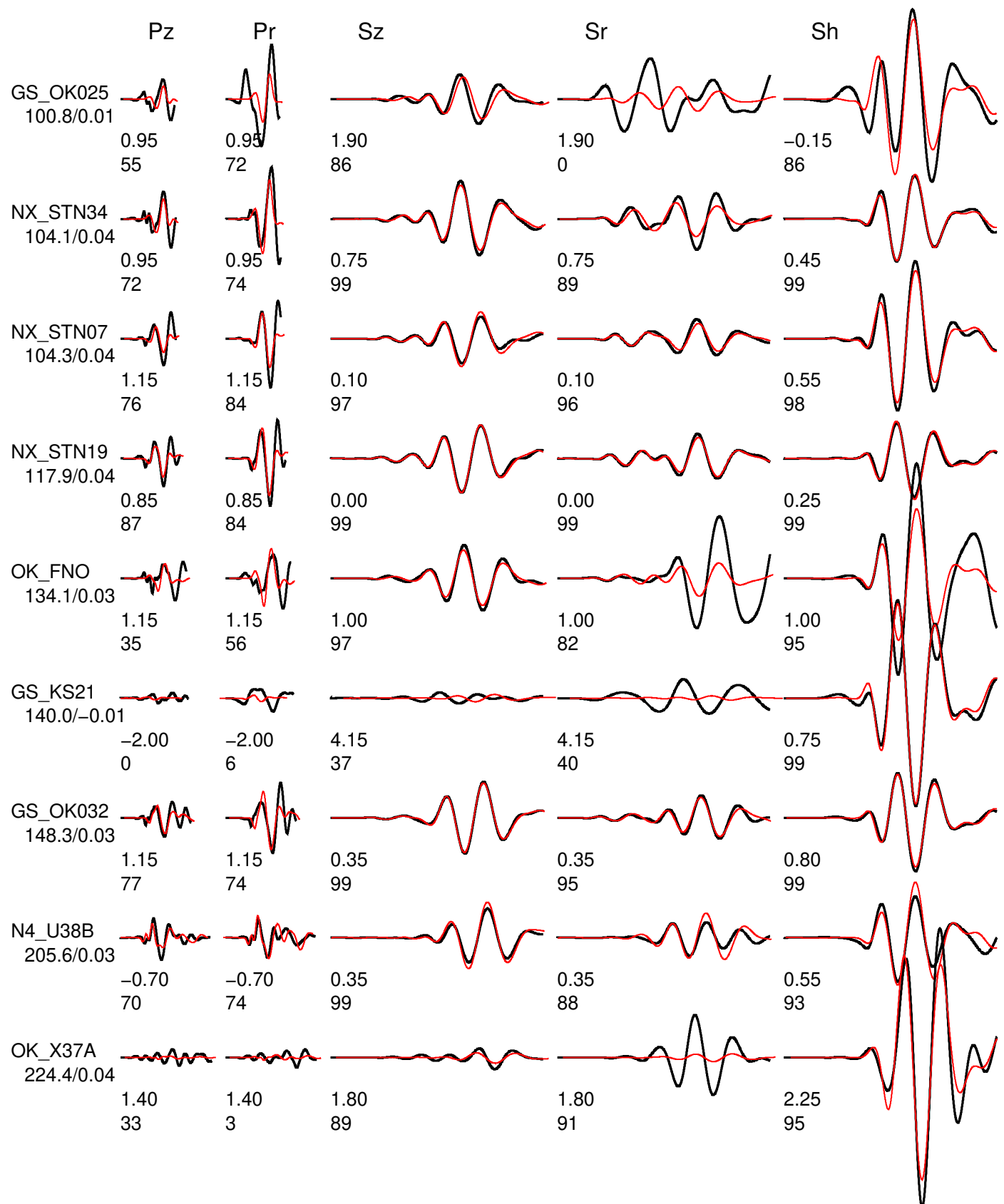




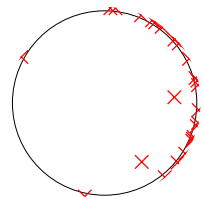
Event data Model and Depth chelsea_4

FM 144 90 9 Mw 3.73 rms 6.117e-06 1396 ERR 0 1 1 ISO 0.00 0.00 CLVD 0.00 0.00

Variance reduction 89.4



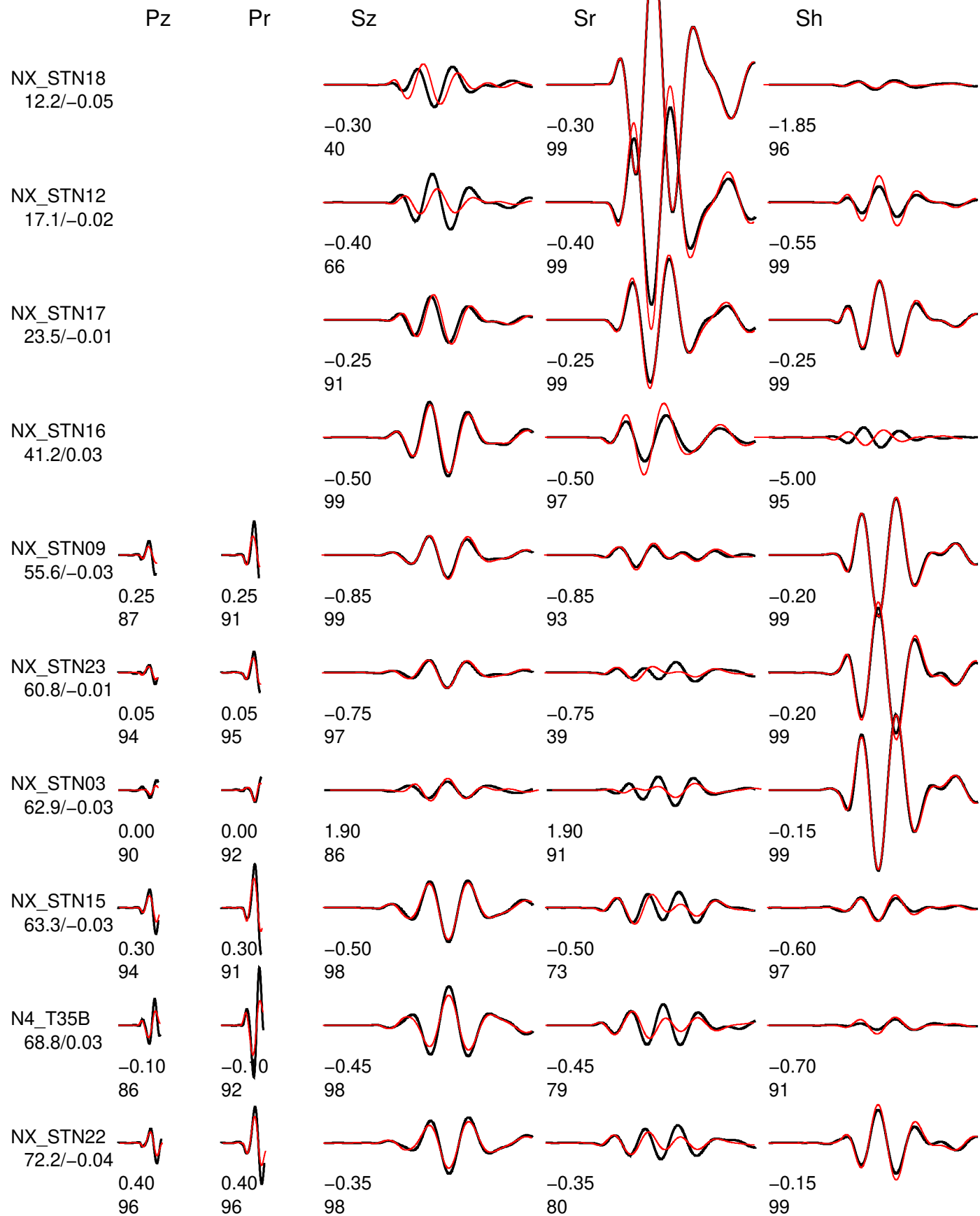
B.4 Inversion Result at depth of 5km

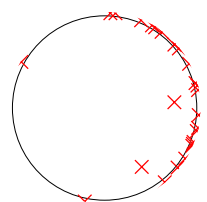


Event data Model and Depth chelsea_5

FM 144 90 12 Mw 3.75 rms 7.231e-06 1396 ERR 0 1 1 ISO 0.00 0.00 CLVD 0.00 0.00

Variance reduction 87.5

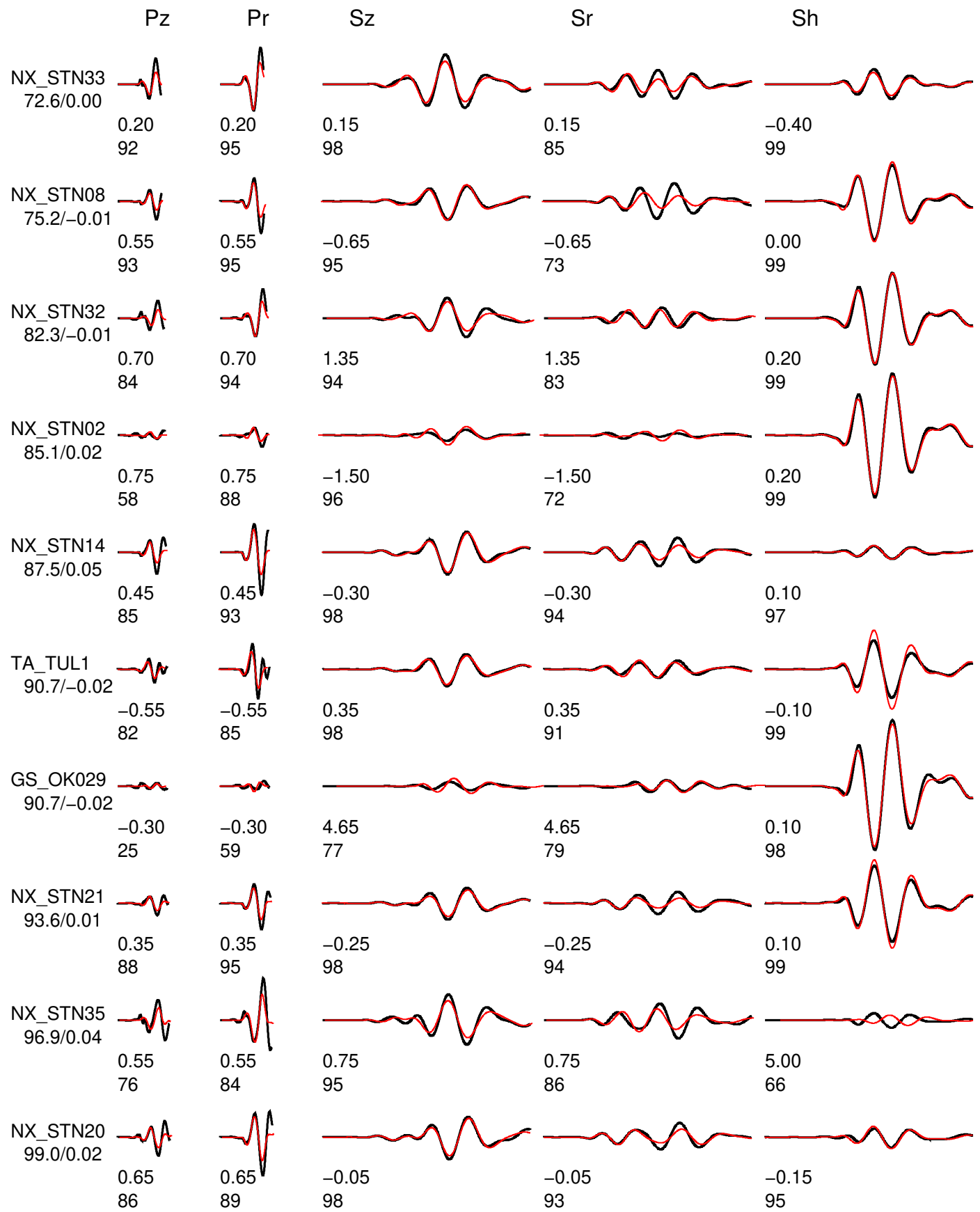


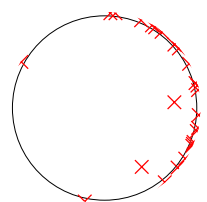


Event data Model and Depth chelsea_5

FM 144 90 12 Mw 3.75 rms 7.231e-06 1396 ERR 0 1 1 ISO 0.00 0.00 CLVD 0.00 0.00

Variance reduction 87.5

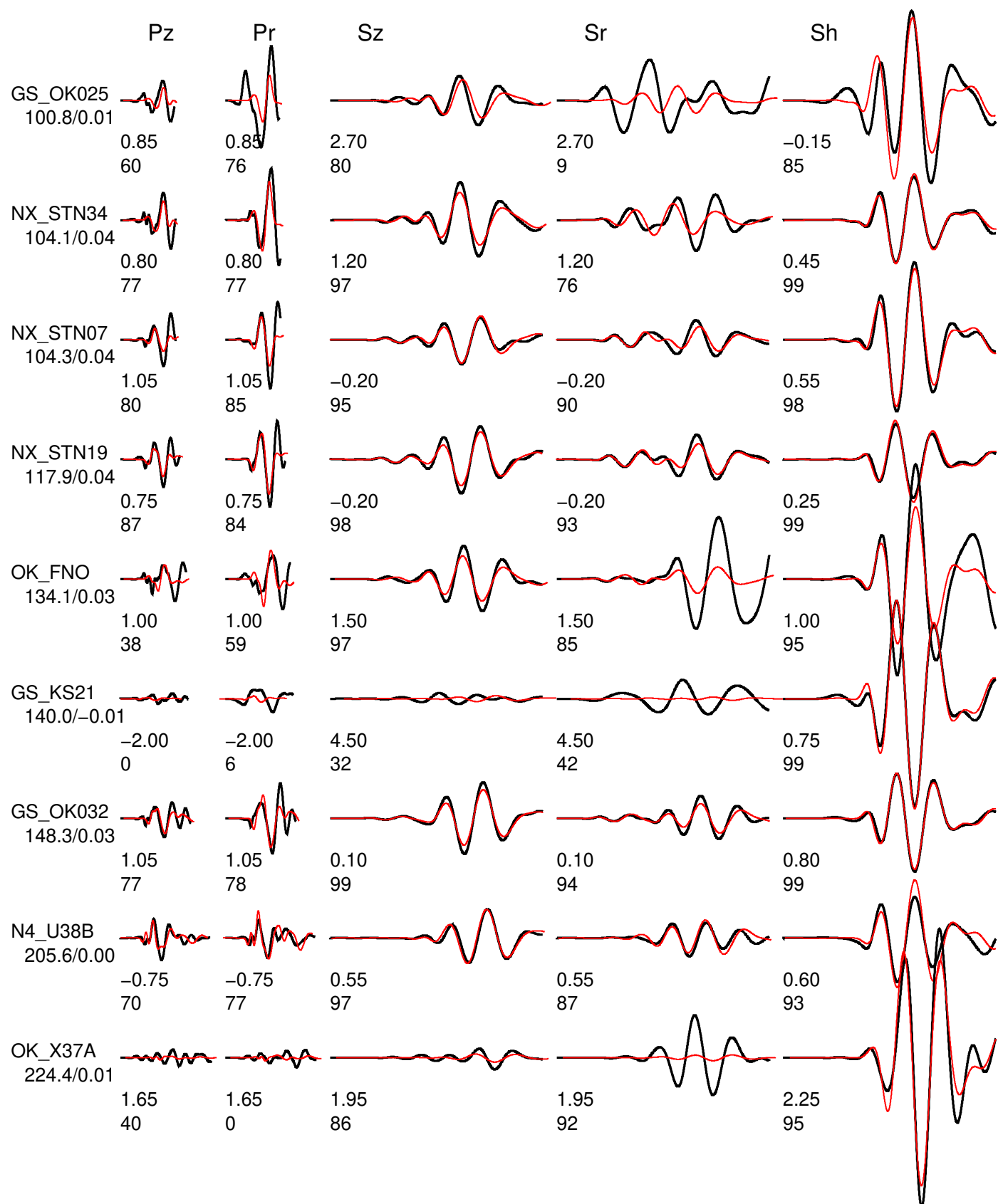




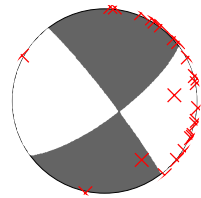
Event data Model and Depth chelsea_5

FM 144 90 12 Mw 3.75 rms 7.231e-06 1396 ERR 0 1 1 ISO 0.00 0.00 CLVD 0.00 0.00

Variance reduction 87.5



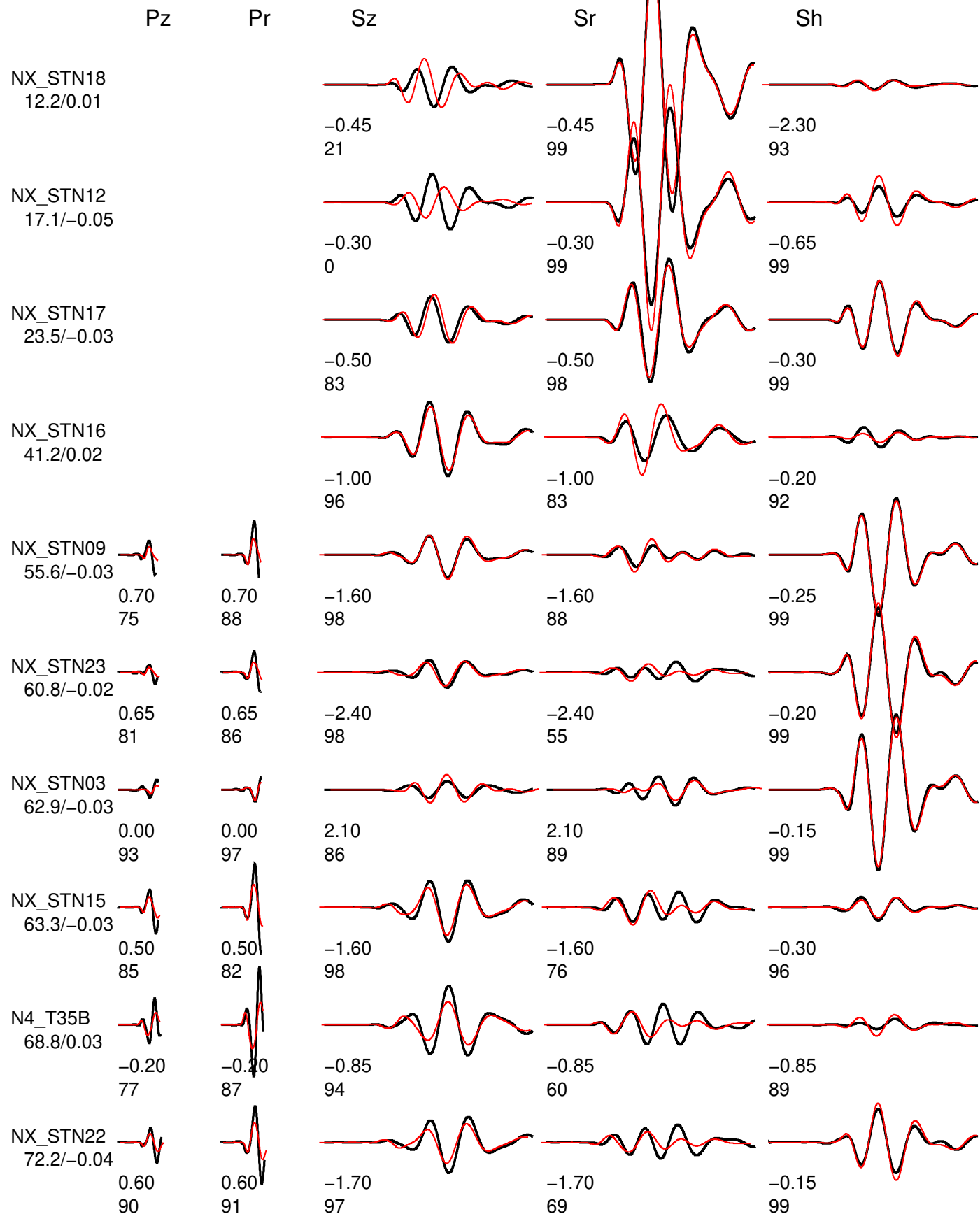
B.5 Inversion Result at depth of 6km

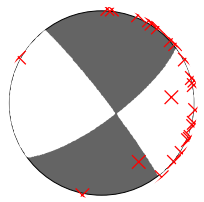


Event data Model and Depth chelsea_6

FM 322 86 -15 Mw 3.76 rms 9.598e-06 1396 ERR 0 1 1 ISO 0.00 0.00 CLVD 0.00 0.00

Variance reduction 83.4

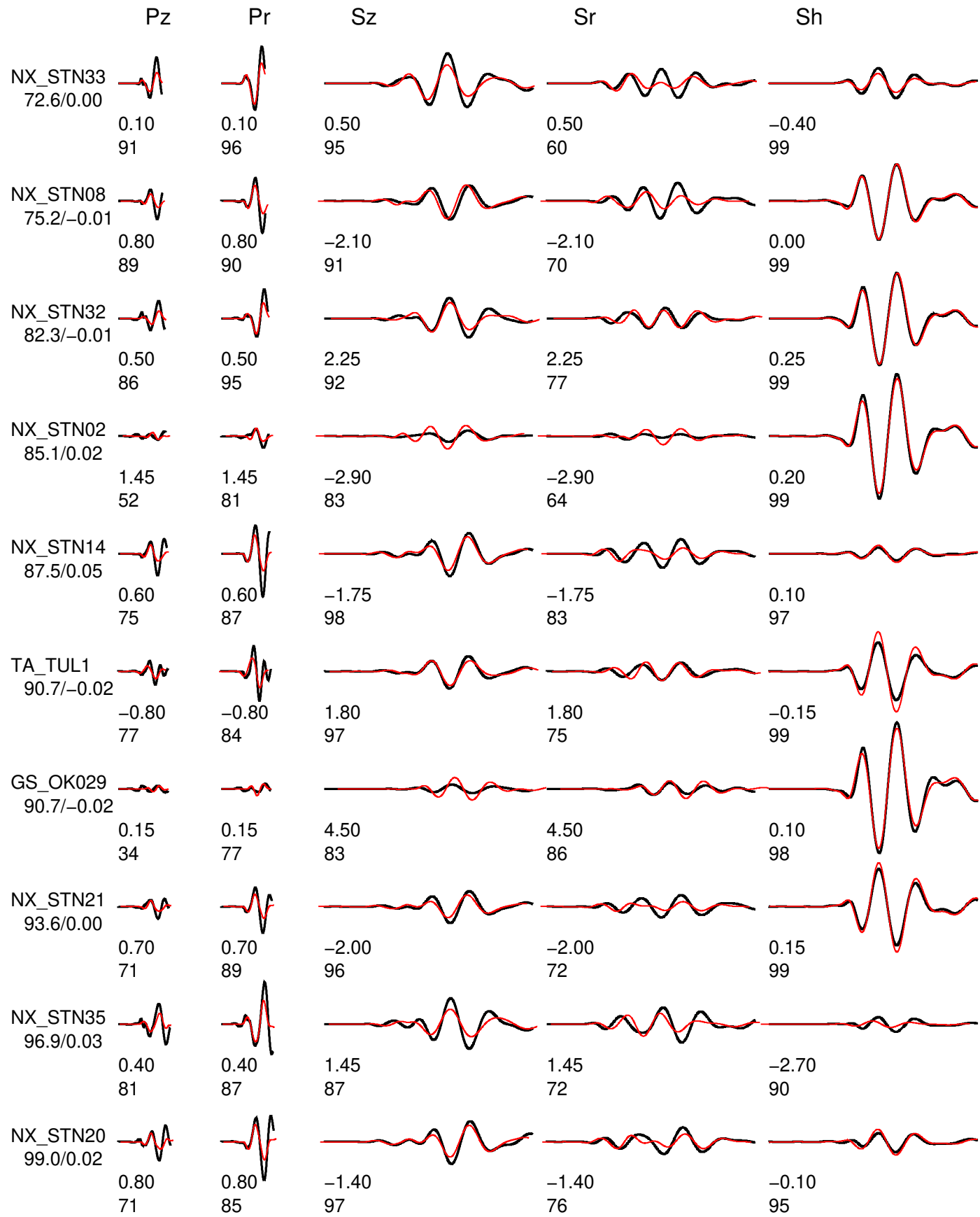


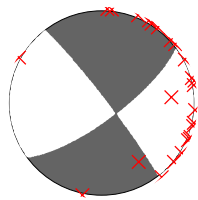


Event data Model and Depth chelsea_6

FM 322 86 -15 Mw 3.76 rms 9.598e-06 1396 ERR 0 1 1 ISO 0.00 0.00 CLVD 0.00 0.00

Variance reduction 83.4

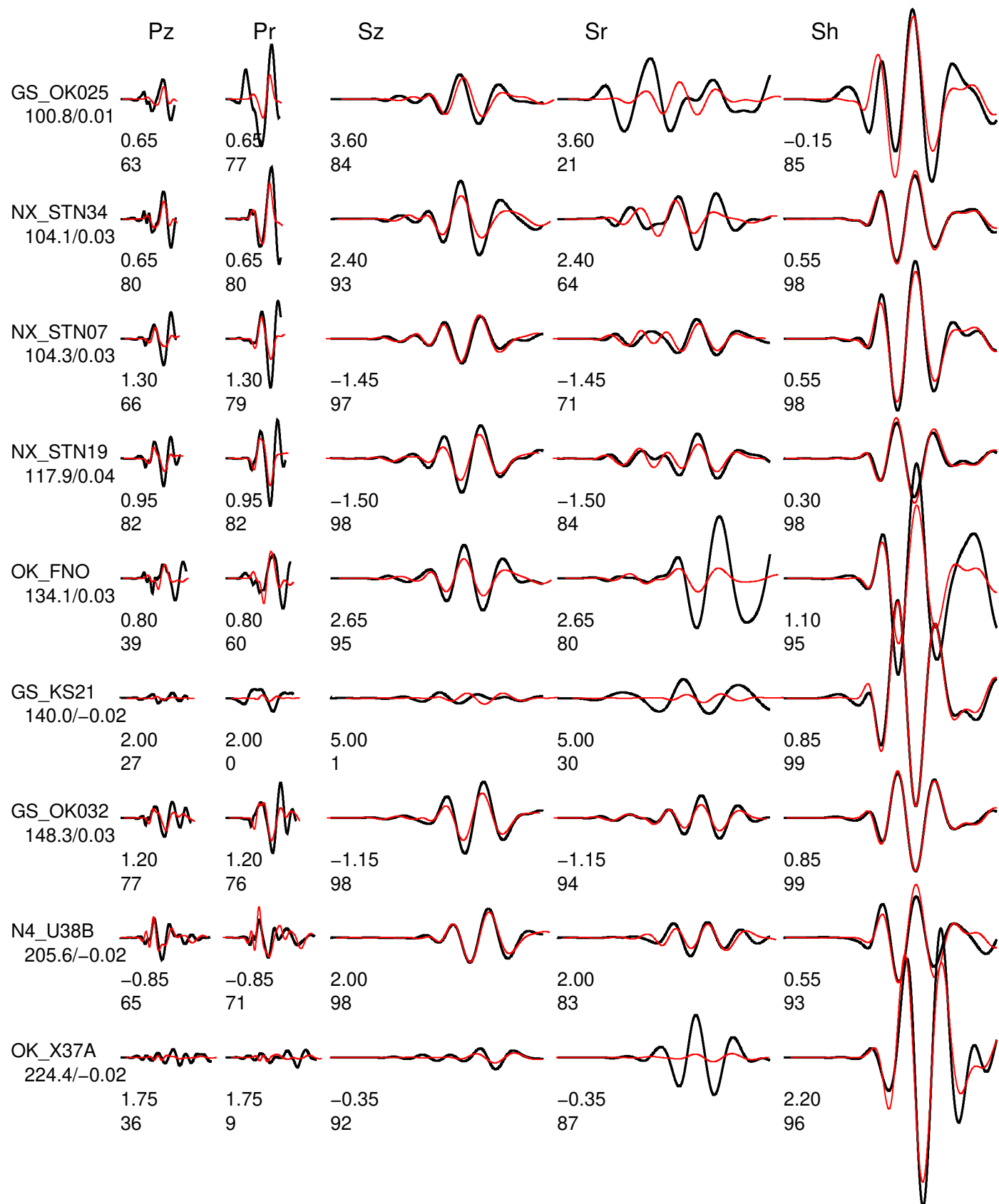




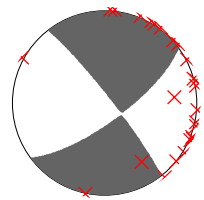
Event data Model and Depth chelsea_6

FM 322 86 -15 Mw 3.76 rms 9.598e-06 1396 ERR 0 1 1 ISO 0.00 0.00 CLVD 0.00 0.00

Variance reduction 83.4



B.6 Inversion Result at depth of 7km



Event data Model and Depth chelsea_7

FM 322 84 -17 Mw 3.76 rms 1.158e-05 1396 ERR 0 1 1 ISO 0.00 0.00 CLVD 0.00 0.00

Variance reduction 79.9

Pz

Pr

Sz

Sr

Sh

NX_STN18
12.2/0.05

-0.65
12

-0.65
99

-2.50
92

NX_STN12
17.1/0.01

-0.40
0

-0.40
99

-0.85
99

NX_STN17
23.5/0.04

-0.70
76

-0.70
97

-0.50
99

NX_STN16
41.2/0.00

-1.15
94

-1.15
75

-0.15
93

NX_STN09
55.6/-0.04

0.85
71

0.85
89

-0.25
99

NX_STN23
60.8/-0.03

0.75
79

0.75
85

-0.25
99

NX_STN03
62.9/-0.04

0.00
89

0.00
96

-0.20
99

NX_STN15
63.3/-0.04

0.60
78

0.60
75

-0.30
96

N4_T35B
68.8/0.02

-0.30
65

-0.30
77

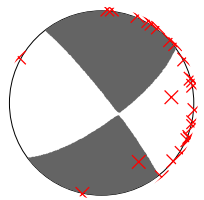
-0.80
89

NX_STN22
72.2/0.05

0.55
83

0.55
86

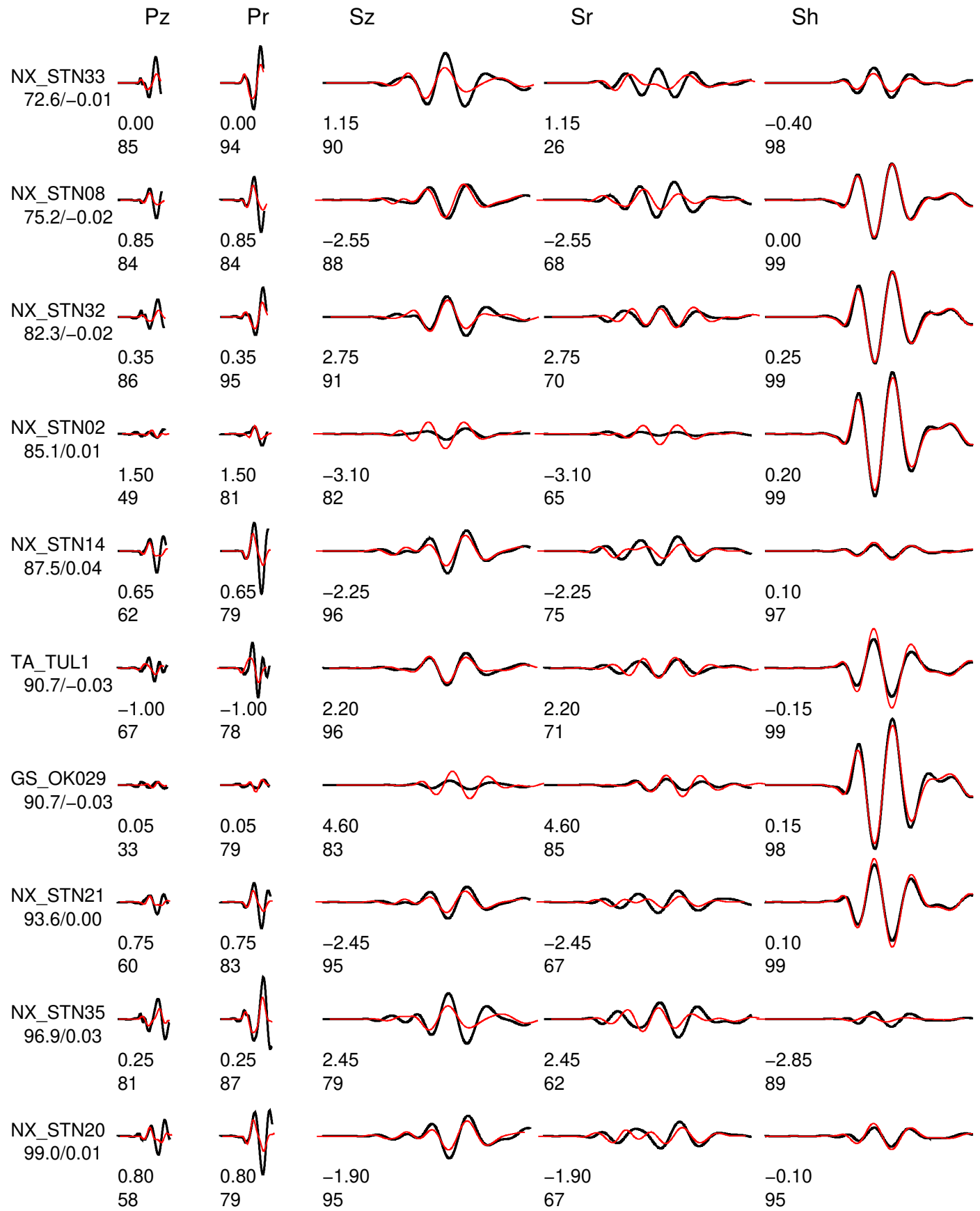
-0.25
99

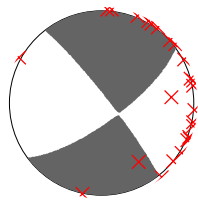


Event data Model and Depth chelsea_7

FM 322 84 -17 Mw 3.76 rms 1.158e-05 1396 ERR 0 1 1 ISO 0.00 0.00 CLVD 0.00 0.00

Variance reduction 79.9

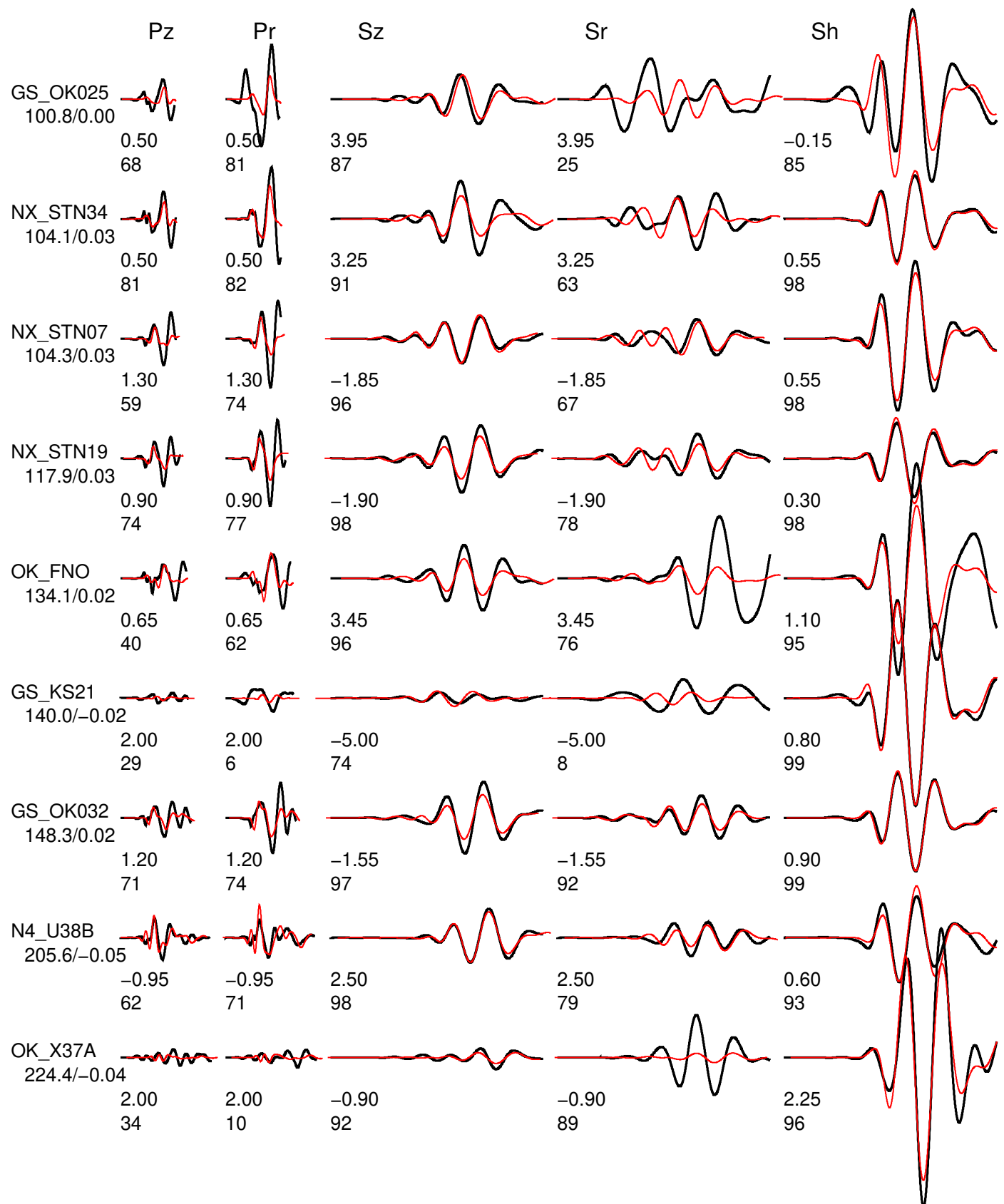




Event data Model and Depth chelsea_7

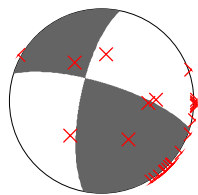
FM 322 84 -17 Mw 3.76 rms 1.158e-05 1396 ERR 0 1 1 ISO 0.00 0.00 CLVD 0.00 0.00

Variance reduction 79.9



C. Full Inversion Result on 2016-09-03 (mainshock M5.8)

C.1 Inversion Result at depth of 2km



Event data Model and Depth chelsea_2

FM 287 74 20 Mw 5.65 rms 7.834e+00 1466 ERR 0 1 2 ISO 0.00 0.00 CLVD 0.00 0.00

Variance reduction 77.2

Pz

Pr

Sz

Sr

Sh

GS_OK034
50.0/-0.00



	Pz	Pr	Sz	Sr	Sh
0.20	96		0.20	42	0.60
					99

GS_OK030
56.7/-0.00



	Pz	Pr	Sz	Sr	Sh
0.30	88		0.30	25	0.70
					99

N4_T35B
66.0/-0.00



	Pz	Pr	Sz	Sr	Sh
-0.55	94		-0.55	16	0.60
					99

GS_KAN13
81.6/-0.00



	Pz	Pr	Sz	Sr	Sh
0.35	87		0.35	80	1.15
					99

GS_OK029
84.3/-0.00



	Pz	Pr	Sz	Sr	Sh
0.50	68		0.50	86	1.40
					99

GS_KAN09
100.1/-0.00



	Pz	Pr	Sz	Sr	Sh
1.50	87		0.70	77	0.70
					53
					1.35
					99

GS_KS20
105.3/-0.00



	Pz	Pr	Sz	Sr	Sh
1.50	87		1.05	77	1.05
					55
					1.70
					93

GS_KAN01
109.6/-0.00



	Pz	Pr	Sz	Sr	Sh
1.55	84		1.15	78	1.15
					50
					1.20
					99

GS_KAN14
109.6/-0.00

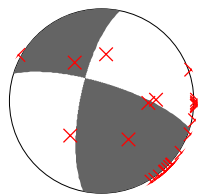


	Pz	Pr	Sz	Sr	Sh
1.50	80		1.70	72	1.70
					36
					1.25
					99

GS_KAN05
113.3/-0.00



	Pz	Pr	Sz	Sr	Sh
1.65	84		2.00	82	2.00
					58
					1.40
					99



Event data Model and Depth chelsea_2

FM 287 74 20 Mw 5.65 rms 7.834e+00 1466 ERR 0 1 2 ISO 0.00 0.00 CLVD 0.00 0.00

Variance reduction 77.2

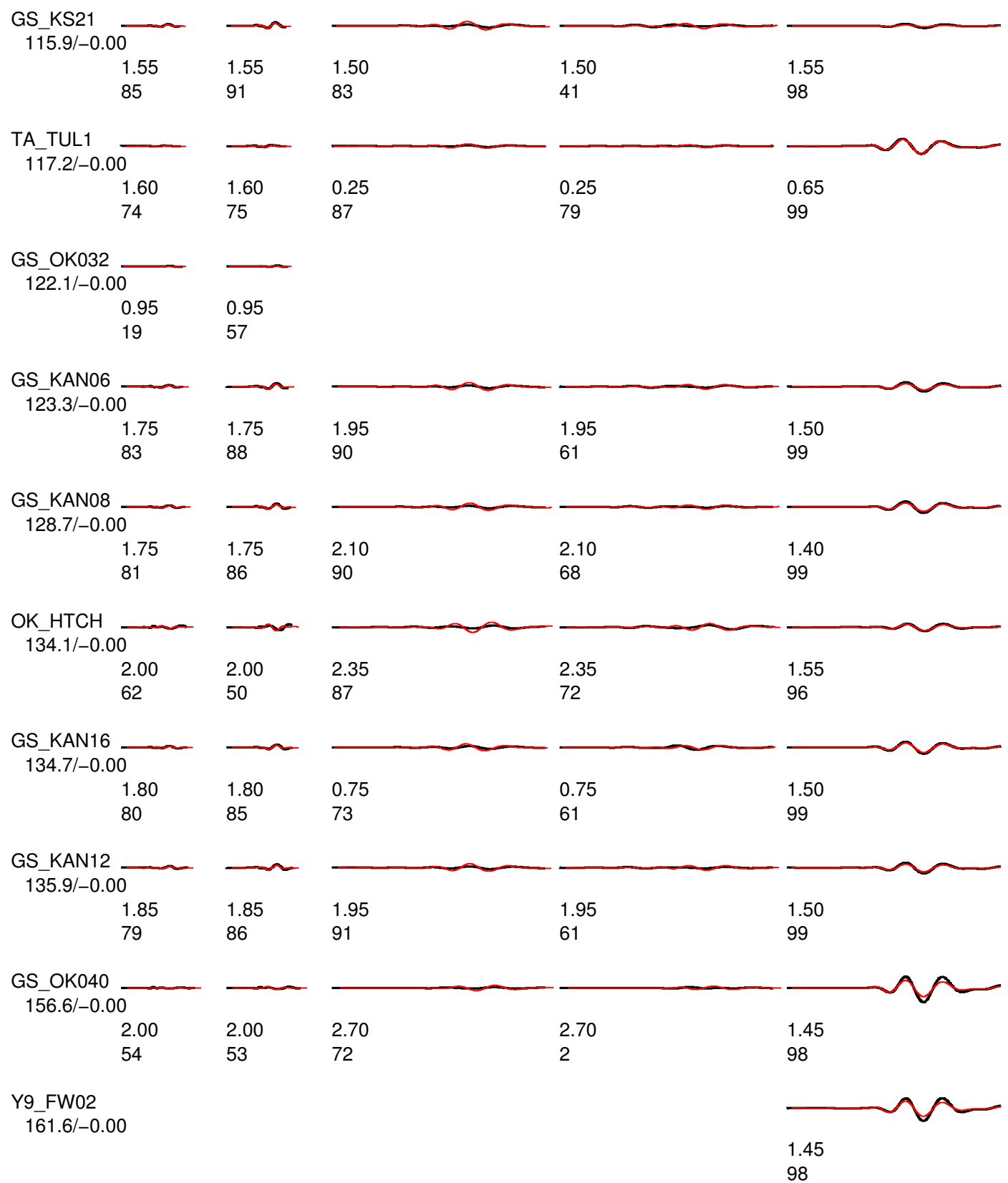
Pz

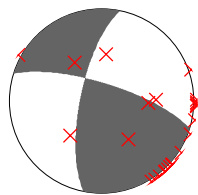
Pr

Sz

Sr

Sh

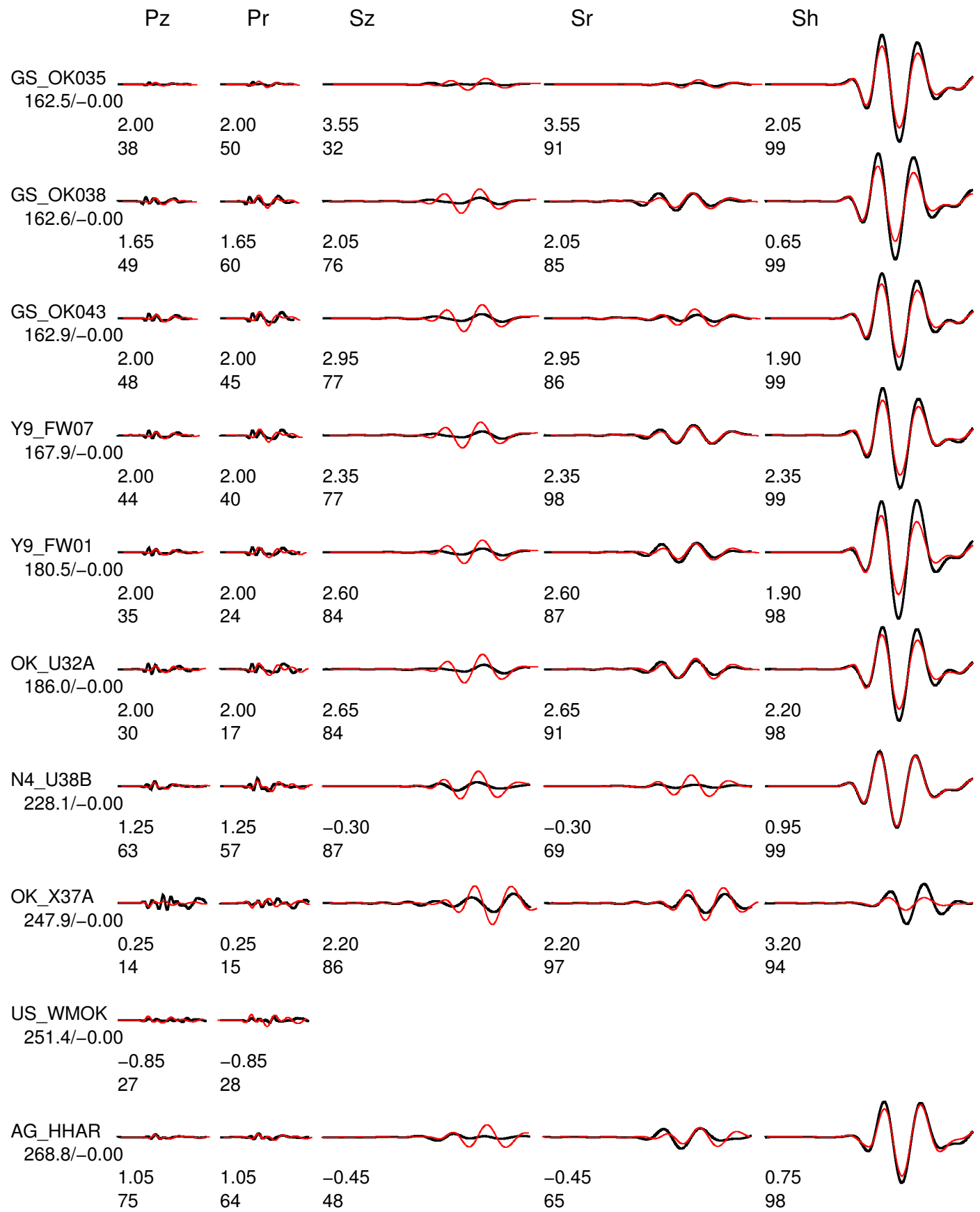


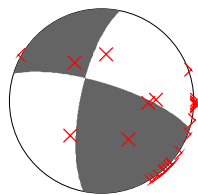


Event data Model and Depth chelsea_2

FM 287 74 20 Mw 5.65 rms 7.834e+00 1466 ERR 0 1 2 ISO 0.00 0.00 CLVD 0.00 0.00

Variance reduction 77.2





Event data Model and Depth chelsea_2

FM 287 74 20 Mw 5.65 rms 7.834e+00 1466 ERR 0 1 2 ISO 0.00 0.00 CLVD 0.00 0.00

Variance reduction 77.2

Pz

Pr

Sz

Sr

Sh

N4_R32B

272.1/-0.00

2.00 2.00 2.95
50 34 85

2.95
95

US_KSU1

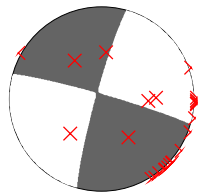
298.3/-0.00

1.40 1.40 2.95
45 33 89

2.95
93

2.30
99

C.2 Inversion Result at depth of 3km



Event data Model and Depth chelsea_3

FM 286 86 5 Mw 5.65 rms 6.098e+00 1465 ERR 0 1 2 ISO 0.00 0.00 CLVD 0.00 0.00

Variance reduction 82.2

Pz

Pr

Sz

Sr

Sh

GS_OK034
50.0/-0.00



0.35	0.35	0.50
97	65	99

GS_OK030
56.7/-0.00



0.45	0.45	0.65
90	39	99

N4_T35B
66.0/-0.00



-0.65	-0.65	0.55
94	27	99

GS_KAN13
81.6/-0.00



0.40	0.40	1.15
90	83	99

GS_OK029
84.3/-0.00



0.65	0.65	1.35
72	88	99

GS_KAN09
100.1/-0.00

1.45
90



0.75	0.75	1.35
81	60	99

GS_KS20
105.3/-0.00

1.45
90



1.05	1.05	1.70
81	64	94

GS_KAN01
109.6/-0.00

1.50
87



1.15	1.15	1.25
82	60	99

GS_KAN14
109.6/-0.00

1.50
85



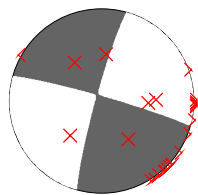
1.55	1.55	1.30
75	50	99

GS_KAN05
113.3/-0.00

1.65
86



1.90	1.90	1.45
85	68	99



Event data Model and Depth chelsea_3

FM 286 86 5 Mw 5.65 rms 6.098e+00 1465 ERR 0 1 2 ISO 0.00 0.00 CLVD 0.00 0.00

Variance reduction 82.2

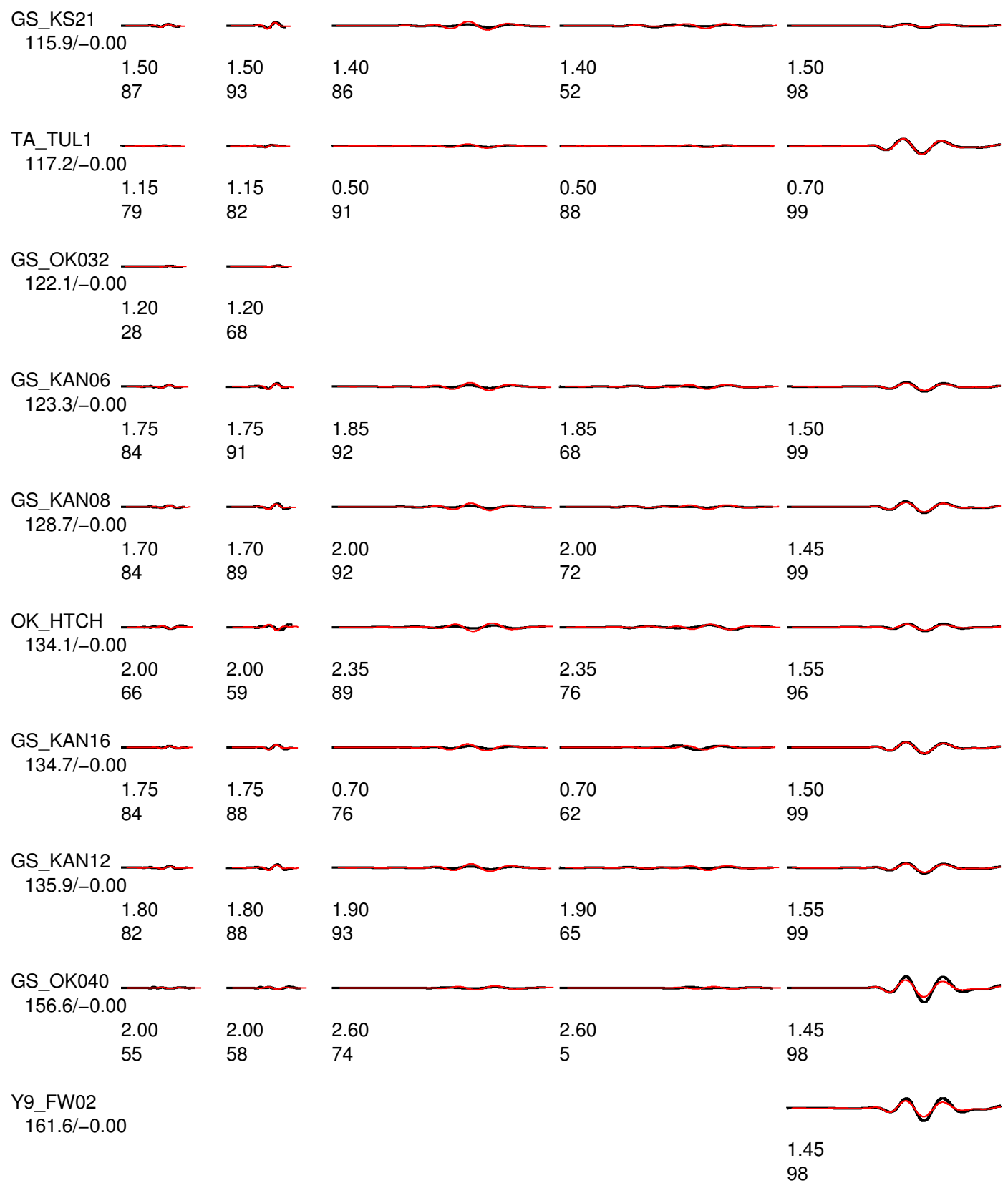
Pz

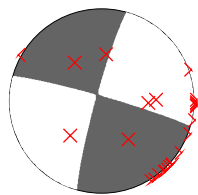
Pr

Sz

Sr

Sh

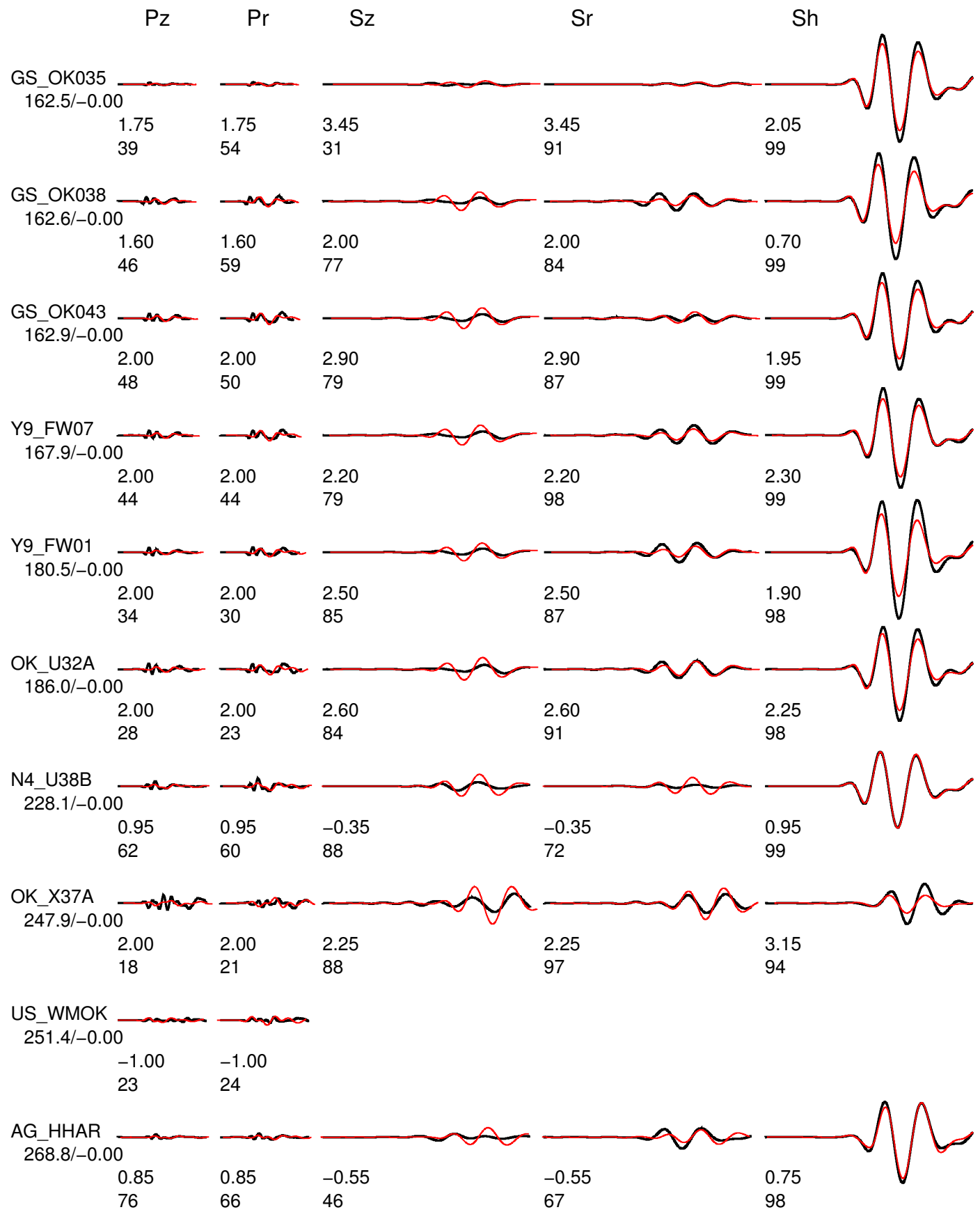


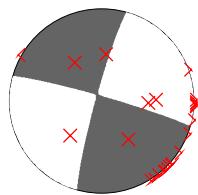


Event data Model and Depth chelsea_3

FM 286 86 5 Mw 5.65 rms 6.098e+00 1465 ERR 0 1 2 ISO 0.00 0.00 CLVD 0.00 0.00

Variance reduction 82.2





Event data Model and Depth chelsea_3

FM 286 86 5 Mw 5.65 rms 6.098e+00 1465 ERR 0 1 2 ISO 0.00 0.00 CLVD 0.00 0.00

Variance reduction 82.2

Pz

Pr

Sz

Sr

Sh

N4_R32B

272.1/-0.00

2.00 2.00 2.85
52 42 88

2.85
95

US_KSU1

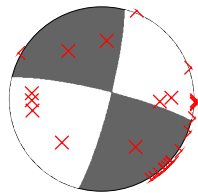
298.3/-0.00

1.55 1.55 2.40
51 48 94

2.40
94

2.35
99

C.3 Inversion Result at depth of 4km



Event data Model and Depth chelsea_4

FM 283 82 -7 Mw 5.69 rms 6.975e+00 1719 ERR 0 1 2 ISO 0.00 0.00 CLVD 0.00 0.00

Variance reduction 83.8

Pz

Pr

Sz

Sr

Sh

GS_OK034
50.0/0.02



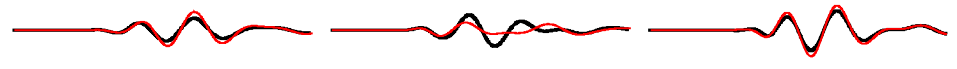
0.45	0.45	0.55
99	92	99

GS_OK031
53.0/0.05



0.75	0.75	1.05
98	87	95

GS_OK030
56.7/0.02



0.40	0.40	0.60
98	58	99

N4_T35B
66.0/0.01



0.15	0.15	0.60
98	79	99

GS_KAN13
81.6/0.00



0.20	0.20	1.55
93	86	99

GS_OK029
84.3/-0.02



0.00	0.00	1.30
78	75	99

GS_KAN09
100.1/-0.03



1.55	1.55	0.75	0.75	1.75
92	95	88	69	98

GS_OK025
100.6/0.01



2.00	2.00	1.45	1.45	1.85
84	82	94	64	94

GS_KS20
105.3/-0.02

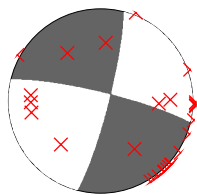


1.55	1.55	0.90	0.90	-5.00
91	95	88	75	87

GS_KAN01
109.6/0.00



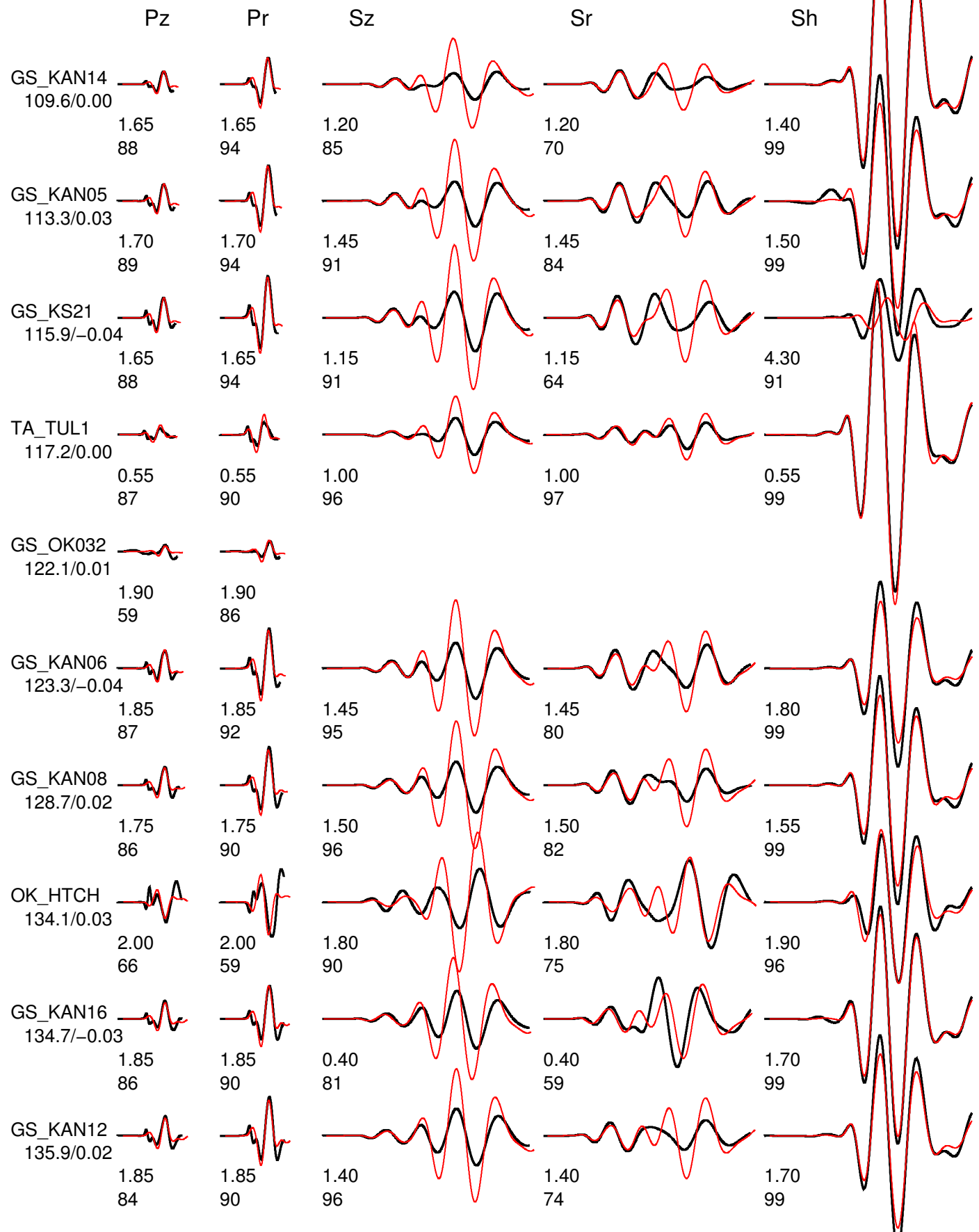
1.55	1.55	1.00	1.00	1.45
90	94	89	72	99

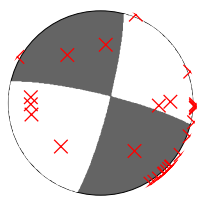


Event data Model and Depth chelsea_4

FM 283 82 -7 Mw 5.69 rms 6.975e+00 1719 ERR 0 1 2 ISO 0.00 0.00 CLVD 0.00 0.00

Variance reduction 83.8





Event data Model and Depth chelsea_4

FM 283 82 -7 Mw 5.69 rms 6.975e+00 1719 ERR 0 1 2 ISO 0.00 0.00 CLND 0.00 0.00

Variance reduction 83.8

Pz

Pr

Sz

Sr

Sh

GS_OK040
156.6/0.02

2.00
43

2.00
44

2.05
65

2.05
22

1.60
98

Y9_FW02
161.6/0.03

1.60
98

GS_OK035
162.5/0.03

-2.00
0

-2.00
0

1.95
3

1.95
66

2.20
99

GS_OK038
162.6/-0.02

2.00
51

2.00
61

0.90
76

0.90
91

0.85
99

GS_OK043
162.9/-0.02

2.00
37

2.00
37

2.10
78

2.10
92

2.15
98

Y9_FW07
167.9/-0.01

2.00
33

2.00
31

1.25
76

1.25
98

2.50
99

Y9_FW01
180.5/0.01

0.35
25

0.35
17

1.50
82

1.50
93

2.15
98

OK_U32A
186.0/0.00

0.40
27

0.40
23

1.75
84

1.75
94

2.40
98

Y9_FW09
189.7/0.05

0.25
22

0.25
27

0.70
75

0.70
90

0.70
92

OK_ELIS
227.2/0.02

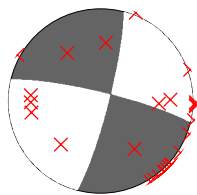
1.00
28

1.00
33

3.70
74

3.70
84

2.75
84



Event data Model and Depth chelsea_4

FM 283 82 -7 Mw 5.69 rms 6.975e+00 1719 ERR 0 1 2 ISO 0.00 0.00 CLVD 0.00 0.00

Variance reduction 83.8

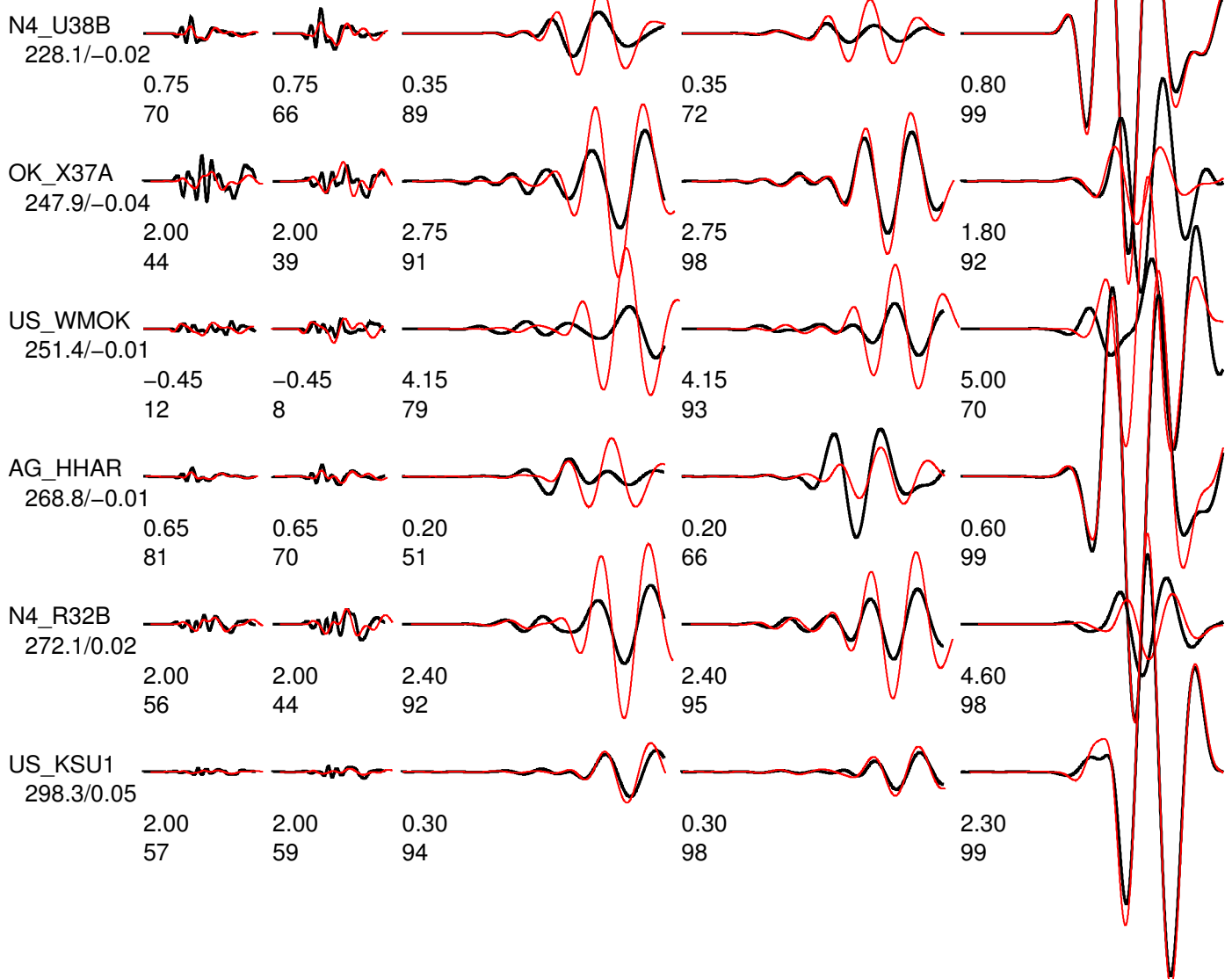
Pz

Pr

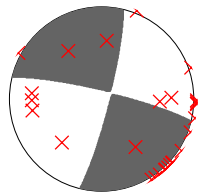
Sz

Sr

Sh



C.4 Inversion Result at depth of 5km



Event data Model and Depth chelsea_5

FM 283 83 -7 Mw 5.70 rms 5.562e+00 1719 ERR 0 1 2 ISO 0.00 0.00 CLVD 0.00 0.00

Variance reduction 87.1

Pz

Pr

Sz

Sr

Sh

GS_OK034
50.0/0.01



GS_OK031
53.0/0.04



GS_OK030
56.7/0.02



N4_T35B
66.0/0.00



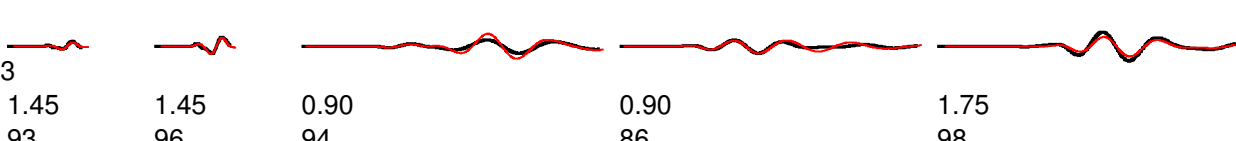
GS_KAN13
81.6/-0.01



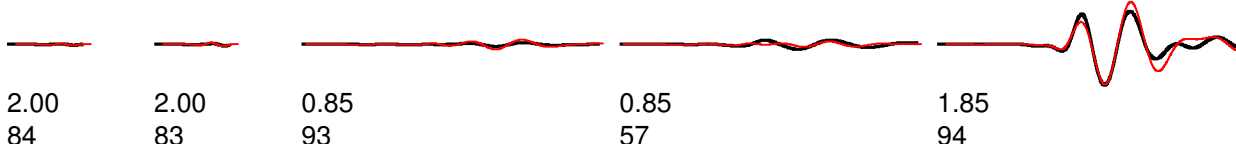
GS_OK029
84.3/-0.02



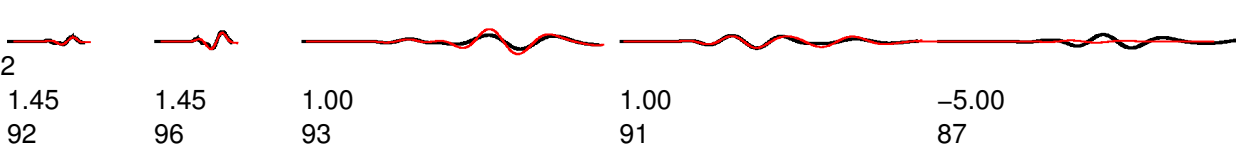
GS_KAN09
100.1/-0.03



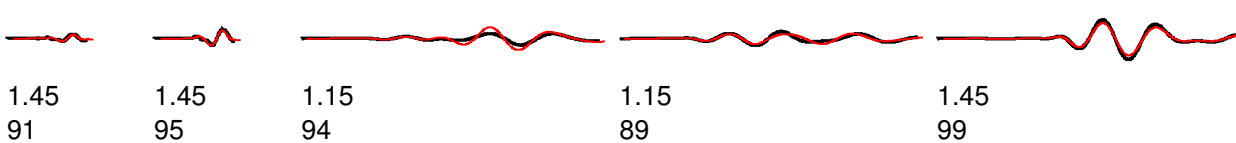
GS_OK025
100.6/0.01

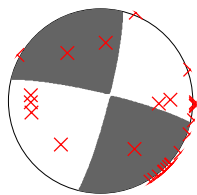


GS_KS20
105.3/-0.02



GS_KAN01
109.6/0.00

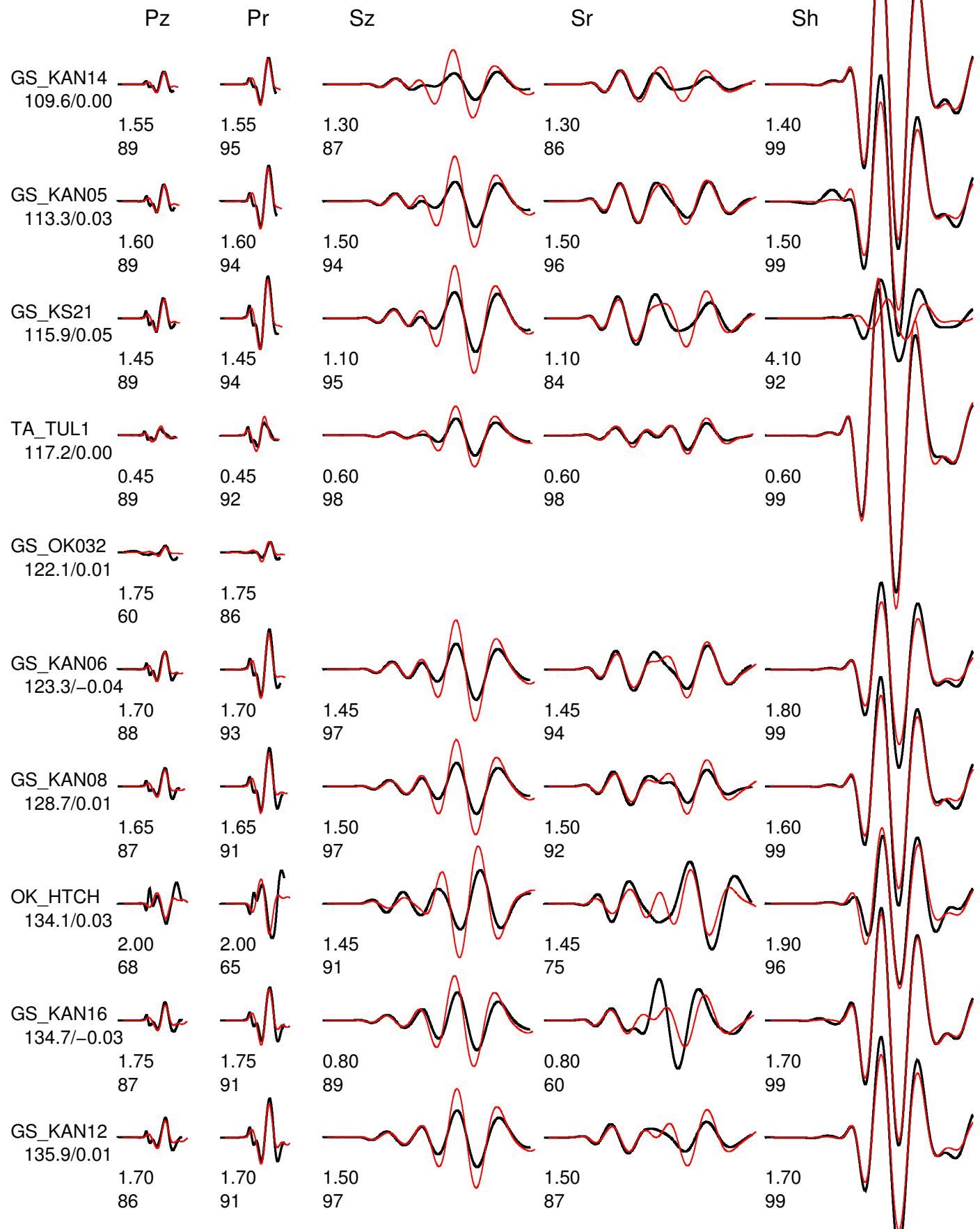


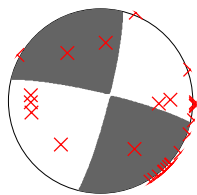


Event data Model and Depth chelsea_5

FM 283 83 -7 Mw 5.70 rms 5.562e+00 1719 ERR 0 1 2 ISO 0.00 0.00 CLVD 0.00 0.00

Variance reduction 87.1





Event data Model and Depth chelsea_5

FM 283 83 -7 Mw 5.70 rms 5.562e+00 1719 ERR 0 1 2 ISO 0.00 0.00 CLMD 0.00 0.00

Variance reduction 87.1

Pz

Pr

Sz

Sr

Sh

GS_OK040
156.6/0.02

2.00
41

2.00
42

1.80
59

1.80
26

1.60
98

Y9_FW02
161.6/0.03

1.60
98

GS_OK035
162.5/0.03

-2.00
0

-2.00
0

2.15
7

2.15
70

2.20
99

GS_OK038
162.6/-0.02

2.00
52

2.00
61

0.45
73

0.45
94

0.90
99

GS_OK043
162.9/-0.02

2.00
34

2.00
37

1.65
76

1.65
91

2.15
98

Y9_FW07
167.9/-0.01

2.00
29

2.00
29

0.85
74

0.85
97

2.55
99

Y9_FW01
180.5/0.01

0.40
27

0.40
18

1.15
79

1.15
95

2.15
98

OK_U32A
186.0/-0.03

0.55
32

0.55
28

1.35
83

1.35
95

2.45
98

Y9_FW09
189.7/0.02

0.30
21

0.30
27

0.35
73

0.35
91

0.75
92

OK_ELIS
227.2/-0.01

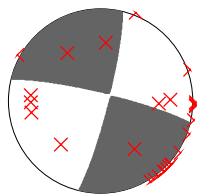
1.15
38

1.15
39

3.35
75

3.35
85

2.75
85



Event data Model and Depth chelsea_5

FM 283 83 -7 Mw 5.70 rms 5.562e+00 1719 ERR 0 1 2 ISO 0.00 0.00 CLVD 0.00 0.00

Variance reduction 87.1

Pz

Pr

Sz

Sr

Sh

N4_U38B
228.1/-0.04

0.60
75

0.60
71

0.80
89

0.80
68

0.80
99

OK_X37A
247.9/-0.04

1.80
46

1.80
43

2.70
94

2.70
98

1.75
91

US_WMOK
251.4/-0.01

-0.10
13

-0.10
0

3.80
82

3.80
92

5.00
70

AG_HHAR
268.8/-0.01

0.45
81

0.45
73

0.65
53

0.65
63

0.60
98

N4_R32B
272.1/0.02

2.00
54

2.00
49

2.35
96

2.35
95

4.75
98

US_KSU1
298.3/0.04

2.00
52

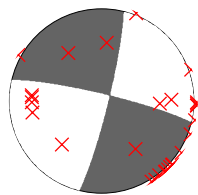
2.00
58

-0.15
93

-0.15
98

2.30
99

C.5 Inversion Result at depth of 6km



Event data Model and Depth chelsea_6

FM 283 84 -6 Mw 5.71 rms 5.082e+00 1719 ERR 0 1 1 ISO 0.00 0.00 CLVD 0.00 0.00

Variance reduction 88.2

Pz

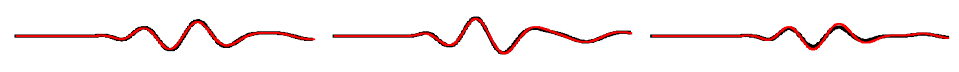
Pr

Sz

Sr

Sh

GS_OK034
50.0/0.01



	Pz	Pr	Sz	Sr	Sh
0.35	99		0.35	99	0.45
					99

GS_OK031
53.0/0.04



	Pz	Pr	Sz	Sr	Sh
1.40	96		1.40	88	1.00
					95

GS_OK030
56.7/0.01



	Pz	Pr	Sz	Sr	Sh
0.05	96		0.05	84	0.55
					99

N4_T35B
66.0/0.00



	Pz	Pr	Sz	Sr	Sh
0.85	98		0.85	89	0.55
					99

GS_KAN13
81.6/-0.01



	Pz	Pr	Sz	Sr	Sh
0.70	99		0.70	98	1.40
					99

GS_OK029
84.3/-0.03



	Pz	Pr	Sz	Sr	Sh
-0.40	83		-0.40	45	1.25
					99

GS_KAN09
100.1/-0.04



	Pz	Pr	Sz	Sr	Sh
1.35	92		1.35	98	1.70
					98

GS_OK025
100.6/0.01



	Pz	Pr	Sz	Sr	Sh
2.00	82		2.00	83	1.85
					94

GS_KS20
105.3/-0.02

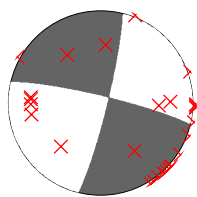


	Pz	Pr	Sz	Sr	Sh
1.35	91		1.35	96	-5.00
					86

GS_KAN01
109.6/-0.01



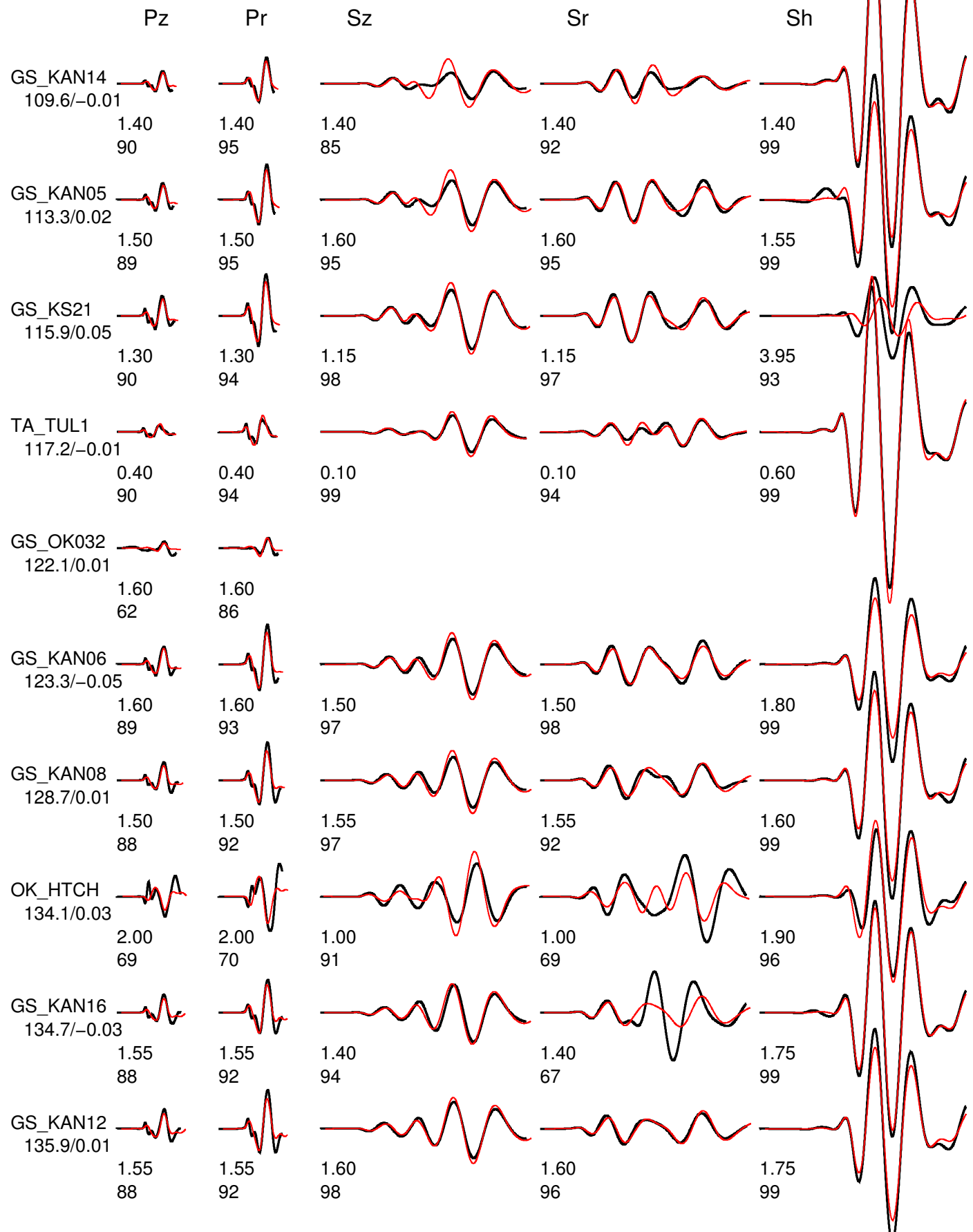
	Pz	Pr	Sz	Sr	Sh
1.35	91		1.35	95	1.45
					99

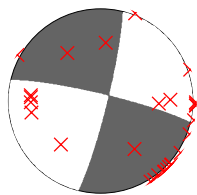


Event data Model and Depth chelsea_6

FM 283 84 -6 Mw 5.71 rms 5.082e+00 1719 ERR 0 1 1 ISO 0.00 0.00 CLVD 0.00 0.00

Variance reduction 88.2





Event data Model and Depth chelsea_6

FM 283 84 -6 Mw 5.71 rms 5.082e+00 1719 ERR 0 1 1 ISO 0.00 0.00 CLMD 0.00 0.00

Variance reduction 88.2

Pz

Pr

Sz

Sr

Sh

GS_OK040
156.6/0.02

2.00
38

2.00
40

1.55
54

1.55
25

1.60
98

Y9_FW02
161.6/0.03

1.65
98

GS_OK035
162.5/0.03

2.00
6

2.00
0

2.25
9

2.25
72

2.20
99

GS_OK038
162.6/-0.03

2.00
53

2.00
59

0.15
70

0.15
95

0.90
99

GS_OK043
162.9/-0.03

2.00
30

2.00
35

1.35
73

1.35
91

2.15
98

Y9_FW07
167.9/-0.01

2.00
25

2.00
28

0.50
72

0.50
97

2.55
99

Y9_FW01
180.5/-0.02

0.55
29

0.55
21

0.90
76

0.90
96

2.15
98

OK_U32A
186.0/0.05

0.55
38

0.55
33

0.90
82

0.90
97

2.35
98

Y9_FW09
189.7/-0.01

0.40
19

0.40
26

0.15
72

0.15
92

0.80
92

OK_ELIS
227.2/-0.03

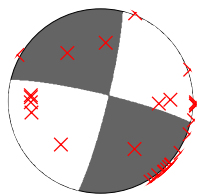
1.20
47

1.20
45

2.95
73

2.95
86

2.80
85



Event data Model and Depth chelsea_6

FM 283 84 -6 Mw 5.71 rms 5.082e+00 1719 ERR 0 1 1 ISO 0.00 0.00 CLVD 0.00 0.00

Variance reduction 88.2

Pz

Pr

Sz

Sr

Sh

N4_U38B
228.1/0.03

0.35
78

0.35
75

1.20
87

1.20
63

0.75
99

OK_X37A
247.9/-0.05

1.55
51

1.55
46

2.60
96

2.60
97

1.75
91

US_WMOK
251.4/-0.01

0.30
19

0.30
0

3.35
84

3.35
92

5.00
70

AG_HHAR
268.8/-0.01

0.30
83

0.30
76

1.05
54

1.05
59

0.55
98

N4_R32B
272.1/0.02

2.00
49

2.00
50

2.35
98

2.35
94

4.90
98

US_KSU1
298.3/0.04

2.00
45

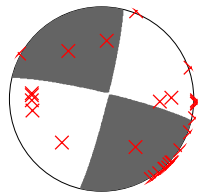
2.00
55

-0.70
90

-0.70
96

2.30
99

C.6 Inversion Result at depth of 7km



Event data Model and Depth chelsea_7

FM 283 84 -5 Mw 5.72 rms 5.207e+00 1719 ERR 0 1 1 ISO 0.00 0.00 CLVD 0.00 0.00

Variance reduction 87.9

Pz

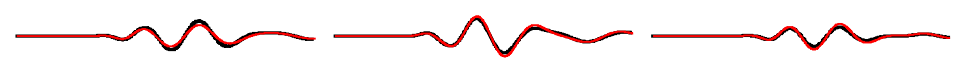
Pr

Sz

Sr

Sh

GS_OK034
50.0/-0.01



0.35
98

0.35
99

0.40
99

GS_OK031
53.0/0.02



1.70
94

1.70
88

0.95
95

GS_OK030
56.7/0.00



-0.15
88

-0.15
88

0.50
99

N4_T35B
66.0/-0.01



1.15
96

1.15
83

0.50
99

GS_KAN13
81.6/-0.02



1.05
98

1.05
87

1.40
99

GS_OK029
84.3/-0.03



-0.90
80

-0.90
25

1.25
99

GS_KAN09
100.1/-0.04



1.25
89

1.25
96

1.70
98

GS_OK025
100.6/0.00



2.00
79

2.00
81

1.85
94

GS_KS20
105.3/-0.03



1.25
88

1.25
95

-5.00
86

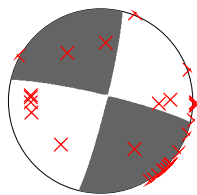
GS_KAN01
109.6/-0.01



1.20
90

1.20
94

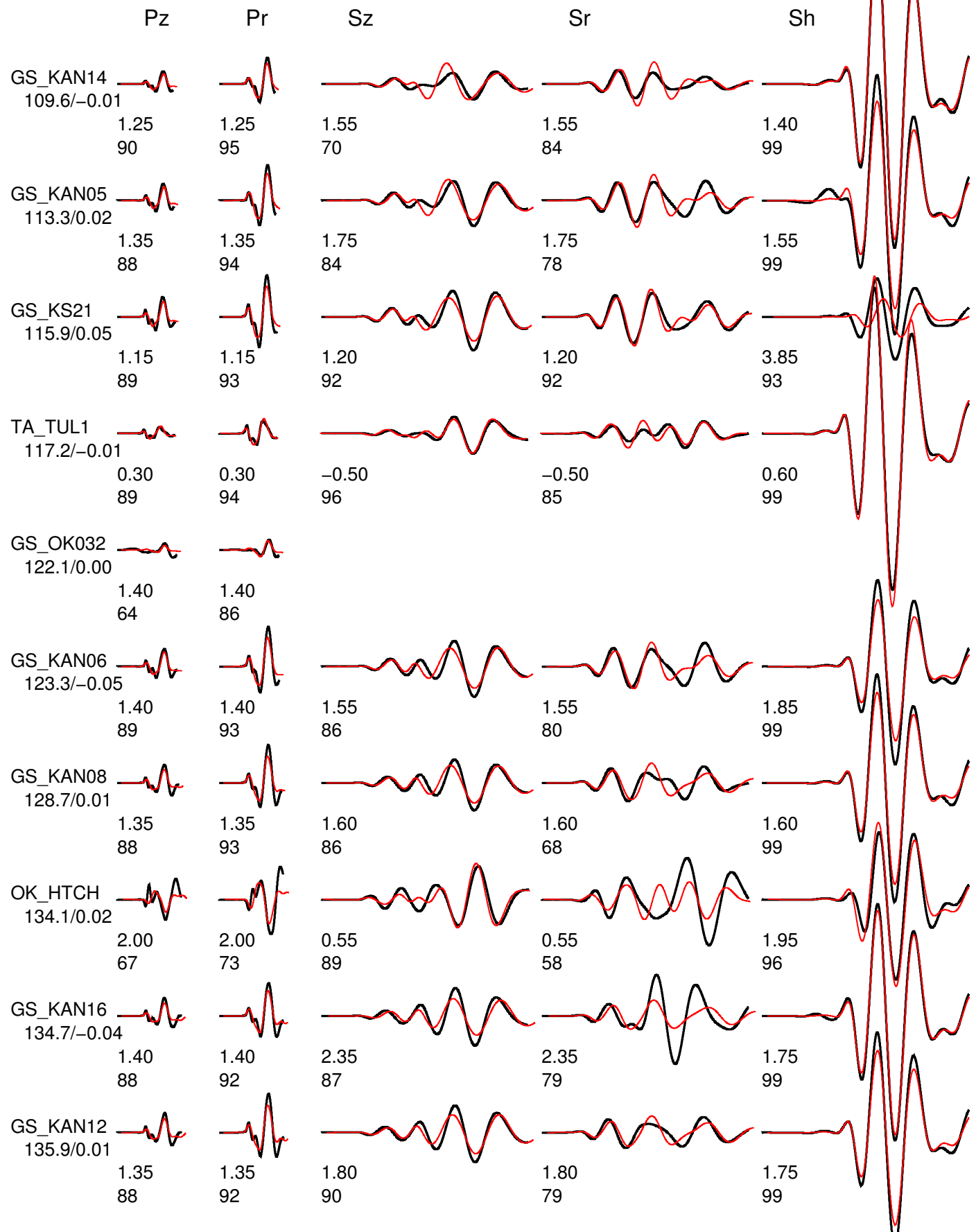
1.45
99

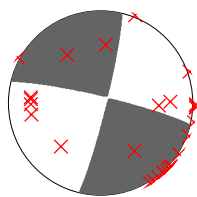


Event data Model and Depth chelsea_7

FM 283 84 -5 Mw 5.72 rms 5.207e+00 1719 ERR 0 1 1 ISO 0.00 0.00 CLVD 0.00 0.00

Variance reduction 87.9





Event data Model and Depth chelsea_7

FM 283 84 -5 Mw 5.72 rms 5.207e+00 1719 ERR 0 1 1 ISO 0.00 0.00 CLMD 0.00 0.00

Variance reduction 87.9

Pz

Pr

Sz

Sr

Sh

GS_OK040
156.6/0.01

2.00
35

2.00
38

1.40
49

1.40
25

1.65
98

Y9_FW02
161.6/0.03

1.65
98

GS_OK035
162.5/0.03

2.00
14

2.00
0

2.30
10

2.30
74

2.25
99

GS_OK038
162.6/-0.03

2.00
53

2.00
57

-0.05
67

-0.05
96

0.90
99

GS_OK043
162.9/-0.03

2.00
25

2.00
33

1.05
70

1.05
89

2.20
98

Y9_FW07
167.9/-0.02

2.00
20

2.00
25

0.25
69

0.25
96

2.60
99

Y9_FW01
180.5/-0.05

0.65
31

0.65
22

0.70
74

0.70
97

2.20
98

OK_U32A
186.0/0.02

0.65
43

0.65
38

0.65
79

0.65
98

2.40
98

Y9_FW09
189.7/-0.03

0.50
18

0.50
23

-0.05
72

-0.05
93

0.80
93

OK_ELIS
227.2/0.04

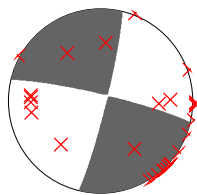
1.15
54

1.15
49

2.45
71

2.45
87

2.70
85



Event data Model and Depth chelsea_7

FM 283 84 -5 Mw 5.72 rms 5.207e+00 1719 ERR 0 1 1 ISO 0.00 0.00 CLVD 0.00 0.00

Variance reduction 87.9

Pz

Pr

Sz

Sr

Sh

N4_U38B
228.1/0.00

0.25
81

0.25
78

1.60
84

1.60
56

0.75
99

OK_X37A
247.9/-0.05

1.35
55

1.35
49

2.45
94

2.45
91

1.70
90

US_WMOK
251.4/-0.01

0.50
21

0.50
0

2.85
85

2.85
92

5.00
71

AG_HHAR
268.8/-0.01

0.10
83

0.10
78

1.35
54

1.35
55

0.55
98

N4_R32B
272.1/0.02

2.00
41

2.00
49

2.30
93

2.30
91

5.00
98

US_KSU1
298.3/0.04

2.00
36

2.00
51

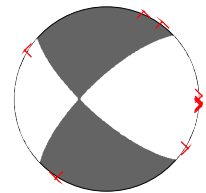
-1.10
87

-1.10
95

2.30
99

D. Full Inversion Result on 2016-09-03 (aftershock M3.7)

D.1 Inversion Result at depth of 2km



Event data Model and Depth chelsea_2

FM 131 73 -18 Mw 3.50 rms 1.414e-06 505 ERR 1 2 6 ISO 0.00 0.00 CLVD 0.00 0.00

Variance reduction 72.4

Pz

Pr

Sz

Sr

Sh

GS_OK033
44.4/-0.15



-0.10
99

-0.10
90

N4_T35B
62.4/-0.08

0.50
77



1.20
26

1.20
51

1.15
88

GS_OK029
88.0/-0.06

1.25
81



0.85
81

0.85
31

0.10
98

OK_CROK
98.4/-0.13

0.85
69



0.85
95

GS_OK025
103.8/-0.08

1.55
51



0.30
97

0.30
92

0.45
97

GS_KAN14
111.7/-0.13

0.25
67



1.45
83

TA_TUL1
115.0/-0.10

0.95
76



-0.25
96

-0.25
82

0.70
99

OK_FNO
139.4/-0.17

1.10
66



0.90
96

0.90
73

0.95
97

Y9_FW06
144.6/-0.11

0.90
28



1.10
98

1.10
71

GS_OK040
160.1/-0.17

1.15
23

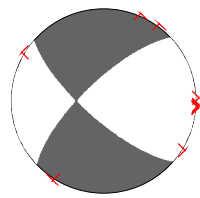


53

96

C. Full Inversion Result on 2016-09-03 (mainshock M5.8)

C. Full Inversion Result on 2016-09-03 (mainshock M5.8)



Event data Model and Depth chelsea_2

FM 131 73 -18 Mw 3.50 rms 1.414e-06 505 ERR 1 2 6 ISO 0.00 0.00 CLVD 0.00 0.00

Variance reduction 72.4

Pz

Pr

Sz

Sr

Sh

Y9_FW10
164.2/-0.10

0.90
4

0.90
41

1.25
95

1.25
87

Y9_FW02
165.3/-0.15

0.05
2

0.05
43

1.40
98

GS_OK038
166.2/-0.11

0.75
89

Y9_FW09
193.2/-0.18

1.75
92

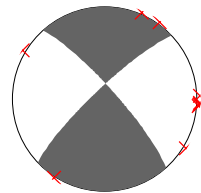
OK_X37A
247.4/-0.27

3.20
84

3.20
89

3.30
95

D.2 Inversion Result at depth of 3km



Event data Model and Depth chelsea_3

FM 318 80 10 Mw 3.50 rms 1.318e-06 505 ERR 1 4 5 ISO 0.00 0.00 CLVD 0.00 0.00

Variance reduction 74.2

Pz

Pr

Sz

Sr

Sh

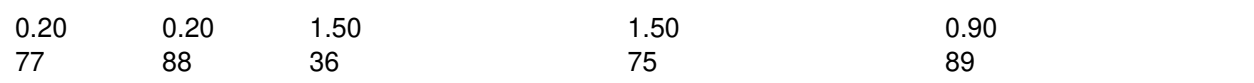
GS_OK033
44.4/-0.05



-0.60
99

-0.60
96

N4_T35B
62.4/0.03



0.20
77

0.20
88

1.50
36

1.50
75

0.90
89

GS_OK029
88.0/0.04



1.25
83

1.25
76

0.10
88

0.10
28

0.10
98

OK_CROK
98.4/-0.03



0.90
76

0.90
87

0.20
97

GS_OK025
103.8/0.03



1.50
53

1.50
67

-0.20
97

-0.20
93

0.50
97

GS_KAN14
111.7/-0.03



0.80
61

0.80
79

-0.20
89

TA_TUL1
115.0/0.00



-0.10
92

-0.10
78

1.25
97

1.25
92

0.65
99

OK_FNO
139.4/-0.06



1.20
70

0.40
96

0.40
77

0.40
97

1.10
97

Y9_FW06
144.6/-0.01



0.95
34

0.95
63

0.40
98

0.40
73

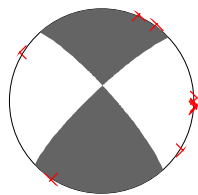
GS_OK040
160.1/-0.06



1.25
25

1.25
58

0.75
96



Event data Model and Depth chelsea_3

FM 318 80 10 Mw 3.50 rms 1.318e-06 505 ERR 1 4 5 ISO 0.00 0.00 CLVD 0.00 0.00

Variance reduction 74.2

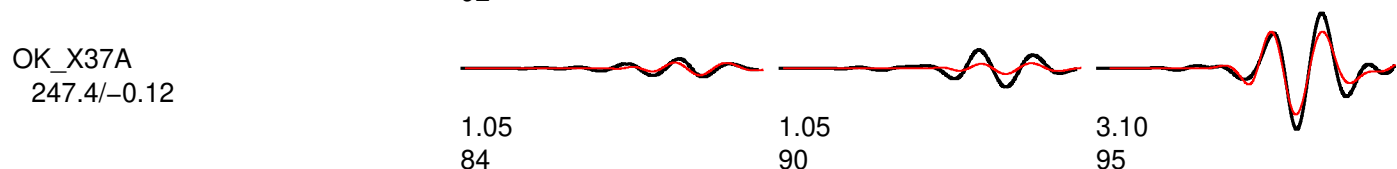
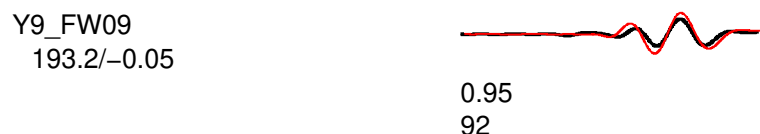
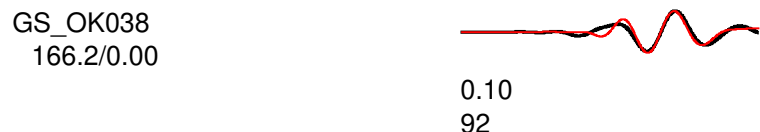
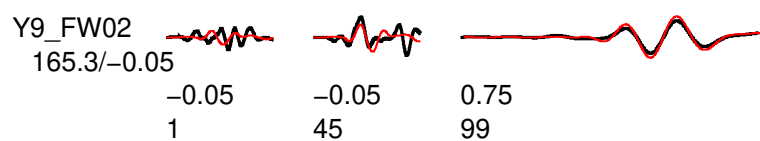
Pz

Pr

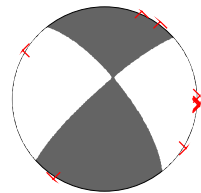
Sz

Sr

Sh



D.3 Inversion Result at depth of 4km



Event data Model and Depth chelsea_4

FM 321 72 10 Mw 3.55 rms 1.255e-06 505 ERR 1 3 6 ISO 0.00 0.00 CLVD 0.00 0.00

Variance reduction 75.4

Pz

Pr

Sz

Sr

Sh

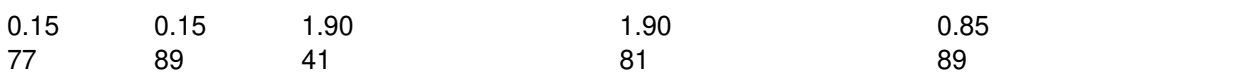
GS_OK033
44.4/-0.04



-0.80
99

-0.80
94

N4_T35B
62.4/0.04



0.15
77

0.15
89

1.90
41

1.90
81

0.85
89

GS_OK029
88.0/0.05



1.20
82

1.20
78

-0.35
91

-0.35
32

0.10
98

OK_CROK
98.4/-0.02



0.85
80

0.85
90

-0.10
98

GS_OK025
103.8/0.04



1.40
55

1.40
65

-0.60
97

-0.60
92

0.50
97

GS_KAN14
111.7/-0.02



0.85
57

0.85
83

-0.80
88

TA_TUL1
115.0/0.01



-0.25
91

-0.25
79

2.05
96

2.05
83

0.60
99

OK_FNO
139.4/-0.05



1.20
73

0.05
96

0.05
79

1.10
97

Y9_FW06
144.6/0.00



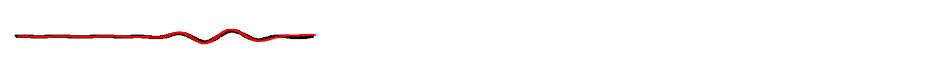
0.90
35

0.90
69

0.10
98

0.10
75

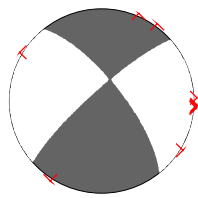
GS_OK040
160.1/-0.05



1.20
28

1.20
58

0.40
95



Event data Model and Depth chelsea_4

FM 321 72 10 Mw 3.55 rms 1.255e-06 505 ERR 1 3 6 ISO 0.00 0.00 CLVD 0.00 0.00

Variance reduction 75.4

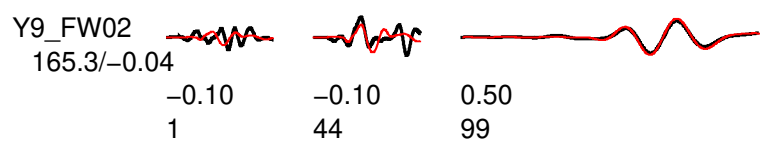
Pz

Pr

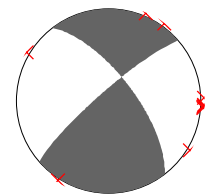
Sz

Sr

Sh



D.4 Inversion Result at depth of 5km



Event data Model and Depth chelsea_5

FM 323 68 10 Mw 3.57 rms 1.273e-06 505 ERR 1 3 4 ISO 0.00 0.00 CLVD 0.00 0.00

Variance reduction 75.1

Pz

Pr

Sz

Sr

Sh

GS_OK033
44.4/-0.04



-1.05
98

-1.05
85

N4_T35B
62.4/0.03

0.05
74



2.30
43

2.30
79

0.80
90

GS_OK029
88.0/0.05

1.20
81



-0.80
92

-0.80
37

0.10
98

OK_CROK
98.4/-0.02

0.75
82



-0.30
98

GS_OK025
103.8/0.04

1.35
56



-1.05
98

-1.05
90

0.50
97

GS_KAN14
111.7/-0.02

0.80
52



-1.30
87

TA_TUL1
115.0/0.01

-0.35
92



2.80
95

2.80
75

0.60
99

OK_FNO
139.4/-0.06

1.25
75



-0.40
95

-0.40
82

1.15
97

Y9_FW06
144.6/0.00

0.85
34



-0.15
97

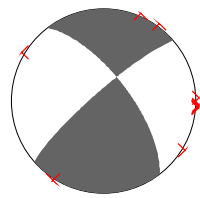
-0.15
74

GS_OK040
160.1/-0.05

1.05
34



0.15
94



Event data Model and Depth chelsea_5

FM 323 68 10 Mw 3.57 rms 1.273e-06 505 ERR 1 3 4 ISO 0.00 0.00 CLVD 0.00 0.00

Variance reduction 75.1

Pz

Pr

Sz

Sr

Sh

Y9_FW10
164.2/0.02

0.40
23

0.40
34

-0.25
89

-0.25
87

Y9_FW02
165.3/-0.04

-0.15
2

-0.15
42

0.25
98

GS_OK038
166.2/0.00

-0.40
96

Y9_FW09
193.2/0.10

0.10
89

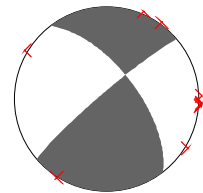
OK_X37A
247.4/0.08

-0.05
88

-0.05
92

2.85
95

D.5 Inversion Result at depth of 6km



Event data Model and Depth chelsea_6

FM 322 64 6 Mw 3.58 rms 1.365e-06 505 ERR 1 2 3 ISO 0.00 0.00 CLVD 0.00 0.00

Variance reduction 73.3

Pz

Pr

Sz

Sr

Sh

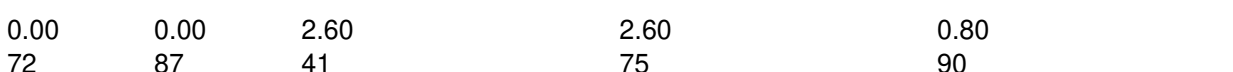
GS_OK033
44.4/-0.05



-1.45
98

-1.45
66

N4_T35B
62.4/0.02



0.00
72

0.00
87

2.60
41

2.60
75

0.80
90

GS_OK029
88.0/0.05



1.45
76

1.45
74

-1.25
90

-1.25
41

0.10
98

OK_CROK
98.4/-0.02



0.75
79

0.75
92

-1.40
97

GS_OK025
103.8/0.03



1.50
46

1.50
57

-1.60
98

-1.60
90

0.55
97

GS_KAN14
111.7/-0.02



0.95
50

0.95
85

-2.25
81

TA_TUL1
115.0/0.01



-0.60
88

-0.60
78

3.85
95

3.85
83

0.65
99

OK_FNO
139.4/-0.06



1.45
76

1.45
94

-0.95
94

-0.95
83

1.25
97

Y9_FW06
144.6/0.00



0.85
34

0.85
81

-1.35
97

-1.35
57

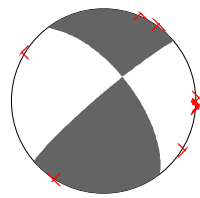
GS_OK040
160.1/-0.06



0.95
43

0.95
55

-0.90
94



Event data Model and Depth chelsea_6
FM 322 64 6 Mw 3.58 rms 1.365e-06 505 ERR 1 2 3 ISO 0.00 0.00 CLVD 0.00 0.00
Variance reduction 73.3

Pz

Pr

Sz

Sr

Sh

Y9_FW10
164.2/0.02

0.15
30

0.15
31

-1.35
88

-1.35
81

Y9_FW02
165.3/-0.04

-0.10
4

-0.10
37

-0.80
97

GS_OK038
166.2/0.00

-1.40
94

Y9_FW09
193.2/0.18

-1.05
94

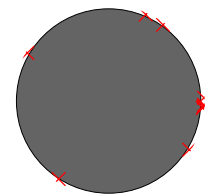
OK_X37A
247.4/0.18

-0.40
90

-0.40
93

2.70
96

D.6 Inversion Result at depth of 7km



Event data Model and Depth chelsea_7

FM 321 90 26 Mw 3.59 rms 1.457e-06 505 ERR 1 2 2 ISO 0.00 0.00 CLVD 0.00 0.00

Variance reduction 71.5

Pz

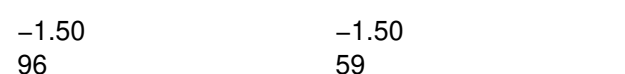
Pr

Sz

Sr

Sh

GS_OK033
44.4/-0.07



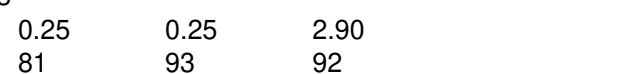
N4_T35B
62.4/0.02



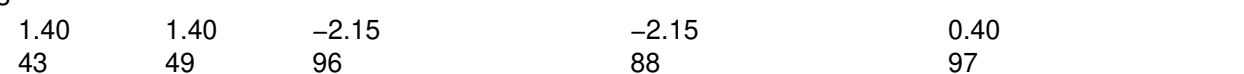
GS_OK029
88.0/0.04



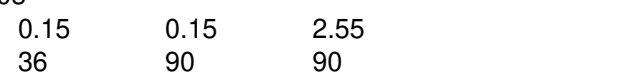
OK_CROK
98.4/-0.03



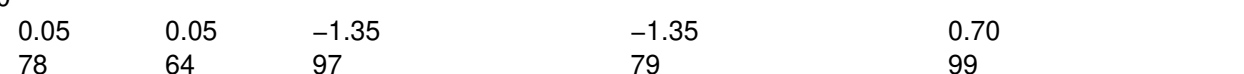
GS_OK025
103.8/0.03



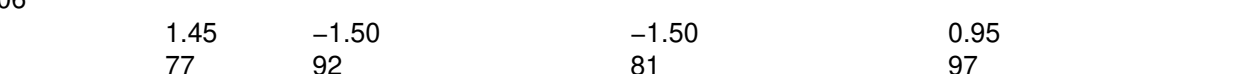
GS_KAN14
111.7/-0.03



TA_TUL1
115.0/0.00



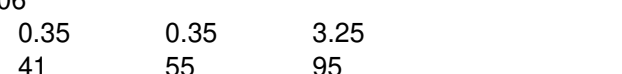
OK_FNO
139.4/-0.06

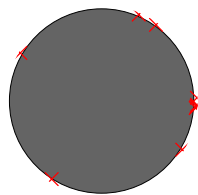


Y9_FW06
144.6/0.00



GS_OK040
160.1/-0.06





Event data Model and Depth chelsea_7

FM 321 90 26 Mw 3.59 rms 1.457e-06 505 ERR 1 2 2 ISO 0.00 0.00 CLVD 0.00 0.00

Variance reduction 71.5

Pz

Pr

Sz

Sr

Sh

